2023

Assessment of potential rooftop solar PV electricity at a suburban scale, and a comparative analysis based on topographical obstruction and seasonality

Alok Singh

UNIVERSITY
OF WOLLONGONG
AUSTRALIA

Assessment of potential rooftop solar PV electricity at a suburban scale, and a comparative analysis based on topographical obstruction and seasonality

By

Alok Singh

This thesis is presented as part of the requirement for the conferral of the degree:

Master of Research

The University of Wollongong

Faculty of Science, Medicine and Health

School of Earth, Atmospheric and Life Sciences

February 2023

Abstract

Long-term climate change mitigation calls for a switch from the current global non-renewable energy system to low greenhouse gas (GHG) emission energy solutions. Many nations have started adopting energy-efficient technology as part of their climate change programs and the built environment has been identified as a key lever for reducing emissions linked to energy efficiency. Building rooftop photovoltaic (PV) system is an effective technology to reduce emissions through the use of solar energy. In recent years, rooftop PV systems have become the main source of solar-generated energy, and forecasting their output is critical when assessing a site's PV energy potential. However, integrating topographical features with seasonal considerations to estimate solar PV energy is challenging. There are some studies available that estimate solar PV energy on rooftops using geospatial tool modeling, but these have limitations in functionality, accuracy, and calculation speed. This study uses a geospatial tool to assess the solar PV potential of suitable rooftops in the suburbs of Wollongong, Australia, namely, Wombarra and Cringila. The model used in this study compares the energy potential of these two suburbs based on the topographical feature (escarpment), seasonality, rooftop slope, and aspect. The digital surface model (DSM) is created using LiDAR data, and then the DSM, building footprints, and suburb boundaries data are used to calculate the solar PV energy potential. A total of 1594 buildings from two suburbs were considered. Subsequently, solar radiation modeling for four common seasons in a year and a comparison of solar radiation output, suitable rooftop area, and electricity output are being done for both suburbs. Wombarra's building rooftops are shadowed by the escarpment, whereas Cringila's aren't. Even though the weather in both suburbs is similar, the escarpment's shadow affects solar PV energy output. Wombarra has 178 kWh/m^2/building lesser yearly solar radiation than Cringila. Hence, Cringila offers more solar rooftop installation potential per building. The average annual potential electricity generation per dwelling in Wombarra is 20.6 kWh/m^2/day, and the same for Cringila is 27.6 kWh/m^2/day. The outcome reveals that 1352 building rooftops, with a usable area of 75481 m^2, are the best locations for installing solar panels. According to the Australian Government's Energy Made Easy statistics, the annual electricity consumption per household in Wollongong is 5707.6 kWh (Australian Energy Regulator 2022). The estimated yearly electricity production is 12705 Mwh (Wombarra: 2778.3 Mwh, Cringila: 9926.7 Mwh), which would be sufficient to meet local electricity consumption. An excess of 17% from Wombarra and 48% from Cringila can be exported back to the grid, which can be used by

neighbouring areas. Tiseo (2021) reported that Australia's power sector released 656.4 grams/kWh of CO_2 in 2020. Therefore, solar PV panels on all suitable rooftops of both suburbs could prevent 8339.5 tonnes of CO_2 emissions. To achieve the goal of clean energy, future development can use the study's findings as a guide. The proposed approach can assist in influencing policies and subsidies to boost deployment. This research can be made more in-depth by taking into account social and economic factors like consumer choices and return on investment, and physically inspecting specific building rooftop impediments.

Acknowledgements

I could not have gotten this far without the assistance of my supervisor, family members, and friends.

I would like to thank my supervisor, Associate Professor Laurie Chisholm. I am grateful to you for all of your suggestions in getting this project started, as well as the continuous feedback and review that you provided throughout the year. The helpful comments and notes for me were a huge help whenever feelings of self-doubt began to creep up on me.

My heartfelt gratitude goes to Korin Brown, without your expertise in geospatial software, I would not be where I am today. I appreciate your insightful comments during the modelling process in the ArcGIS Pro GIS tool.

I'd like to express my gratitude to Sharmishtha, my spouse, for her unwavering support. I am grateful for your support throughout this journey. Finally, and most importantly, I am and will always be grateful to my parents and in-laws. Their unending love, support, and compassion are the driving forces behind all of my accomplishments.

Certification

I, Alok Singh, declare that this thesis submitted in fulfilment of the requirements for the conferral of the degree Master of Research, from the University of Wollongong, is wholly my own work unless otherwise referenced or acknowledged. This document has not been submitted for qualifications at any other academic institution.

Alok Singh

Date: 01/02/2023

List of Abbreviations

2D	Two Dimensional
3D	Three Dimensional
ABS	Australian Bureau of Statistics
AEMO	Australia's energy market operator
ArcGIS	GIS mapping software
ArcPy	ArcGIS Python package
ARIMA	AutoRegressive Integrated Moving Average
ASR	Area Solar Radiation
BIM	Building information modelling
BoM	Bureau of Meteorology
CNN	Convolutional neural network
CO_2	Carbon dioxide
CSIRO	Commonwealth Scientific and Industrial Research Organization
CSP	Concentrated Solar Power
DC	Direct current
Dcceew	Department of Climate Change, Energy, the Environment and Water
DEM	Digital Elevation Model
DNI	Direct normal irradiance
DSM	Digital Surface Model
ESRI	Environmental Systems Research Institute
GeoJSON	Geospatial JavaScript Object Notation
GHG	Greenhouse Gas Emissions
GIS	Geographic information system
Gt	Gigatonne

IEA	International Energy Agency
Mt	Megatonne
Gw	Gigawatt
Kwh	Kilowatt hours
kWh/m^2	Kilowatt-hours per square metre
Kwp	Kilowatt peak
LAS	LASer File Format; A file format for the interchange of 3-dimensional point cloud data
LFA	Leased Federal Airports
LiDAR	Light Detection and Ranging
LSTM	Long short-term memory
MAPE	Mean Absolute Percentage Error
MATLAB	Matrix Laboratory software
NOAA	National Oceanic and Atmospheric Administration
NREL	National Renewable Energy Laboratory
NSRDB	National Solar Radiation Database
NSW	New South Wales
PV	Photovoltaic
PVSYST	Energy Modelling tool
PVWatts	Web application for estimating the energy production
RETScreen	Renewable Energy Project Analysis Software
SunSPoT	Three-Dimensional mapping software
USA	United States of America
Wh/m^2	Watt-hours per square metre
SVR	Support Vector Regression
NN	Neural network

Table of Contents

List of Figures

List of Tables

1. Introduction

1.1 Background

Electricity is an important facet of contemporary life, and the various ways in which it benefits us cannot be overstated. We rely on electricity for several different things, such as illuminating, cooling, heating, and refrigerator, as well as for the functioning of gadgets, electronics, computers, and transportation systems, among other things (Schiffer 2009). In this day and age, we would be nothing without the aid of electricity. A secondary source of energy is the electricity that we require for our day-to-day activities. Electricity is created through the transformation of fundamental and natural energy sources including nuclear energy, natural gas, coal, wind, and solar energy, into electrical energy (Salehabadi et al. 2020). This process is of utmost significance in the improvement of human lives and the revitalization of the national economy.

The generation of electricity through the use of resources that are not replenishable (non-renewables) is a major cause of environmental concern. Since industrialization in the 18th century, traditional fossil fuels have been extensively used to generate electricity (Sen 2008), resulting in the release of several greenhouse gases and thus, migrating the climate. The consumption of fossil fuels is to blame for environmental issues such as global warming and air pollution, both of which contribute to the deterioration of people's health and the overall quality of life in their respective communities (Breeze 2014). Coal and oil are two major examples of polluting fossil fuels that are contributing to environmental degradation.

The most significant contribution that humans have made to the problem of climate change is the generation of energy through the combustion of fossil fuels, in particular coal (Ng et al. 2019). Because one of the major sources of carbon dioxide (CO_2) emissions is electricity generation using fossil fuels, governments have investigated the feasibility of switching from polluting energy sources to clean energy sources (Ellabban et al. 2014). Even if some countries have reduced their emissions, greenhouse gas (GHG) emissions are still rising. Over the last decade, the widespread implementation of renewable energy sources has emerged as a primary concern for governments and decision-makers across the board in industrialized economies, developing markets, and a large number of developing nations. As a result of this, a great number of nations have initiated a paradigm shift by embracing technology that is more energy efficient and fuels that emit less pollution as part of their initiatives to combat climate change (International Energy Agency (IEA) 2021b). The shift from conversation to

action, on the other hand, frequently proves to be a great deal and more challenging than was first imagined. These changes have repercussions and necessitate adjustment at all levels of decision-making, management, and economic planning. Such adjustments require a full understanding of the many capacities, such as finances, infrastructure, as well as the climatic and topographic circumstances at a location, in order to ensure a seamless transition to an energy system. Renewable energy sources are a foundational component of sustainable practices for meeting the needs of the underprivileged and fostering long-term economic expansion (Moriarty & Honnery 2012). Renewable energy will assist millions of people to have better access to modern energy services, reduce economic risk by assuring energy security, and minimize the likelihood that climate change will occur. All of these benefits are achieved by cutting emissions (Reddy & Nathan 2013).

There was a 6% increase in worldwide energy-related CO_2 emissions from 2020 to 2021, bringing the total to 36.3 Gt of CO_2 emissions in 2021 (IEA 2022). The production of electricity and heat saw the largest growth in CO_2 emissions of any industry in 2021, with a 900 Mt increase in the amount of gas released into the atmosphere. As a result of this, 46% of the worldwide rise in emissions may be attributed to it, since the use of all fossil fuels grew to assist in meeting the growing demand for energy (IEA 2022). Buildings account for around 40% of the world's total energy use, giving them an important place in the energy industry (World Economic Forum 2021). It is anticipated that the demand for energy from buildings will continue to rise around the globe in the next decades. In addition to this, the construction industry has a considerable impact on how natural resources are utilized (Sartori & Hestnes 2007). Therefore, structures, even though that they provide facilities for human needs and their innumerable advantages to society, cannot be overlooked, buildings have also had detrimental effects on the environment over the previous few decades (Zuo & Zhao 2014). The annual increase in CO_2 emissions from the building industry was 81 Mt in 2019, which resulted in 167 Mt of CO_2 emissions from the building sector in 2021. (IEA 2022).

As the global population continues to rise, so has the need for electric energy in all kinds of daily uses like entertainment, transportation, healthcare, outdoor, household, commercial, and office. As a direct result of human activity, the extraction of non-renewable resources such as natural gas, coal, and oil has led to major negative effects on the surrounding environment as well as on society. The transition to a more sustainable and environmentally friendly method of producing electricity is urgently required. Solar energy is recognized as a clean source of energy that does not incur any cost in transportation, is endless, widely

available, easily accessible, inexpensive, and beneficial to the environment. As a result, solar energy exceeds other forms of renewable energy as well as fossil-based energy resources. (Lukač et al. 2013).

The transition to solar energy instead of continuing with conventional fossil fuels for electricity production has significant benefits. According to The Australia Institute Climate of the Nation, 83% of the population aged between 18 and 34 years has a concern about climate change (Quicke 2021). It is identified that solar energy is a major alternative to powering homes and heating water so it can help to reduce carbon emissions and lead to a more sustainable lifestyle (Kabir et al. 2018). Electricity production from solar panels is also not harmful to humans, wildlife, and ecosystems because there is no impact on the land and air quality as occurs in electricity production from oil and gas. Therefore, solar energy can help to reduce climate change and decrease the use of fossil fuel-based energy production, which includes carbon emissions, air pollution, and other adverse impacts on the environment (Shahsavari & Akbari 2018). Further, solar energy also helps to achieve sustainable development goals. For instance, SDG goal 3: Good health and well-being are achievable when there is lesser carbon emission to whom an individual has exposure. SDG goal 7: clean and affordable energy is also achievable, as there is almost no impact on the environment (Güney 2019).

Solar energy is one of the most abundant natural energy resources. It has the potential to significantly cut CO_2 emissions, and solar photovoltaics (PV) is one of the most effective methods to convert it into electricity (Freitas & Brito 2019). A photovoltaic system is a group of cells that work together to convert solar radiation into electricity. Each cell has layers of a semi-conducting material. Light striking the cell generates an electric field that reaches across its layers, causing electricity to flow. Each cell generates a particular amount of electrical power, which is proportional to the amount of light that hits it (Tyagi et al. 2013). The cost of solar photovoltaic (PV) systems has decreased noticeably all over the world with time, and globally, the process of converting solar energy to electricity has significantly increased. This is largely due to the lower cost of PV cells as well as their higher conversion efficiency (Baurzhan & Jenkins 2016). Consequently, PV technology is a beneficial investment because it lowers greenhouse gas emissions and results in cost reductions over the long term. It has been anticipated that solar photovoltaic electricity will reduce annual utility expenses in Abu Dhabi, United Arab Emirates, by $3.3 million (Harder & Gibson 2011).

Australia's electricity generation production increased significantly in 2020-21, reaching a capacity of 266 tWh, which was the highest total generation as compared to previous years (Australian Energy Market Operator 2021). Coal and natural gas are the main sources of energy to produce electricity in the country. 71% of the total electricity is generated in Australia using fossil fuels such as coal, gas, and oil. Coal is contributing to producing more than half of the total energy in Australia (Department of Climate Change, Energy, the Environment and Water (dcceew) 2022a). However, the subsequent environmental impacts are driving the country toward the usage of renewable energy sources (Kabir et al. 2018). A comparison from the beginning of the century, there is almost a 30% reduction in the use of coal, whereas an increase of 5% is observed for the use of renewable energy sources in 2021 in comparison to 2020 (IEA 2021a). Currently, solar energy is the most prominent renewable energy source in Australia, and it is contributing to 12% of total electricity production (dcceew 2022a). Apart from this, 17% of the total electricity production is coming outside of the national electricity sector as it is contributed by households and businesses (dcceew 2022a).

In New South Wales, the contribution of coal to total electric energy production is still dominant and most of the energy is coming from the electricity sector in the country. Only a small portion of the country's electricity is generated by businesses and households (Department of Planning and Environment 2019). But since 2009, the country has adopted solar energy significantly more frequently as a renewable energy source, and it is anticipated that solar energy will play a big role in the nation's future electricity production (Ravimohan et al. 2014). As of 2019, there were nearly two million PV solar energy dwellings and the penetration level is around 60% at a global level, Australia leads the globe in implementing distributed residential PV solar energy and around 60% of solar panel installations are for the residential sector (Narayanan et al. 2021).

Considering the benefits of solar energy, Australia is continuously focusing on achieving sustainability and meeting net zero carbon emission goals set to be achieved in 2050 (IEA 2021b). In 2020, Australia was generating 21.6% of its total electricity using solar PV panels and in 2021, it had increased to 31.8% (Geoscience Australia 2022a). In the next ten years, the average annual growth rate is expected to be 33.6% for solar PV panels for energy production (Geoscience Australia 2022a). Solar energy has the potential for remote areas to deliver off-grid electricity to them. As of December 2020, 2.7 million solar PV systems were installed, and they covered 27.3% of houses in Australia. In New South Wales, solar energy

has been adopted using 8275 installations that are generating around 37,000 kW of capacity (Clean Energy Council 2022). Further, the rapid growth of hospitals, commercial buildings, schools, and businesses is creating a need to control electricity costs, so people are moving toward solar energy. Governmental initiatives and policies are also major factors in uplifting the adoption of solar energy in Australia (Rahman & Vu 2020). It indicates that there is a significant transition toward solar energy sources. In 2021, Australia broke its previous record for rooftop solar system construction by building around 380,000 new systems (Taylor 2022). These installations have a combined capacity of 3.2 gigawatts when all their power is combined. As a result, Australia's total amount of renewable energy produced in 2021 was 72.5 Twh, a 23% increase over the amount produced in 2020 (Taylor 2022). After installing the largest generator in Australia, that total capacity increased to 17 gigawatts, which is equivalent to the count of rooftops of more than 3 million, and that's where Australia leads the globe in rooftop solar PV energy (Taylor 2022). However, in 2020, total energy consumption from renewables account for only 6% (Li et al. 2020). In 2020, fossil fuels account for 76% of Australia's electricity generation, with solar energy accounting for only 22.3% of the nation's yearly renewable electricity output (Clean Energy Council 2020).

Although Australia receives more sun than any other continent on Earth, its major energy consumption is powered by solar energy, which accounts for less than 1% of Australia's overall consumption (Yu & Halog 2015). Security of energy supply to meet rising demand, universal access to energy services, and limiting the impact of energy on climate change are the three main global energy concerns. Human progress and energy availability are intertwined (Asumadu-Sarkodie & Owusu 2016). The Energy Networks Australia (2017) forecasts that by the year 2050, rooftop solar installations will cover 40% of all rooftops in Australia. Solar power is one of the most eco-friendly forms of renewable energy, and Australia has abundant solar radiation per square metre (Bahadori & Nwaoha 2013). PV systems have the ability to meet urban energy needs while relieving strain on the grid infrastructure. With the support of the grid, customers can generate their energy and even export it back into it when they don't need it. Many commercial and industrial buildings have vacant roof space that might be converted to solar photovoltaics (Sewchurran & Davidson 2021). Distributed generation, driven by rising power prices and falling PV costs, is having an impact on the electricity system, notably on the management of the transmission networks (Rathore et al. 2019). A better understanding of the magnitude and distribution of all rooftops' potential would help network design and support tailored strategies for PV solar

energy development (Rathore et al. 2019). Future expansion in the global usage of solar energy is predicted to be driven mostly by government regulations, as well as decreasing investment costs and risks (Bahadori & Nwaoha 2013).

It is crucial to establish effective and precise geospatial frameworks for evaluating and categorizing rooftops as per slope, aspect, and suitable area for PV systems across local government areas in order to support informed planning and investment decisions. Solar radiation on different earth's surfaces varies significantly regarding intensity, and it is because of atmospheric and astronomical factors. In calculating solar photovoltaic energy potential, it is essential to predict how solar radiation is distributed in the selected site because of variations in solar radiation from one surface to another.

Australia is found in the southern half of the globe, and as the earth revolves around the sun, the Southern Hemisphere experiences more daylight hours for half of the year, i.e., spring and summer, due to the Earth's inclination axis. The axis tilts away during the other half of the year, which results in less sunlight reaching the southern hemisphere during autumn and winter (Singh 2022). Considering this phenomenon, the overall amount of solar radiation for a site in Australia varies in a cyclical variation. The number of variations in solar radiation results in various seasons. Besides these, there is also the impact of topographical factors on the distribution of solar radiation incoming to a site. For instance, topographical features can result in shadows on most of the site's area, reducing the solar panel area's exposure to sunlight. If solar panels are positioned in an area covered with shade, there is a loss of revenue because of the lower energy potential of each solar photovoltaic cell. Therefore, analyzing shadow casting on a site in the different seasons due to topographic features is essential to considering evaluating solar radiation distribution and calculating solar photovoltaic energy (Doorga et al. 2019). Additionally, there is a major impact on the location where solar panels are being installed. The location of the dwelling, the tilt angle of the rooftop, along with its orientation for sunlight, are important factors, as they determine the overall sunlight density in a unit area of the surface (Ghaleb & Asif 2022).

Solar PV panels capture the energy of sunlight and convert it into electricity, and it is one of the most efficient ways of converting solar energy into direct current (DC). Given a specific area, the efficiency of solar PV is determined by two key factors: the distribution of solar radiation over a suitable rooftop area and its intensity. Even though the number of rooftop

assessment tools and methods for PV is growing, these methods must consider some important variables collectively in the assessment, like considering solar insolation variation at each hour for different seasons, including obstruction of topographic features, vegetation, and other buildings, sun direction over the seasons and a day, and rooftop characteristics (slope and aspect).

1.2 Research Aim and Objectives

This research aims to investigate the impact of topographical structure on the solar energy output. In order to accomplish this, two suburbs are selected, namely, Wombarra and Cringila, located in Wollongong, NSW, Australia. In Wombarra, the escarpment is close to dwellings, resulting in a varying amount of shadow cast across the seasons. On the other hand, in Cringila there is no shadow from an escarpment due to its distance from dwellings. The study will estimate and statistically compare the solar PV potential of all type of building rooftops based on topographical obstructions and seasonal variation. The estimation of seasonal solar energy for each building in these suburbs will be conducted through the utilization of LiDAR data in a geospatial technique. This approach provides an effective and accurate method to assess the potential energy output of solar panels on rooftops, allowing for better decision making when it comes to installing solar panels. By using LiDAR data and GIS, we can accurately measure the size of roofs, calculate their orientation and tilt angles, as well as determine the amount of sunlight that each building receives throughout the year. With this information in hand, we can then estimate how much solar energy each building is likely to produce throughout the year. The data collected through this research will help us better understand how these factors affect the solar PV potential of dwelling rooftops. There are few studies that have provided assessments of the shading effects of topographical features to estimate the solar PV potential of all rooftops. A detailed evaluation of all kinds of obstructions around buildings, including topographical features, on a suburban scale, is necessary to assess the solar PV potential of rooftops during the various seasons of the year.

The following are the objectives of this study:

a. Validate the estimated mean solar radiation data in the selected suburbs for four seasons, against the Wollongong weather stations' data.

b. Estimate the amount of solar radiation falling on each building rooftops, and the distribution of suitable rooftop areas of the selected suburbs for each of the four seasons and over the course of a year.
c. Calculate the potential solar photovoltaic energy output of all building rooftops in selected suburbs by using the estimated solar radiation, and the distribution of suitable rooftop areas.
d. Compare the energy output of selected suburbs and estimate average loss of solar PV energy due to escarpment shadow in one of the suburb in kWh/m2/day/building.
e. Estimate the possible change in CO_2 emissions based on the potential solar PV energy production of both suburbs.

1.3 Research Outline

Chapter 1 Introduction: This chapter presents the background, research aim, and objectives of the study that was carried out. This introductory chapter outlines what kind of information is organized and managed in various chapters so that it provides a clear understanding of the research content. In addition, it is helpful to establish a background to develop a fundamental understanding of the research area. The subsequent chapters are structured as follows:

Chapter 2 Literature review: This chapter provides a literature review and includes the research articles that are pertinent to the modeling of PV energy and determining solar radiation by applying the impacts of topographic obstacles in the estimation process. This chapter discusses the contributions of various authors to developing and modeling the solar PV system at different scales. It also discusses the relevancy of the case studies and the application of estimations for the selected area of interest. This chapter also focused on research methodology and tools used in various studies, and it includes the identification of the importance of topographical feature and their analysis of solar radiation.

Chapter 3 Regional Setting: This chapter is focused on the study area, taking into consideration the landscape, dwelling structures, climate, and the vision of the local council in order to accomplish the objective of creating a sustainable city. Additionally, the criteria that were utilized to pick Cringila and Wombarra as two places in which to collect and analyze the data to estimate solar PV energy potential.

Chapter 4 Research Methodology: In this chapter, the primary emphasis is placed on providing an explanation of the research method to facilitate the development of an accurate solar PV energy estimation model utilizing the geospatial application ArcGIS Pro. It then continues to give an outline of the aims and objectives of the research and justifies how the methodologies can be applied to attain the particular purpose. In addition to presenting the utilization of data and sources, the study also discussed the relevant parameters for the model that was used to process the data.

Chapter 5 Results: This chapter contains results and analysis produced by using the geospatial method, and provides adequate visual and statistical representations of the output. Statistical representation describes distribution and variations and provides the solar PV energy potential for the selected suburbs while undertaking a comparative analysis of outcomes for both suburbs. At last, the model is validated, and for that, it contains a comparison of the data generated by simulations with the data generated by bureau stations, and the mean absolute percentage error (MAPE) method is used to evaluate the percentage difference.

Chapter 6 Discussion: This chapter discussed the findings and their implications in light of pertinent literature, as well as the study's limitations.

Chapter 7 Conclusion: This chapter outlines the conclusions from the research in this thesis and highlights the prospects for further research in this area.

2. Literature Review

2.1 Introduction

The potential of rooftop PV systems to generate electricity from solar energy is estimated using a variety of methods, as mentioned in (Freitas et al. 2015) and (Margolis et al. 2017). These techniques have been used to determine the technical potential of PV and rooftop suitability factor for many cities and countries, including the European Union (Defaix et al. 2012), Australia (Teofilo et al. 2021), Seoul (Hong et al. 2017), Switzerland (Buffat et al. 2018), Australia (Rana & Rahman 2020), Wheatbelt region (Clifton & Boruff 2010), New South Wales (Almaghrabi et al. 2021), City of Neom (Alqahtani & Balta-Ozkan 2021), Municipality of Laghouat, Algeria (Boulahia et al. 2021), Netherlands (Calcabrini et al. 2019), and Greece (Karteris et al. 2013). Finding a location's solar energy potential before installing solar panels is one of the most challenging tasks. As a result, a variety of studies are being conducted to determine whether or not the potential for solar radiation is sufficient to meet the energy needs of a particular region. The amount of solar radiation that strikes a PV system has the greatest impact on the overall energy generation efficiency of the system. To install an effective PV system in a specific location, it is necessary to have accurate and reliable information about the variables involved in assessing solar PV energy potential. In addition to this, data on solar radiation is essential for determining the system design and accessibility of the photovoltaic system (Labed & Lorenzo 2004). Installing measuring equipment such as pyrheliometers at a spot is the most basic way to gauge the amount of solar radiation at any location (Schüler et al. 2016). On the other hand, maintaining and supervising their daily record is a time-consuming and expensive task, particularly in rural and mountainous locations. Therefore, there isn't enough data available to measure solar radiation for a given area, particularly in rural and mountainous areas (Benti et al. 2022). Incoming solar radiation on a dwelling surface is influenced by a number of variables, including the structure of the roof, the topography of the area, the surface features, and the amount of solar insolation (Zalamea & Alvarado 2014). Earlier approaches for calculating the PV potential relied on computed solar radiation methods that were either top-down or were unable to capture either complicated rooftops or the likely shade that would be caused by the impediments (Ineichen 2016). Then, a mix of computer models and geospatial methodologies arose to enhance the solar irradiance estimations and for the estimation of both technical (Wiginton et al., 2010) and socio-economic potential (Gooding et al. 2013). On the other hand, geospatial-based methods, help capture the spatial and temporal

fluctuations of solar irradiation and, as a consequence of this, PV yields (Nguyen & Pearce 2010). Aerial imagery, digital surface models (DSM), and LiDAR data are examples of the types of geographic data that are used as the foundation for the vast majority of geospatial-based methodologies (Redweik et al. 2011; Tovar-Pescador et al. 2006). These methodologies start with varying presumptions. Therefore, their levels of precision and functionality are not comparable to one another. The assumption that every place on the rooftop receives the same quantity of solar radiation, regardless of the shading factors, slope, and aspect, is the most prevalent one considered in models. These kinds of assumptions frequently result in inaccurate conclusions (Jakubiec & Reinhart 2013). When it comes to the preparation of maps or the creation of PV potential tools, it is essential that the model be customized to suit the geographical area. This is because solar radiation and the weather parameters that are associated with it change significantly according to the location and time. These methods still lack seasonality assessment of solar radiation due to topographical features outside the boundary of the area of interest that will lead to variation in shading and suitable rooftop area at different time periods in a year. Scale, rooftop characteristics, landforms, and solar insolation are the most important factors since the same processes cannot be applied at the local, regional, or national levels (Buffat et al. 2018). As a consequence of this, researchers were forced to begin their work all over again from scratch and develop their very own data models (Farzaneh et al. 2019). The determination of the amount of solar potential in urban areas plays an essential part in the promotion of adaptive policies and financing programs, as well as in the gradual movement of cities toward a low-carbon energy transition (Wiginton et al. 2010).

There are a variety of ways to deal with solar estimations and among many different approaches to calculating solar PV energy, the three-step approach is used the most frequently: (i) solar irradiance calculation of the selected site (ii) estimation of the suitable roof area (iii) calculation of the power of the PV (Julieta et al. 2022). In order to do an analysis of the solar potential of varying building densities as well as the total roof area that is available, the climatological circumstances and the selected site settings that are employed are both considered to be input data.

2.2 Extent of the study area

In the recent few years, there has been a lot of focus placed on the viability of installing large-scale solar panel systems on the rooftops of residential buildings. In previous studies,

numerous study scales have been used to estimate and increase solar potential. Starting at the continental scale (Defaix et al. 2012; Teofilo et al. 2021), country scale (Buffat et al. 2018; Rana et al. 2020), city scale (Almaghrabi et al. 2021; Alqahtani & Balta-Ozkan 2021; Boulahia et al. 2021; Clifton & Boruff 2010) to the urban block scale (Calcabrini et al. 2019; Karteris et al. 2013). An analysis of the various approaches suggests that scale and the availability of data are two factors that are essential to the production of an accurate estimate of solar photovoltaic energy (Julieta et al. 2022). Therefore, depending on the desired outcome, several distinct methods, technologies, and tools have been applied, ranging from solar constant approaches with straightforward 2D display maps to the most advanced 3D modeling and the utilization of remote sensing data (LiDAR) (Gagnon et al. 2018; Ghosh & Vale 2006; Jo & Otanicar 2011; Odeh & Nguyen 2021; Suomalainen et al. 2017).

2.2.1 Solar PV assessment at a country scale

In order to determine the PV potential of a 2250 square kilometre area with a spatial resolution of 0.5 m^2, a simulation was done for more than 3 million structures in Switzerland (Buffat et al. 2018). Images of solar radiation captured by the satellite were integrated with the technical parameters of photovoltaic (PV) technology contained in the model (Buffat et al. 2018). The footprints of individual structures were acquired by utilizing a combination of Open Street Map, cadastral surveys, and SwissTLM because there was no single source that could cover such a huge area (Buffat et al. 2018). A Digital surface model (DSM), which was produced from LiDAR,(remote sensing data) was provided by Swisstopo to determine slope and aspect (Buffat et al. 2018). There is a significant possibility that some of the data would be duplicated, and there is also the possibility that some of the data would be completely absent because this research covers such a vast area and uses such a diverse range of technologies to achieve the same results. Because of the greater area, it was necessary to collect more than one DSM, and the data that was gathered had to be smoothed. Second, the simulation of a wider region that makes use of numerous tools at the same time requires a lot of computational effort, in addition to the compatibility and integration of these tools, which is necessary to migrate data from one tool to another. Both SwissTLM3D and Swisstopo are exclusive to their namesake country of Switzerland and are not available anywhere else.

For the whole United States, the technical potential of rooftop solar photovoltaics was examined (Gagnon et al. 2018). US Department (2006-14) LiDAR data was used, which covers

23% of the footprints of US buildings. The counts of medium and large buildings were based on data from an energy consumption survey of commercial buildings. To estimate the number of small structures, a regression model was created (derived from survey data of zip codes and population density). To get the total roof area, a random sample of buildings in Zip Codes with LiDAR data was selected, and the extrapolation was performed for all of the structures in the vicinity. The slope, azimuth, and shadowing of roofs were determined by using LiDAR data. For the roof suitability validation, Google Project Sunroof was employed (Gagnon et al. 2018). Even though it is possible to estimate a wide area's solar potential, doing so requires manual intervention in filling the gap for missing data, which is time-consuming and error-prone. In addition, the Google Project Sunroof feature is only available in the United States and has not yet been rolled out to Australia. Here, LiDAR data only covered 23% of the buildings, and the remaining data were dependent on surveys, making the accuracy of the information in those areas suspect.

Teofilo et al. (2021) developed a geospatial-based methodology to assess large-scale commercial rooftop PV installations (located at 21 airports around Australia) and provided an overview of their great potential at the country level. To complete the tasks of digitizing roof polygon outlines and computing rooftop area, the World Imagery feature of ArcGIS Pro 2.4 was utilized (Teofilo et al. 2021). Geoscience Australia provided the digital elevation data that was used to determine the elevation of the ground. The 3D imagery that was supplied by MetroMap was used to obtain data on the height of the buildings (Teofilo et al. 2021). The Area solar irradiation tool was used to identify the solar irradiation. The PV Watts calculator was used to figure out the optimal tilt angle for the solar panels (Teofilo et al. 2021). This methodology requires less time and effort and is more scalable.

Jung et al. (2019) used digital numerical map-oriented estimates to determine the solar energy potential on the slopes of South Korea's national highways. The national geographical institute was the source of the spatial data that was collected for estimating purposes to support efficient land utilization. The coordinates for the maps were derived from spatial data in a 3D vector form (Jung et al. 2019). In addition, DEM was used so that continuous digitalization of topographic surfaces could be accomplished. It was used in both the examination of terrain and the estimation of solar radiation. A digital numerical map was utilized to extract vector-type elevation contours, and then these elevation contours were translated to raster data in order to obtain an elevation value for each cell that was contained

inside the grid (Jung et al. 2019). In addition, an estimation of the shaded area and the possible area for use with the national road network were included in the study. In order to complete the study, manual digitization of contour maps was required, and MATLAB was utilized for further calculation (Jung et al. 2019). MATLAB necessitates the construction of GIS packages, which is a time-consuming process and cannot be automated.

2.2.2 Solar PV assessment at a state scale

Almaghrabi et al. (2021) conducted research on PV power forecasts for all PV plants in New South Wales, Australia. To develop the forecast model, solar performance data provided by Australian Energy Market Operator (AEMO) was aggregated over 494 days (2019-2020) in NSW (Almaghrabi et al. 2021). The data were normalized to prepare regional-level time series data. Then, the ARIMA model and Deep Learning algorithms (CNN and LSTM) were applied to evaluate spatial patterns over different time intervals in the time series data, and the prediction was made considering only historical solar power data (Almaghrabi et al. 2021). The limitation includes that this study used only previous recorded data and did not take into account shading analysis due to the obstructions in the sunlight path and roof statistics.

An energy estimating model for solar PV systems that makes use of a deep learning algorithm and data from remote sensing was proposed by Jiang et al. (2022). To record the patterns of solar radiation, geostationary satellite photos were used, which had a low spatial resolution. The overall area of the study was 107,200 km^2, and it is located in the province of Jiangsu in China (Jiang et al. 2022). The hourly solar radiation was determined by using a deep learning algorithm to analyze the collected satellite photos along with the associated time and location data. Using a technique called deep learning segmentation, the footprints of buildings were extracted from high-resolution photographs. The model was trained using a convolutional neural network (CNN) based on the collected historical data and estimation was carried out. The modeling of photovoltaic (PV) electricity output made use of the Global Solar Energy Estimator (GSEE) and Python module. In this model, the limitations consist of rooftop characteristics and topographical structure, both of which are crucial to derive shading impact and suitable rooftop areas.

2.2.3 Solar PV assessment at a city scale

Jo & Otanicar (2011) developed a method for evaluating the potential energy production of the city of Chandler, Arizona, by utilizing data from remote sensing, geographic information systems (GIS), and simulations of renewable energy sources. While Quickbird remote sensing data photographs and GIS building footprints were utilized for the detection of building rooftops using an object-orientated approach (Definiens developer program) (Jo & Otanicar 2011). Google Sketch was utilized for the loss calculation due to shadows that were cast by the buildings. After importing the data into ArcGIS, the computation of the area was carried out. A total of 150 buildings were inspected, and visual examination was employed to locate obstructions on the roofs of 20 of those buildings (Jo & Otanicar 2011). This method takes a long time and cannot be scaled up.

Boulahia et al. (2021) proposed an engineering-statistical technique for evaluating the photovoltaic solar potential on the rooftops of residential buildings. The study focused on Laghouat, which is located in the Central Southern region of Algeria. The full roof area was provided by the urban master plan developed by Laghouat in 2009 (Boulahia et al. 2021). The Ladybug tool performed an analysis of solar radiation in which shading losses, solar irradiance, tilt angle, and azimuth were taken into consideration (Boulahia et al. 2021). On the other hand, Ladybug is a three-dimensional tool that simulates one building at a time and then hypothesizes about the rest of the buildings in the simulation. This method is time consuming and sample building results were extrapolated for the estimation of all buildings.

The study by Suomalainen et al. (2017) focused on residential structures located in Auckland, New Zealand which spans an area of 2250 square kilometres. LiDAR data was used to develop the DSM. This data contains building topography as well as trees. The shapefile that was used was based on census data from 2013 to compute the area of building footprints and was provided by the Auckland Council. Estimating annual solar radiation in ArcGIS requires the use of a solar radiation tool that takes into account DSM and shapefiles (Suomalainen et al. 2017). This tool took into account many different factors, including time zone, climate, slope, surface orientation, and the effect of surrounding buildings and trees. The building footprint information supplied by the council takes into account garden blinds and garages, as a result, the findings are exaggerated as a direct result of the inclusion of these factors.

Ghosh & Vale (2006) developed a model to estimate the potential for rooftop solar energy in Glen Innes, which is located in Auckland. The ArcGIS application made use of aerial photographs in order to find a suitable area for solar energy generation (Ghosh & Vale 2006). This process considered factors such as the orientation and slope of the roof. In light of previous investigations, both the size of PV panels and their efficiency were taken into consideration. On the other hand, seasonality and topographic features were not taken into account in this investigation.

Odeh & Nguyen (2021) devised a technique to evaluate the potential of installing photovoltaic (PV) systems on rooftops in the residential areas of Sydney. The SunSPoT tool was used to calculate the annual energy production for every roof that had an area that was greater than or equal to 4 square metres on more than one side (Odeh & Nguyen 2021). Roof samples from each neighbourhood were considered, and the results were used to determine how much energy could be produced by each roof. This tool calculated the annual energy production of a rooftop by taking into consideration a wide range of factors, some of which include solar irradiation, PV area, orientation, and tilt angle, amongst others (Odeh & Nguyen 2021). The process is time-consuming since the SunSPoT tool, calculates the amount of solar photovoltaic (PV) electricity produced by a single residence at a given time. Also, this tool is currently not accessible in the Wollongong region.

Clifton & Boruff (2010) assessed the potential of Solar PV energy in the Wheatbelt area of Western Australia. This model was prepared considering DSM data with a resolution of 0.5-metre square, including topography, solar radiation, and land usage, in conjunction with the geospatial software ArcGIS. The two Bureau of Meteorology stations that are geographically near to the Wheatbelt region were used to collect the monthly average direct normal irradiance (DNI) data (Clifton & Boruff 2010). The ArcGIS solar radiation model was then used to derive solar radiation data. In this particular investigation, the aspects and PV elements were not taken into account when assessing concentrated solar power (CSP).

Using machine learning techniques, Mahmud et al. (2021) evaluated the amount of solar electricity generated in the city of Alice Springs, Northern Territory, Australia. Solar irradiance from the nearest weather station, as well as short-and long-term forecasts of PV power generation, were included in the data set (Mahmud et al. 2021). The investigation of roof tilt and orientation, as well as shading, were not included in this study.

Nettesheim et al. (2015) studied soil and litter variation patterns in a tropical region (Marambaia is in Rio de Janeiro, Brazil) with opposing slopes that intercept different amounts of solar radiation at different times of the year. Based on study goals and terrain, two sampling sites were chosen. Each site's element concentrations were determined by analyzing soil and litter samples. DEM was used to create geospatial models for each sample site. These findings suggest that topography influences soil and litter variation in mountainous tropical landscapes (Nettesheim et al. 2015). The geographic orientation of slopes determines soil and litter variation patterns in regions with varying topography (Nettesheim et al. 2015). However, the project did not consider solar PV potential and the variability of seasons in solar radiation calculation.

Fu & Rich (2002) proposed a geometric model for solar radiation to determine its applications in forestry and agriculture. They conducted the study at the Rocky Mountain Biological Laboratory in Colorado. They have selected a topographic area with significant differences, covering an area of 300 square kilometres. Their study recorded temperature for each hour and an insolation-modified adiabatic model for temperature measurement was used to create temperature maps for the selected topographical surfaces. They have created insolation maps to determine topographical influences such as the impact of elevations, sky obstructions, and surface orientation. Second, they have constructed temperature maps to identify the minimum temperature at the locations. Later, correlation analysis was used to measure the temperature of soil with insolation and elevation. They conducted the study for a month and used the 30-m DEM method. Their study revealed that topographical features have a significant contribution to solar radiation at a location.

2.2.4 Solar PV assessment for a few dwellings

Rana & Rahman (2020) assessed the solar PV energy of a single-built area in Queensland, Brisbane, Australia. Data on solar electricity used in this study was gathered from a 1.22 MW PV system placed at the University of Queensland buildings in Brisbane, Australia. Over a period of two years, data on solar power generation were gathered and pooled at 1-minute intervals. The methods used for forecasting were Support Vector Regression (SVR) and Neural Network (NN) based machine learning models. Scholars did forecast based on historical time series data and did not consider the seasonality of solar radiation, aspect, and tilt angle.

Alqahtani & Balta-Ozkan (2021) investigated the potential of rooftop solar PV energy generation for meeting residential loads on three dwellings in Neom, Saudi Arabia. The model made use of a Homer Pro simulation model as part of the PV system assessment and load profile design. This model utilized graphic location parameters and economic factors in addition to PV system design in order to determine the maximum battery capacity and panel size in order to maximize electricity production. A fixed tracking system was assumed with an assumption of a tilt angle of 28-degrees and a 0-degree aspect angle. The level of sensitivity of the system was determined by Homer Pro and was based on the availability of resources as well as the cost of the different components (Alqahtani & Balta-Ozkan 2021). The analysis of shadowing and obstructions was made more difficult since the study did not include DSM data. In the same vein, the parameters of solar radiation known as azimuth, slope, and direction were not the primary focus of this investigation.

Jung et al. (2020) proposed a monthly solar PV potential forecasting model for South Korea. Their study has utilized time series datasets for 164 PV sites for over 63 months. It included data such as weather conditions, electrical trading, power plant capacity, and estimated solar radiation. The authors have used historical data to produce a machine-learning-based forecasting model to determine the estimated monthly PV potential for a new power plant. The dataset-trained model is used to acquire temporal patterns for multiple sites, and for that, long short-term memory layers were used to process the monthly data. It was used for topographical and temporal variations in weather and solar irradiation conditions. The digital elevation method is adopted to determine topographical conditions at various sites. However, the method contained time-series data and machine learning dependent models. The estimation was done to complete the data as well as rooftop characteristics like slope and aspect historical data were not considered.

Heo et al. (2021) investigated in their study how the performance of solar power estimation has an impact on topographic and meteorological data obtained from other PV sites. The authors have proposed a solar power estimation model utilizing multi-channel CNN. This model was tested for its capability to collect and use raster map data such as temperature, solar irradiation, wind speed, and perception at various sites. The study emphasized the evaluation of a multi-channel CNN-based prediction model so that the monthly capacity for solar PV can be estimated. Geographical and meteorological characteristics of the solar photovoltaic site are extracted from image data resembling with map. The CNN algorithm

was used to capture spatial data from the image, and it was further used to identify spatial patterns in meteorological and terrain information. The national spatial data infrastructure of Korea is used to obtain spatial data and input datasets for terrain information. Continuous numerical maps are processed to extract data for contour maps and DEM. In this model, the boundary lines of roads, contours, and administrative boundaries are used as major aspects of spatial information for estimation. The study was conducted on a national scale, with estimation used to complete the data and historical data not taken into account for rooftop characteristics like slope and aspect.

2.3 Summary

2.3.1 Methodology assessment

There are four common approaches used in the field to determine whether solar PV energy is acceptable for solar photovoltaic panels. The first type is known as the constant-value method, and it is used to extrapolate the number of usable rooftops based on assumptions about factors like the percentage of flat roofs and sloped roofs, the count of buildings with the optimum rooftop aspect, the area affected by building impediments (i.e., ventilation and heating), and shading (Melius et al. 2013). This method is widely used, especially as a starting point for area calculation. It requires less time and resource input and can be easily applied to large regions compared with other methods (Alqahtani & Balta-Ozkan 2021; Gagnon et al. 2018; Melius et al. 2013). However, the trade-offs are that the uniqueness of individual buildings is not captured, which results in little validation (Melius et al. 2013).

The second kind is manual selection methods. Google Earth and other forms of satellite or aerial photography are used in the manual selection processes. PVWatts, developed by the National Renewable Energy Laboratory, manually determines the allowable area of the rooftop, yielding more accurate results than constant-value approaches (Margolis et al. 2017; Melius et al. 2013; Odeh & Nguyen 2021). The investigation examined each building in the vicinity. As a result, this approach requires a lot of work, and it might not be suitable for doing an exhaustive examination of a region and is not considered a scalable methodology.

The third kind is a machine learning based forecasting model which requires time-series historical data of solar energy production, i.e., solar radiation data, slope data, and aspect data (Isaksson & Karpe Conde 2018; Mahmud et al. 2021). However, the trade-off is that shading analysis for any kind of topographical structure is not included in this model.

The fourth kind is geospatial-based methods. For geospatial-based methods, instead of using fixed values or selecting structures manually, the suitability is determined by geospatial software after each characteristic value of what makes a suitable rooftop is fed to a computer model (Boulahia et al. 2021; Jo & Otanicar 2011; Melius et al. 2013; Teofilo et al. 2021). Moreover, the 3-D model generated from orthophotography, or LiDAR data, is the primary tool for analyzing the effect of solar resources and shadow (Boulahia et al. 2021; Jo & Otanicar 2011; Melius et al. 2013; Suomalainen et al. 2017; Teofilo et al. 2021). Geospatial-based methods are exceptionally efficient when calculating total solar energy generation potential because they consider slope, orientation, building structure data, and obstructions; produce versatile outputs like creating maps for slope, aspect, and solar radiation for any given period; and automatically calculate skyview factors and viewshed (Ghosh & Vale 2006; Melius et al. 2013; Suomalainen et al. 2017).

When compared to constant-value, hand-selected methods, and machine-learning based methods, a geospatial-based procedure yields more accurate results. This procedure can be applied to larger spaces than the manual selection method (Margolis et al. 2017). Given the advantages of objectivity, high accuracy, and high resolution of the LiDAR data due to technological development, geospatial-based methods have become the most popular method to estimate rooftop suitability for PV (Melius et al. 2013). The constant-value method is excluded because using it in a complex-built environment would cause significant inaccuracy. The manual selection method could be applied to the study site due to its small scale and high accuracy, but it does not provide a systematic and efficient method that could be used elsewhere. As a result, the geospatial-based method is the best to find a balance between accuracy and efficiency. Moreover, this method gives both 2D and 3D views of the study site, which makes the demonstration of the building more accessible. Thus, this research methodology will mainly focus on the utilization of the geospatial method.

2.3.2 Data availability and extent of the study area

Further, the assessment of the solar PV potential in various studies is subjected to data availability and differences in spatial area. The evaluation depends on the scale of the study and various methods have been suggested, combining satellite images, LiDAR data, DSM model, building footprints, quantification of the available rooftop areas, and PV sizing. Estimates at the country scale involve extensive computation, data collection from many sources, and data aggregation due to the sheer vastness of the territory and the ensuing data volumes (Buffat et al. 2018). While comparing previous studies conducted for solar PV energy

estimation, these were centred either on major cities in the USA (Gagnon et al. 2018), Saudi Arabia (Alqahtani & Balta-Ozkan 2021), and Switzerland (Buffat et al. 2018) or the country scale because a larger part of these territories is covered by major cities where data availability is not a constraint and also there is an absence of natural landforms which obstruct the direct sunlight on dwelling rooftops, while comparing to regional areas. Therefore, not much attention has been given to the evaluation of solar PV energy estimation for regional areas. However, Australia has a significant regional population and just five of its large cities have a population of over one million, as shown in Figure 1a. These are Sydney, Melbourne, Brisbane, Adelaide, and Perth (Glenn 2022), while the Inner Regional area (Baxter 2011) is home to 20% of the Australian population (Figure 1b).

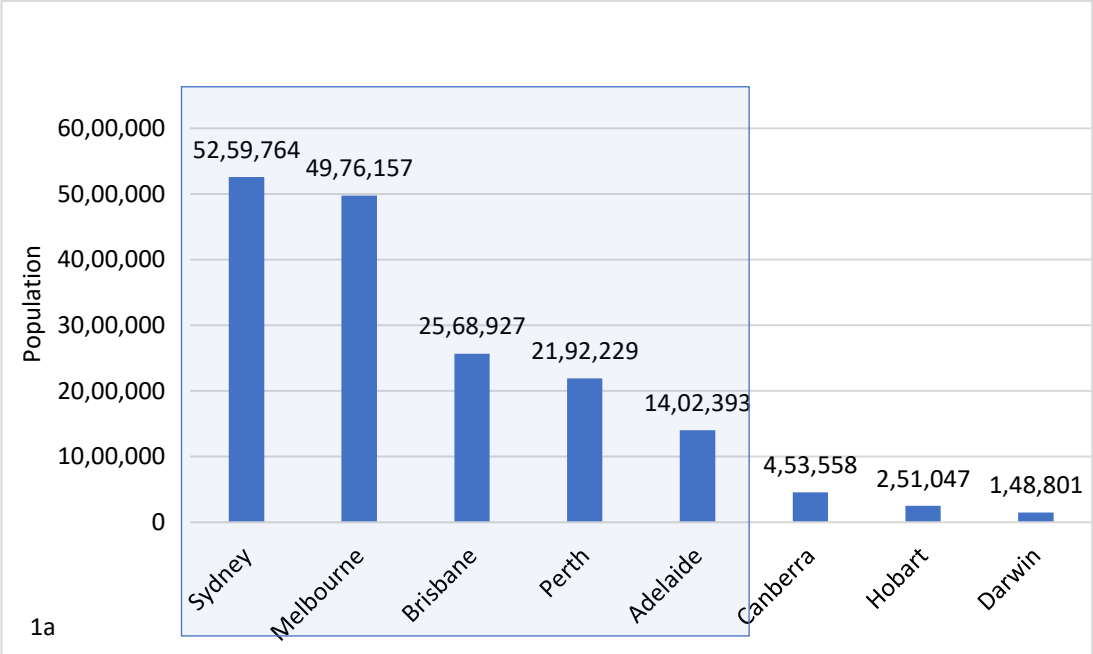

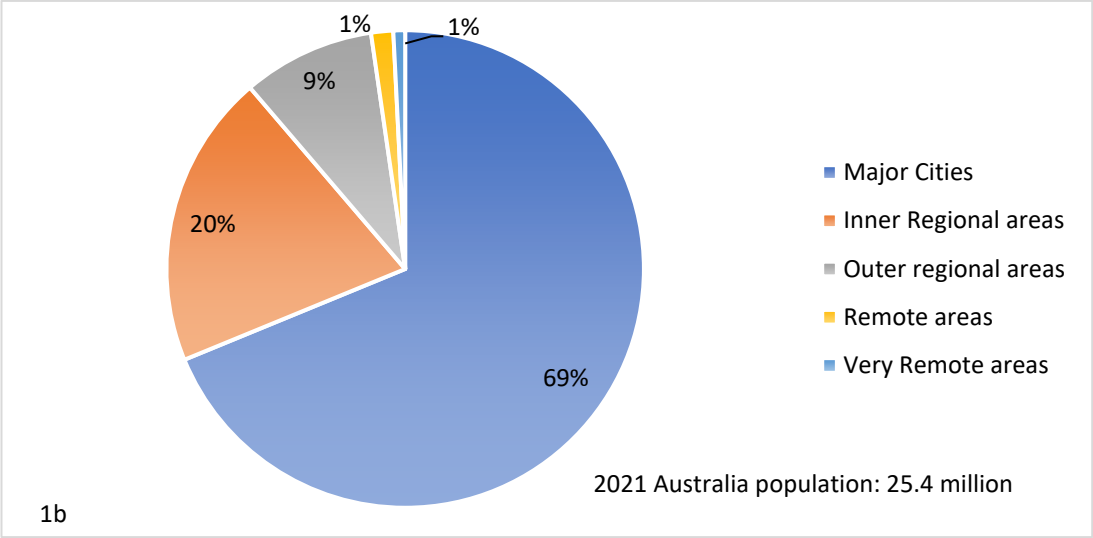

Figure 1a: The Population of more than 1 million in five major cities in Australia on 30 June 2021, indicated in the light blue box (ABS, 2021c); Figure 1b: Population distribution in Australia by major cities, inner regional areas, outer regional areas, and remote areas (Baxter 2011) and total population of Australia in 2021 is 25.4 million (ABS 2022).

For inner regional areas like Wollongong, no research has been done to forecast the use of solar PV electricity. Recently, cross-border migration and its effects on host nations have received a great deal of attention on a worldwide scale. But it is increasingly evident that local community groundswell in regional areas is much more prevalent than international migration. Some of the factors that cause them to relocate include politics, society, and the

environment. This extensive migration increases resource consumption and affects the climate over time (Meyerson et al. 2007). Two essential actions that can reduce climate migration are reducing greenhouse gas emissions and considering climate migration when planning future development. A concerted action is required to mitigate climate migration caused by population growth in regional areas, and this research will aid in estimating solar PV energy and will help the decision makers in considering an integrated approach to understanding the solar energy potential at the local scale. Therefore, Australia's regional areas are physically favourable and can significantly contribute to the country's overall PV estimations and as a case study being conducted in the areas of Wollongong.

As per Wollongong city 2030's sustainable planning, the Wollongong council is visioning a climate-resilient and sustainable city. Wollongong City Council needs long-term solutions to climate change and environmental degradation. 78 percent of 2018/19's emissions came from energy use (Wollongong City Council 2020). To achieve this sustainable planning mission, it is imperative to use a scalable solar PV energy modeling technique for this area in order to bridge the gap in energy supply and demand (Wollongong City Council 2020). While considering decision making for strategic changes on a large scale, it is good to have a bottom-up approach and be driven by local strategic changes. Strategic planning and policy making at the municipal and local governments/suburb levels help make decisions at the state and country level. Hence, municipalities and local governments can facilitate any innovative strategy effectively (Dwyer 2018) and one of the objectives of this study is to analyze solar PV potential at the suburban scale, which can help LGA to gauge the gap in current energy usage and the potential.

2.3.3 Research limitations

In the current literature, there is a dearth of studies that implemented automation while calculating skyview factors and viewsheds, including variation at one-hour intervals, and accurate seasonal shading analysis including topographic features, and there is still potential for advancement in determining the variation in area suitability factors in different seasons for all building footprints. Some studies did not include the elevation data needed to analyse the impacts of impediments and topographic features (Alqahtani & Balta-Ozkan 2021; Boulahia et al. 2021; Odeh & Nguyen 2021). Some studies have used software not deployed to Wollongong; these are Google Project Sunroof, Swisstopo, SwissTLM and SunSPoT (Buffat et al. 2018; Gagnon et al. 2018; Odeh & Nguyen 2021). Some of the earlier studies made use

of manual procedures like the visual assessment of buildings for load and obstructions, which are known for their high level of accuracy but are very time-consuming. Other studies, on the other hand, made use of ratios of rooftop area based on assessing a smaller area and extrapolating the results on a national norms or assumptions basis. Very few studies have included topographical features for solar radiation modeling, but the objectives of some of those were finding soil properties (Nettesheim et al. 2015; Fu & Rich 2002), finding solar PV potential using machine learning methods emphasizing more on temporal patterns to find topographical feature effects (Jung et al., 2020), and finding potential sites for the installation of a solar PV installation (Jung et al. 2019). None of the studies included seasonal outcomes of solar radiation modeling, which is affected by landforms/topographical features and leads to the calculation of suitable rooftop areas for each dwelling and results in potential solar PV electricity for the area of interest. Along with solar power density, rooftop area, and alignment of the solar PV panels, there is a significant impact of seasonality and topographical obstructions on solar radiation distribution and determining the suitable rooftop area for PV installation. The shadow cast by escarpment and its variability during the seasons can reduce the conversion of solar energy to electricity through solar PV panels. This thesis focuses on the estimation of the solar PV energy potential of two suburbs, namely, Wombarra and Cringila, which are located in Wollongong, NSW, Australia. These two suburbs are chosen to demonstrate the comparative analysis of shading effects (how solar insolation varies in different seasons) due to topographical features (escarpment). Both suburbs have similar climatic conditions, rainy days, and dwelling structures (Australian Bureau of Statistics (ABS) 2021a; ABS 2021d; World Weather Online 2022). On the other hand, Wombarra is right beside the escarpment, and Cringila has no effect of shading due to the escarpment. As a result, even if the climatic conditions are identical, the solar PV energy output will differ due to the shadow cast by the escarpment.

An examination of a variety of methodologies revealed that geospatial-based methods provide several benefits, the most notable of which are scalability, efficiency, and accuracy (Julieta et al. 2022). In addition, LiDAR data, DSM model, and building footprints are widely utilized in conjunction with the widely used robust geospatial software ArcGIS when calculating the power produced by solar PV systems. This paper makes a two-fold contribution for the reasons stated above: first, it presents a scalable approach for estimating solar PV potential and power generation on building rooftops across two suburbs by using LiDAR data, building footprints, and geospatial software. Second, this method compares the

result of the PV potential of these two suburbs in different seasons, which is affected by the shadow of an escarpment, vegetation, and other buildings. This study simulates the solar PV potential in Australia at a suburban scale, including geographical features in shading analysis in consideration of seasons, which has not yet been covered in previous studies.

Appendix A contains a tabular listing of the literature discussed in “section 2.2: Extent of study area”. It is a comparison of studies and their methodologies, including the factors considered. Additionally, it examines whether or not any validation is being done.

3. Regional Setting

3.1 Landscape and climate setting

The study was conducted on two suburbs located in the inner regional area of Wollongong, NSW, Australia, at a distance of approximately 80 Km south of Sydney. Wollongong is located on New South Wales' south coast, between the Illawarra escarpment and the Tasman Sea (Figures 2a and 2b). The average annual maximum and minimum temperatures for the city are 21°c and 15°c, respectively (World Weather Online 2022). There are four distinct seasons in the city: summer (December-January), autumn (March-May), winter (June-August), and spring (September-November) (World Weather Online 2022). The city has a mild winter and warm summer climate. January is the warmest month, and July is the coolest, with maximum temperatures of 26°C and 16°C, respectively (World Weather Online 2022). Its unique environment includes escarpment and lush rainforests. It is one of New South Wales's largest cities, with an area of approximately 683.8 square kilometres (Informed Decisions 2021), and a city council population forecast for 2022 is 223,684 (Wollongong City Council 2020). As per the Informed Decisions (2022), the population of Wollongong will increase by 24.62% from the year 2022 to 2041, which is an average annual growth of 1.13%. Hence, this local community groundswell will lead to the utilization of more resources, specifically non-renewable resources, and consequently will result in climate change degradation. As per the Wollongong City Council (2020), climate change adaptation is required in the city. The statistics of 2018/19 show that emissions from energy consumption were 78%, population of Wollongong will increase by 20% in 2036 and hence emissions as well (Wollongong City Council 2020). The vision is to adopt net zero emissions by 2030. The City Council is working with the community to reduce the city's emissions and increase renewable energy usage (Wollongong City Council 2020). One of the positive actions is installing solar panels and improving home energy efficiency.

Figure 2a: Location of Wollongong City in NSW, Australia indicated by dark blue dot; Figure 2b: Wollongong City map with city and suburb boundaries in dark blue.

Wollongong is home to a population of around 214,657 people of many different cultural backgrounds, and it is surrounded by and defined by the escarpment (Figure 3) (Macquarie 2013). The Illawarra Escarpment is a sandstone cliff that has a long steep slope, where elevation changes suddenly, as well as it is covered with dense vegetation (Macquarie 2013). This 200–400 metre vertical ascent is a wall of sandstone cliffs and slopes covered by forest. Around 120 kilometres long, the Illawarra Escarpment is covered in plant slopes that descend from cliffs (Macquarie 2013). Throughout the year, the average amount of daily DNI that Wollongong receives is 4.5 kWh/m^2, as reported by the Bureau of Meteorology (BOM) (2019) (higher in summer and lower in winter). That's to conclude, for every 1 kilowatt-hour produced by solar panels, using the conservative estimate that the solar array's efficiency is around 85%, the generated electricity is about 3.9 kWh of power (Sykes 2022).

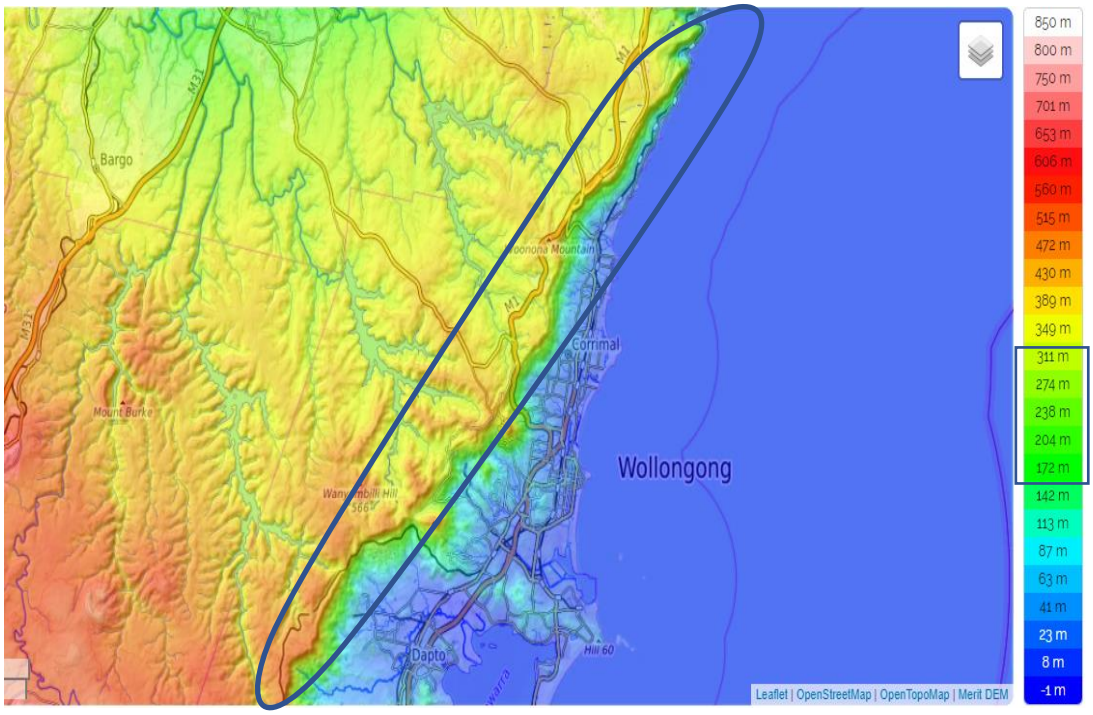

Figure 3: The Illawarra Escarpment elevation range from 172 metres to 311 metres is indicated in green inside the oval on the west side of Wollongong city (OpenStreetMap 2022).

3.2 Study Area

The chosen suburbs for study in Wollongong are Wombarra and Cringila. These have been selected to compare the impact of shading as an effect of geographical characteristics on solar PV energy potential in different seasons. Both suburbs are in Wollongong, New South Wales, Australia; Wombarra is a seaside suburb located on the north side of Wollongong, and Cringila is located on the south side (Figures 4a, 4b, and 4c). , They are 66 and 89 kilometres, respectively, from Sydney via the Princes Highway.

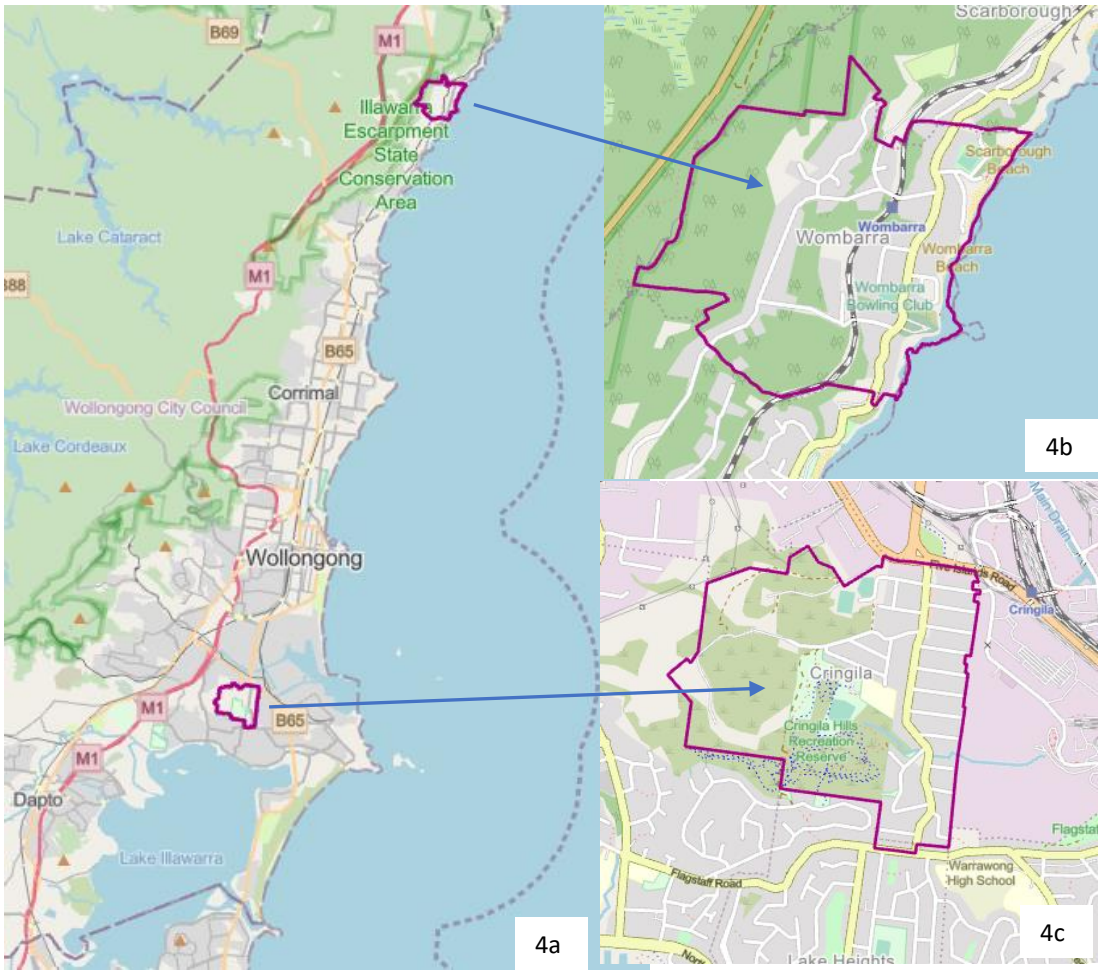

Figure 4a: Location of Wombarra and Cringila suburbs' red colour boundaries in Wollongong city; Figure 4b: Wombarra Suburb boundaries in red; Figure 4c: Cringila suburb boundaries in red.

In terms of sunshine hours per day, suburbs that are located adjacent to the escarpment experience fewer sunshine hours than other suburbs, and it varies in different seasons. In the Wombarra suburb, the escarpment is on the west side and adjacent to the dwellings, which is around 350 m tall and casts a shadow on the dwelling rooftops, and it varies across the seasons (Macquarie 2013). The Illawarra escarpment cast a shadow on the rooftops of dwellings close by, however Wollongong's southern suburbs are not exposed to the escarpment. As per the 2021 census data (ABS 2021a; ABS 2021d), among them, in Wombarra, 96% of the dwelling structures are separate houses, which is closely matched with Cringila (93.5%) (Table 1). While comparing the two locations, the comparison of the annual mean of PV energy per dwelling is appropriate when most of the dwellings are similar in structure. Therefore, in order to examine which suburb has higher solar PV energy

potential per dwelling in all seasons, Cringila, a southern suburb without escarpment shade, can be compared to Wombarra, which is adjacent to the escarpment.

Table 1: The number of dwelling structures in Wombarra and the southern suburbs of Wollongong, their percentage of total dwellings, and the light yellow colour indicate that Cringila has most of the dwelling structures similar to Wombarra (ABS 2021a; ABS 2021d).

Dwelling structure	**Separate house**	**Semi-detached, row or terrace house, townhouse, etc**	**Flat or apartment**	**Another dwelling**
Wombarra	321	0	13	0
%Wombarra	96.4	0	3.9	0
Mount Saint Thomas	507	36	7	0
%Mount Saint Thomas	92.3	6.6	1.3	0
Primbee	524	68	51	0
%Primbee	81.6	10.6	7.9	0
Cringila	664	3	39	3
%Cringila	93.5	0.4	5.5	0.4
Coniston	451	159	273	4
%Coniston	50.9	17.9	30.8	0.5
Mangerton	748	122	168	6
%Mangerton	71.7	11.7	16.1	0.6
Windang	946	113	42	75
%Windang	80.2	9.6	3.6	6.4
Lake Heights	1,236	88	168	3
%Lake Heights	82.5	5.9	11.2	0.2
Warrawong	1,167	256	355	3
%Warrawong	65.2	14.3	19.8	0.2
Port Kembla	1,540	133	316	10
%Port Kembla	76.7	6.6	15.7	0.5
Wollongong	1,318	702	7,365	108
%Wollongong	13.8	7.4	77.3	1.1

The climates in both suburbs are similar. In the summer, both have average maximum and minimum temperatures of 25°C and 18°C, respectively (World Weather Online 2022). In autumn, the average maximum and minimum temperatures are 22°C and 16°C, respectively (World Weather Online 2022). In the winter, the average maximum and minimum temperatures are 16°C and 10°C, respectively (World Weather Online 2022). In the spring, the average maximum and minimum temperatures are 21°C and 14°C, respectively (World Weather Online 2022). Similarly, the average number of rainy days in these suburbs in summer, autumn, winter, and spring is 17, 12, 10, and 14, respectively (World Weather

Online 2022). Both the suburbs have direct normal irradiance (DNI) of around 4.0-5.0 kWh/m^2/day (BOM 2019). Even though the climate is same, the solar PV energy output will differ because the escarpment casts a shadow on one of the suburbs' rooftops.

Commonly, there are four seasons in Australia (summer, autumn, winter, and spring) (Chiew et al. 2009), and solar radiation that falls on dwelling roofs is obstructed by escarpment and other impediments vary across the seasons as the solar angle changes daily and seasonally during a year. Hence, the average solar radiation reaching rooftops varies according to the season of the year. During winter, the average annual solar radiation of the area of interest can be as low as 2.4 kWh/m^2/day, while in summer this value can be higher at around 6.3 kWh/m^2/day (BOM, 2022). Figure 5 shows DNI in Australia, and indicated area shows DNI in Wombarra, and Cringila, which is around 15 to 18 megajoules/m^2/day and in kWh it is around 4.0 - 5 kWh/m^2/day (BOM 2019). As a result, there is a massive potential for generating electricity through solar PV in the Wombarra and Cringila suburbs.

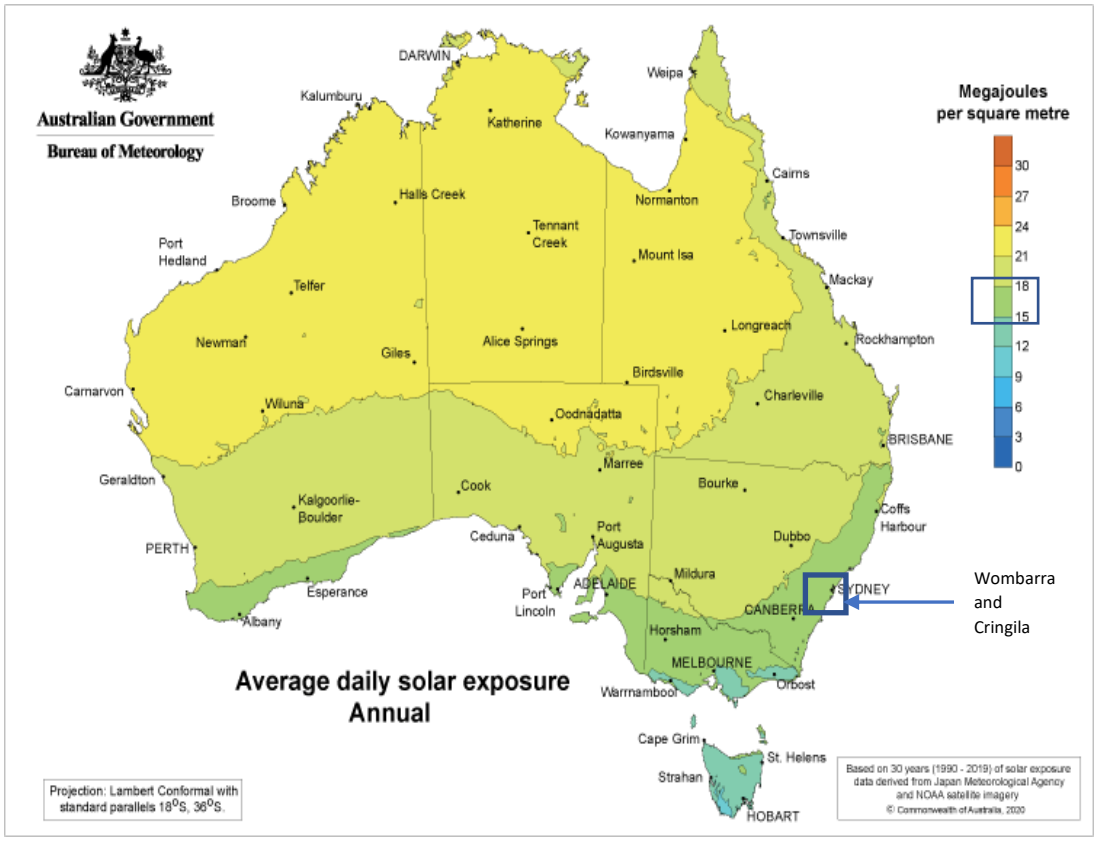

Figure 5: Australia's DNI is highest in red (>30 MJ/m^2/day) and lowest in blue (<3 MJ/m^2/day). Wombarra and Cringila are located in the blue square indicated area by arrow and are close to Sydney, NSW; indicated area is green and has a DNI range of 15–18 MJ/m^2/day (4.0–5 kWh/m^2/day) as shown in the legend (BOM 2019).

4. Research Methodology

The research strategy and methods used in this study are described in this section. This approach was chosen to fill gaps in the existing literature (described in Section 2) and to achieve the stated goal of estimating solar PV energy and comparing shading effects based on topographical obstruction by using a geospatial method and accounting for seasons. The model for estimating solar PV energy was created using a geospatial-based methodology for Wombarra and Cringila suburbs. The amount of solar radiation that reaches the surface of the earth fluctuates by season and even during a day. Furthermore, the shadow cast by the landform (escarpment) changes during the seasons and fluctuates solar radiation amount, having a substantial impact on the amount of power produced by solar energy (Benson et al. 1984). As per Chapter 3, these suburbs are in the same city, have similar solar radiation, and have similar kinds of dwelling structures, a comparative analysis was done to demonstrate the difference in the electricity produced in different seasons due to the effect of escarpment shading.

Active remote sensing is widely used in attempts to locate rooftop assets and infrastructural features that may limit the rooftop's overall applicability (Florio et al. 2021). High-resolution maps of entire cities are possible with the help of active remote sensing techniques and aerial or satellite platforms (Taminiau & Byrne 2020). LiDAR data, which uses active remote sensing to construct a 3D point cloud of observations, is frequently utilized since it can create a 3D model with high-resolution and comprehend the profile of the chosen area. When calculating solar PV potential, high-suitability rooftop areas were identified using DSM data and solar radiation modeling. After that, ideal values for rooftop attributes (slope and aspect) were entered into a computer model. As a result, it was easier to quickly and accurately determine which rooftops are suitable for PV installation.

Figure 6 depicts the flow of the methodology. The flow is divided into two basic stages: the solar radiation estimation phase and the electric potential computation phase. The initial stage involved gathering and processing data, which included downloading building footprints, Wombarra and Cringila suburb boundaries, and LiDAR data. Then, the DSM raster was processed and combined with the vector (suburb boundaries and building footprints) data. Following that, hillshade analysis and solar radiation modeling were performed on the combined data. The next stage was to create aspect and slope rasters, which were then combined with solar radiation data to estimate electricity potential. Finally, CO_2 reduction

was calculated based on the estimated electricity potential. Figure 6 shows green colour blocks representing raster data, orange colour blocks representing vector data, and blue colour texts representing geospatial software built-in toolkits.

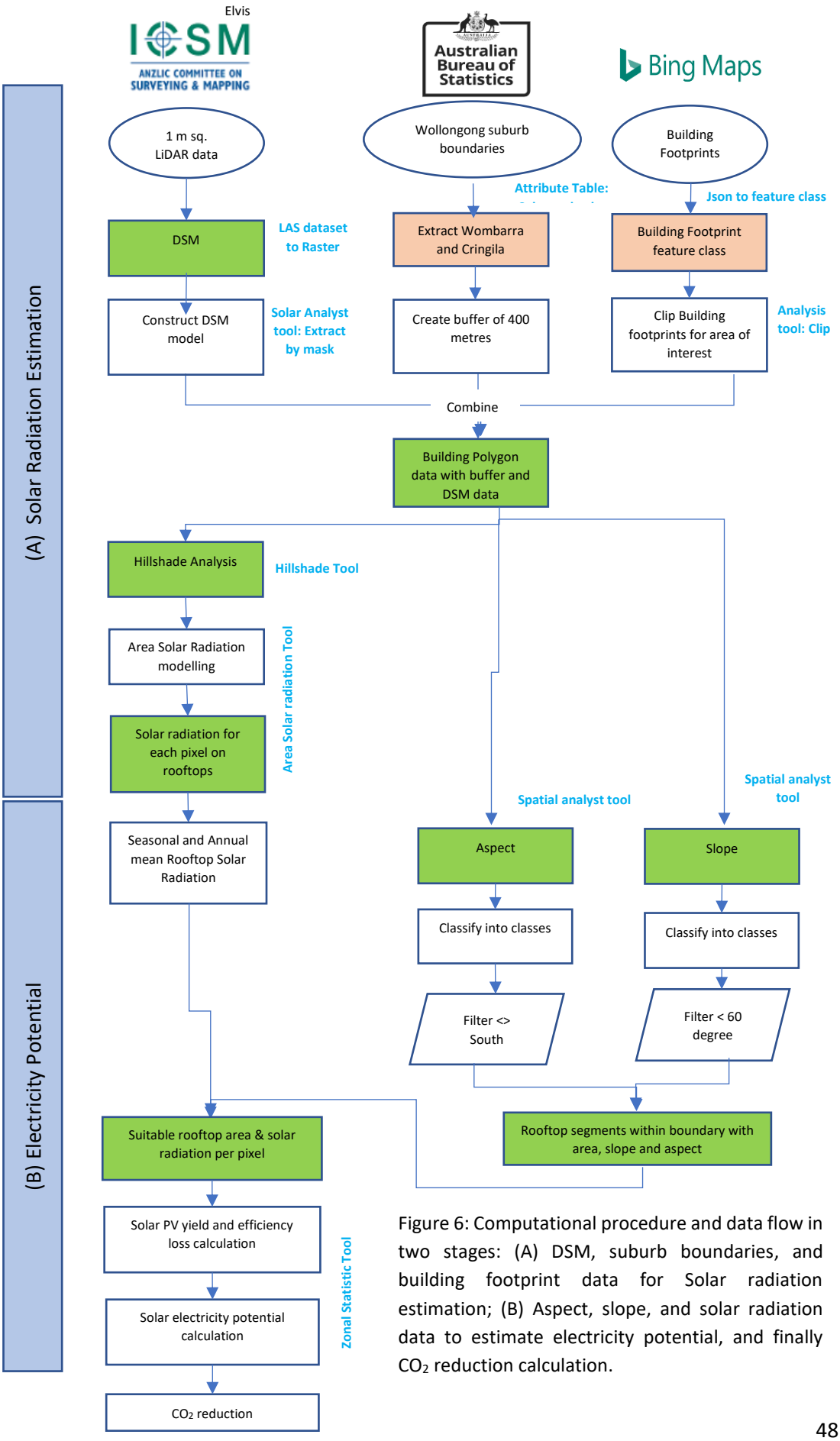

Figure 6: Computational procedure and data flow in two stages: (A) DSM, suburb boundaries, and building footprint data for Solar radiation estimation; (B) Aspect, slope, and solar radiation data to estimate electricity potential, and finally CO_2 reduction calculation.

4.1 Solar radiation model validation

Each season's average solar irradiance data must be validated to ensure accuracy. This is due to the fact that the findings of seasonal solar irradiance for the area of interest during each season are essential input parameters for calculating the solar PV energy potential. The solar irradiance data obtained from the model before applying the filters for rooftop slope, aspect, and minimum area conditions was validated with the dataset from the Wollongong city weather stations by using the Mean Absolute Percentage Error (MAPE) method. This method compared the model data and the stations' data and then provided the error percentage of the output.

Another statistical test was performed to test the difference in solar radiation in both suburbs due to the topographical obstruction. The t-Test unpaired two samples for means was conducted for Welch's t-Test to determine whether null hypothesis can be discarded or not. To perform the t-Test, a sample population of 40 buildings from Cringila and 40 buildings from Wombarra has been taken. In this study, the null hypothesis was that the average annual solar radiation per m^2 obtained from the geospatial model has the sample population mean of Cringila equivalent to Wombarra. The alternate hypothesis indicates that means are significantly different due to topographical differences, and it rejects the null hypothesis, it also implies that the outcomes are quite accurate. If p-value is lower than 0.05, the alternative hypothesis is supported.

4.2 Solar Radiation Estimation

Inputs required for area solar radiation modeling were suburb boundaries, LiDAR data, and building footprints**.**

4.2.1 Suburb Boundaries

Suburb boundaries were required to analyze the rooftops of buildings within the scope of this study. Wollongong suburb boundaries were acquired from the Australian Bureau of Statistics (ABS) (2021b) in the shapefile format. It was important to extract suburb boundaries because it would limit the area of analysis within these boundaries and would reduce the computation time. The suburb boundaries shapefile was imported as vector data and an attribute table was used to select Wombarra and Cringila suburbs. Keeping in mind that any landform, building, or vegetation outside the boundaries that were casting shadows on the dwellings inside the boundaries must be included in the analysis. To achieve that, a

visual inspection of the vector data was done to include escarpment in the analysis by creating a buffer to extend the area of interest.

4.2.2 LiDAR data

The LiDAR data was collected with a resolution of 1 square metre via a cloud-based technology called Elvis Elevation and Depth (Geoscience Australia 2022b). According to the National Oceanic and Atmospheric Administration (NOAA) (2021), the underlying idea of LiDAR data is a remote sensing technique that employs laser beam at regular intervals to detect ranges (different distances) from the Earth. It provides precise information about the earth's surface. Specifically, a sensor would emit laser beams toward a target during the flight, and the laser would be reflected by the target and received by the sensor, as shown in Figure 7 (ESRI 2019). The sensor precisely records the time of transmission and reflection to calculate the distance between the target and the sensor. Post-processed spatially organized LiDAR data is point cloud data (NOAA 2021). With ArcGIS Pro's conversion tool LAS Dataset to Raster, the LAS dataset (LiDAR point cloud data) was transformed into a raster for use in making the 0.5 square metres DSM. To generate the DSM, the method of triangulation interpolation was performed, which assigned the maximum point value to each cell in the output raster, which represents the top surface of the terrain (Rogers et al. 2020). To simulate Hillshade analysis and solar radiation modeling, a digital surface model (DSM) model was required. A DSM model consists of surface features, which include all objects above ground level, such as flora, buildings, and landforms. In DSM, elevation is presented like a grid, and a value for elevation is assigned to each cell of the grid.

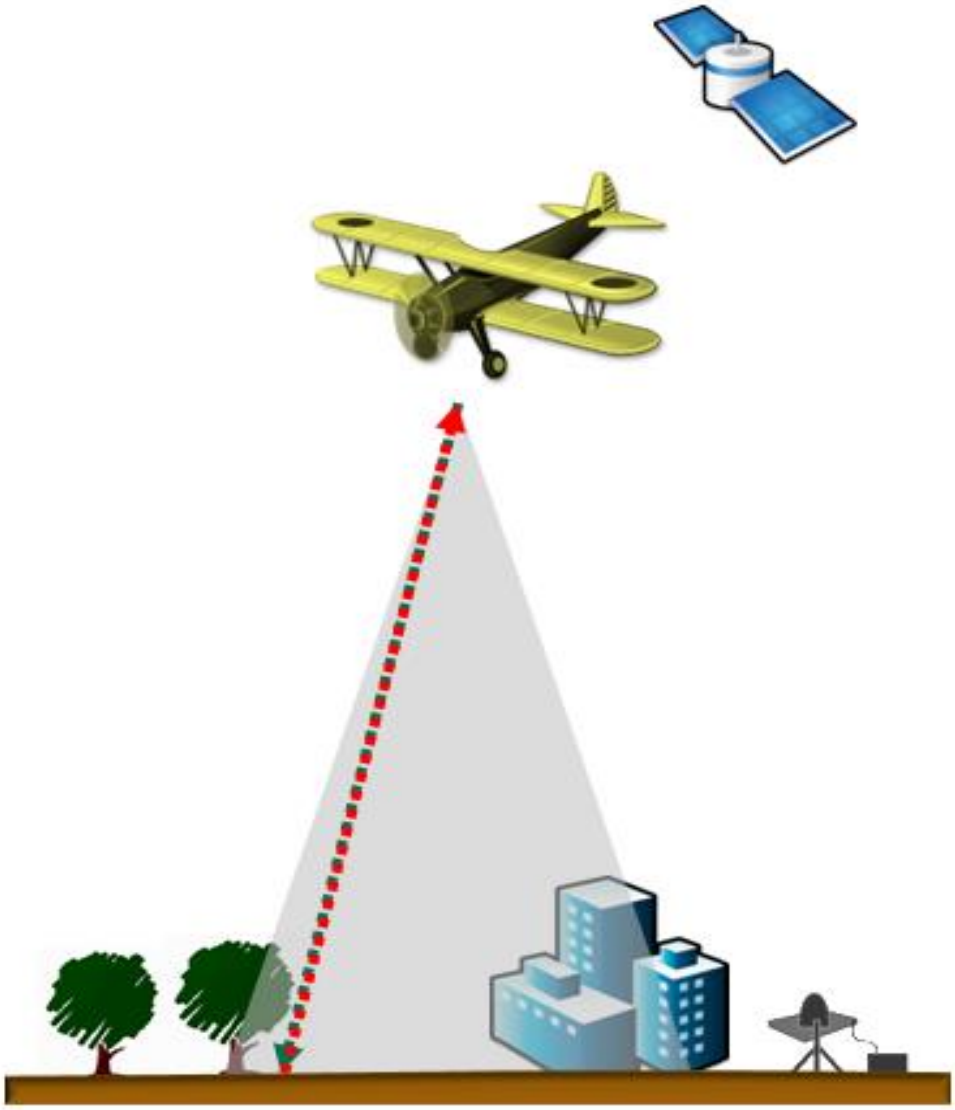

Figure 7: Basic Principle of LiDAR data collection (ESRI 2019).

4.2.3 Building footprints

A building footprint vector data displays the outline of a facility traced along its external surfaces, along with a description of its actual dimensions, frame, and location. In terms of spatial characteristics, distribution, and correlation with other buildings and other objects, it depicts a building's total area and gives a more accurate representation of its spatial properties than a point representation. To determine the rooftop points, building footprints were used as vector data (Zhang et al. 2006), and this provided building counts and rooftop areas for each building. Building footprints were acquired from Microsoft (2020), and Microsoft used Bing satellite imagery to create the roof outline. The satellite imagery for this extraction process was provided by Maxar (2020). Using a semantic segmentation and polygonization technique, the collection includes 11,334,866 building footprints. Microsoft

used self-supervised training and unsupervised domain adaptation to create a validated product for building footprints in Australia Microsoft (2020).

The vector data utilized for building footprints included all rooftops in both suburbs. Furthermore, all portions of these rooftops are included in vector polygons of each building. The building footprint data was imported into the geospatial tool and clipped for the area of interest. Visual verification of maps in the tool is being performed to verify that all rooftops are covered. These polygons include spatial information that is used to calculate the overall rooftop area. Given that the total rooftop area of the suburbs under consideration may vary, comparisons will be made using annual average values expressed in kWh/m2/day per building.

4.2.4 Hillshade analysis and Area solar radiation modeling

Following the collection of building footprints, suburb boundaries, and the DSM model, these data points were intersected to conduct additional analysis on the area of interest.

Since shade can drastically cut down on a "system's" power generation, it is crucial to analyze the effects of shading while calculating PV potential. A Hillshade function was applied to DSM, which results in a 3D grayscale representation of the terrain surface that is shaded according to the relative position of the sun (ESRI 2021c). Hillshade analysis differentiates between houses, trees, and other topographical characteristics, as well as roofs. Area solar radiation (ASR) was then used to process the DSM (ESRI 2021b).

Solar irradiation on a rooftop is affected by a number of spatial and temporal factors, such as the sun's position and the presence or absence of obstacles in the path of direct sunlight. Irradiation on rooftops is directly proportional to the sun’s irradiation potential. While solar irradiation potential is not technology dependent, the PV system's ability to convert that potential into usable power is. The technical purpose of this phase was to estimate the solar radiation for each pixel on the rooftops of the buildings using the Area Solar Radiation tool in ArcGIS Pro (Ghosh & Vale 2006). This identified the rooftops with the feasibility of producing solar energy in the right position and one can find the best spot for PV panels to install in order to maximize energy output. The length and direction of shadows cast by structures change throughout the day and with the seasons, making it challenging to do shading analysis for each day of the year. Despite this, a monthly and annual average irradiation loss estimate is possible by performing shading analysis using the geospatial tool (ESRI 2021a).

The parameters that are given in the ASR model were:

- Latitude: The default value of the area of interest was mentioned.
- Time configuration: Multiple Days, so that the desired start and end day for the analysis can be defined; in this study, the multiple days parameter was chosen to include all of the seasons in a year.
- Year: It is restricted to input one year at a time. To achieve the aim of the study, that is, seasonality analysis, the most recent full year (2021) was mentioned so that all the seasons could be captured. Landforms that were included in the study area by creating a buffer would cast shadows differently in different seasons, and thus they would affect the electricity and solar radiation output. Subsequently, a comparison of these outputs was done to showcase the shading effect of the landform.
- Start Day and End Day: Input was given for the four seasons separately (autumn: March to May; winter: June to August; spring: September to November; summer: December to January).
- Day and Hour Interval: In this case, solar insolation at each season was required, and it should be differentiating between different times of the day. As sun tracks within three days usually overlap, depending on the size of the sky and the season, day intervals greater than three are advised (ESRI 2021b). Because of this, a default value of day interval of 14 days and hour interval of 1 are capable of showing the variation in solar radiation in a season (Falklev 2017). For every season of the year, the insolation was estimated at hourly intervals, and the computation can take hours or days to complete.
- Topographic Parameter: The foundation for the creation of the ArcGIS Pro Spatial Analyst Tool (SAT) is related to viewshed and the estimation of direct and diffuse solar radiation (Fu & Rich 1999). Viewshed calculations for the selected location can be made using the ASR modeling in the SAT tool. The term "viewshed" refers to a map that shows how the topography in the area blocks the view of the visible sky with respect to the aspect, and the DSM model is the basis for viewshed calculation (Fu & Rich 1999). For a specific set of directions (azimuth divisions), the viewshed algorithm requires calculating the irradiation horizon angles, which are then interpolated as a hemispherical view of the sky. Valid values for azimuth divisions are in multiples of 8, and an increased number of azimuth divisions is a concern when output is required at hour or day level and for a complex topography (ESRI 2021b),

but in this case, output was at seasonal and annual scale as well as the complexity of the topography was low (Figure 8). The study area is not complex, as it has an escarpment on one side of Wombarra, and the height of the escarpment is constant between 337 m and 364 m. Hence, a fewer number of directions (16) was sufficient for solar radiation output, and it will also minimize the calculation time.

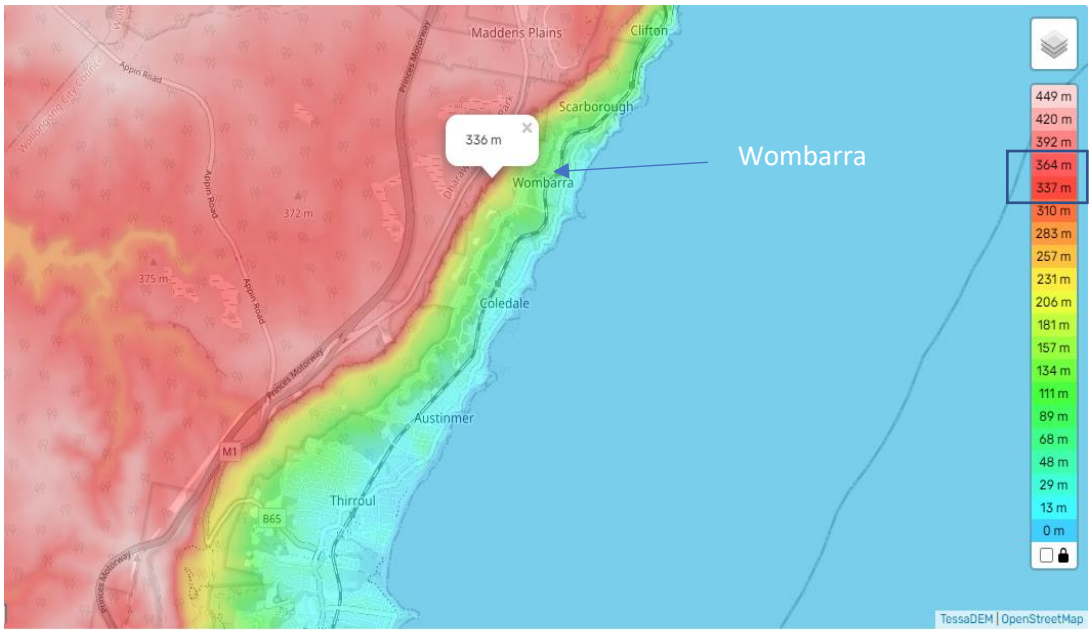

Figure 8: Elevation of the escarpment to the west side of Wombarra (OpenStreetMap 2022).

Model parameters for transmissivity (T) and diffusivity (D) were calibrated from the data by using the Solar Radiation model (Fu 2000). T and D depend on the sky condition, and the spatial analyst tool (SAT) estimates them automatically based on the input days/months/season as a parameter, in this case, 4 seasons were taken as input. ESRI (2021e) explains that the model estimates irradiance levels on a daily, monthly, and annual basis, as well as for a given time range. In this study, calibration was done for two scenarios with a seasonal and yearly temporal resolution of one hour each, to provide more accurate data for future projections. This extensive computation can take a few hours or many days to complete tasks such as geographic data analysis, data conversion, data administration, and map automation (Chow et al. 2014), and to make it efficient, the Arcpy package that is based on the Python scripts is used by ArcGIS Pro (ESRI 2021e). To avoid having to manually run and cycle through all of the possible combinations of D and T values, the ArcPy package has the capability to perform all permutations and combinations to evaluate all atmospheric parameters of the model.

The horizontal solar insolation values are based on pixel with a watt hours per sq. metre (Wh/m^2) unit as this is the default result of the ASR module in ArcGIS Pro. To make these calculations more manageable, the measured solar radiation in pixels was converted to area-based values in kilowatt-hours per sq. metre (kWh/m^2). To do this, the "Zonal Statistics as Table" feature was used, which generates an aggregate statistical representation of all pixel values. New columns were added to the original table to display information like the average solar radiation value in kWh/m^2 for each building polygon feature over a specified time period, the total number of pixels in the feature, and the total area of the rooftop feature in square metres.

Since the ideal slope of a surface for PV systems varies with latitude, these classifications are crucial when determining eligible locations. So essentially, based on the orientation, this stage identified rooftops that would get the most solar radiation throughout the season and span of the year.

4.3 Electricity Potential

4.3.1. Rooftop slope and aspect

The degree to which a surface drops off abruptly is measured in terms of its slope. No slope (flat) corresponds to a value of 0 degrees, whereas a value of 90 degrees represents a perfectly vertical surface. According to ESRI (2021d), the surface slope is determined by averaging the elevation differences between a particular cell and its eight neighbouring cells. After determining the slope using the Spatial Analyst tool, the results were organized using a classification scheme based on how well they would support the installation of a PV system. While many prior studies divide houses into two categories—those with flat roofs (slope of less than 10 or 20 degrees) and those with sloped roofs (slope of greater than 10 or 20 degrees and less than 60 degrees) (Alexander et al. 2009). For this study, as shown in Table 2, reclassification was done for five classes. The minimum value of the first class and maximum value of the last class was defined by default as per the min and max slope values available in the area of interest. Since the ideal slope of a surface for PV systems varies with latitude, these classifications were crucial when determining eligible locations. Within these classes, results do not vary much, and on the basis of these classes, results can be generated to demonstrate the optimum tilt angle. So essentially, based on the orientation, this stage identified rooftops that would get the most solar radiation throughout the season and span of the year.

Table 2: Slope values reclassification.

Slope	**Class**
0.018-10	1
10-20	2
20-40	3
40-60	4
60-87.323	5

The aspect of a slope is its relative orientation, and solar radiation varies on the basis of the aspect. In this case, the area of interest lies in the southern hemisphere. As the sun stays the majority of the year in the northern direction in the sky, north-facing roofs are recommended for the construction of solar PV systems (in the southern hemisphere) (Li & Liu 2017). The aspect of the surface slope at the dwellings is identified by the cardinal and ordinal directions, and these directions must be aligned with the sun's path in order to maximize the energy outcome. The evaluation of each building's aspect and slope served to offer additional rooftop attributes so that the output of the solar radiation analysis could be merged with these parameters. Aspect ranges from 0 to 360 degrees, in a clockwise direction. As shown in Figure 9, the aspect was categorized into 8 categories: (i) (337.5-22.5) north, (ii) (22.5–67.5) northeast, (iii) (67.5–112.5) east, (iv) (112.5–157.5) southeast, (v) (157.5–202.5) south, (vi) (202.5–247.5) southwest, (vi) (247.5–292.5) west, (viii) (292.5-337.5) northwest. A flat roof was assigned an aspect ratio of -1. Aspect values were derived from DSM using the aspect tool in the Spatial Analyst Toolbox.

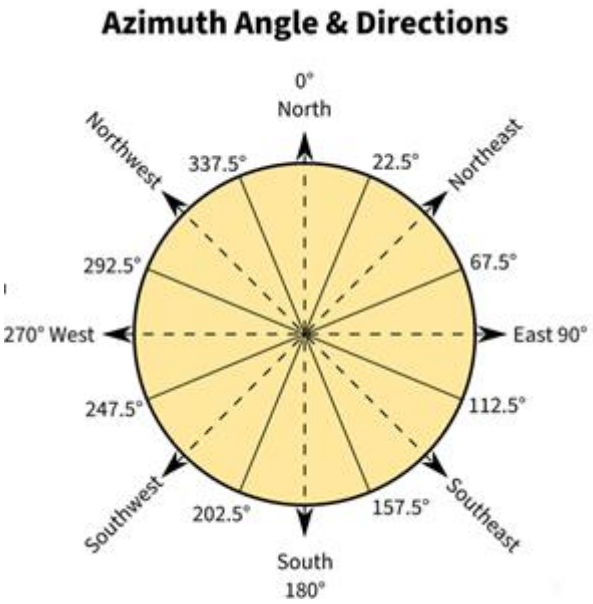

Figure 9: Azimuth angle and direction (SolarSena 2021).

4.3.2 Solar electricity potential calculation

Once the solar radiation layer was generated and slope and aspect were calculated, filtering was done to extract suitable rooftops on the basis of the four factors applied to rooftop slope, rooftop aspect, area of a single dwelling, and a minimum value of solar radiation. Rooftops with a slope of less than 10 degrees were considered flat. Given that higher slopes receive less sunlight, the rooftop slope should be less than or equal to 60 degrees. Above 60-degree slopes were categorized as unsuitable because they had very steep angle values for installation and energy production from solar radiation would be very low, thus not economical (Yesilmaden & Dogru 2019). As per the Bureau of Meteorology's climate data provided by the weather station (068219 Wollongong (Appin) NSW), the mean of monthly solar radiation data calculated for the years (1990 to 2022), mentioned in Table 3, the annual mean solar radiation in Wollongong is 4.4 kWh/m^2/day and the lowest is 2.4 kWh/m^2/day (876 kWh/m^2/year) in the month of June (BOM 2022). Hence, rooftops in Wollongong are getting at least 800 kWh of average solar radiation per square metre annually and the same cut-off is kept for solar radiation while calculating electricity potential. The roof shouldn't have a south-facing aspect because southern hemisphere rooftops absorb less sunshine (Li & Liu 2017). Rooftops with a roof area smaller than 10 square metres are not worth the investment for solar PV installation, as the cost would be higher than the profit made by solar energy production. Hence, the space required for the roof must be greater than 10 square

metres (Bergamasco & Asinari 2011). Thus, an expression where AREA is greater than or equal to 10 was built in the Select by Attributes window.

Table 3: Monthly mean solar radiation in Wollongong (kWh/m^2/day) (BoM 2022).

Statistic	Jan	Feb	Mar	Apr	May	Jun	Jul	Aug	Sep	Oct	Nov	Dec	Annual
Mean	6.1	5.3	4.5	3.7	2.9	2.4	2.7	3.6	4.6	5.4	5.8	6.3	4.4
Lowest	5.3	4.5	3.2	2.7	2.3	1.9	2.2	2.9	4	4.6	4.3	5.1	4
Highest	7.6	6.2	5.8	4.5	3.2	2.8	3.1	4.1	5.4	6.8	7.4	7.3	4.8

Following the application of the parameters, viable building rooftop locations were found, and maps of seasonal and annual radiation were created for the targeted area. In order to calculate the energy potential of each selected rooftop, the results were then compiled.

This PV system model is essentially a calculation to determine a PV system's solar energy output. The worldwide formula to estimate the electricity produced in the output of a PV system is (Markos & Sentian 2016):

$$E = A_s * Y_s * S_r * P_r \quad \text{- - - - - - - (3.1)}$$

Using Eq. (3.1), the solar energy potential in kWh was calculated. A_s denotes the total area of the PV panels in metres square. Performance ratio coefficient and PV panel efficiency are denoted by P_r and Y_s respectively, these are two additional factors that depend on the PV panel feature. Values for these parameters were chosen based on construction material and PV panel efficiency. Annual solar radiation S_r in kW h/m^2 was estimated in the ArcGIS zonal statistics table tool.

The function of the zonal statistics table is explained below:

The power per building was calculated in this study using the Zonal Statistics Table tool. This tool aggregates all suitable cells found inside the footprint polygon of each building. The building_id had been set as a zone field so that every building had been taken into account since each had a unique Id. The raster input value was set to suitable_cells. The average solar radiation (kWh/m^2) for each building was calculated using the mean field of statistics type, and the results were presented as a table. The Join Field tool would connect AREA and MEAN, the average solar radiation, to the map based on the building footprints. The selected buildings were exported into a new feature class using the Export Features function in the

Contents pane. The usable solar radiation was calculated and displayed in the attribute table. The usable solar radiation was then calculated as MEAN times AREA, divided by 1000, and expressed in megawatt-hours. Another field that represents electricity production was calculated. The data type and number format would be the same as the usable solar radiation. There was an 86 percent performance ratio for the solar panels, allowing them to convert 17.5% of the sun's energy into power. Thus, the available solar radiation was multiplied by 0.175 and 0.86 to get the amount of electricity produced (dcceew 2022b).

In Australia, the two most common varieties of panels are polycrystalline and monocrystalline (Solar Market 2022). In a solar panel, each cell contains silicon that uses the photovoltaic effect to transform sunlight into direct current (DC). The performance of solar PV panels is measured in efficiency, which is the fraction of the solar radiation that is converted into energy output. Polycrystalline panels are made from several silicon crystals, whereas monocrystalline panels are made from a single continuous silicon crystal structure. As per the website of the Australian Government, while polycrystalline panels are marginally less efficient than monocrystalline ones, with an efficiency range of 13 to 17%, monocrystalline panels are more efficient, with a range of 15 to 20% (dcceew 2022b). The average value of monocrystalline panels' efficiency (17.5%) was taken into the final electricity calculation.

4.4 CO_2 reduction calculation

The reduction of CO_2 emissions is the main goal of using solar energy, as was indicated in the introduction. In the years 2016–17, the consumption of fossil fuels was the primary contributor (78%) to the overall emissions of Wollongong (Wollongong City Council 2020). Residential structures account for 16% of fossil fuel emissions, commercial buildings account for 7%, and the industrial sector accounts for 55% (Wollongong City Council 2020). CO_2 emissions from electricity generation totaled 3.07 million tonnes in the fiscal year 2018-19, accounting for 37% of total emissions (Ironbark Sustainability 2021). As a result of the COVID-19 epidemic, which temporarily reduced emissions, emissions fell to 2.84 million tonnes in 2020–21 (Ironbark Sustainability 2021). However, it is expected to grow beginning in 2022 (Knight et al. 2021). This study assessed the viability of the sustainable Wollongong 2030 strategy plan and sought to determine whether or not the suburbs of Wollongong City Council are capable of establishing a sustainable future for the city by utilizing the full potential of solar energy. In NSW, the average amount of CO_2 released by the power sector

for the production of energy in 2021 was 0.81 Kg of CO_2 per kWh (Zhao et al. 2021). The annual CO_2 emission reduction was calculated by multiplying 0.656 Kg and the annual solar electricity potential output in kWh for two suburbs. Then, this result was divided by the number of dwellings to find out the volume of CO_2 emission reductions per building

5. Results

5.1 Solar radiation model validation

To measure the accuracy of the model, error variance for direct normal irradiance (DNI) was produced. The method for calculating the model's error was Mean Absolute Percentage Error (MAPE). To calculate MAPE, the absolute errors of measured and predicted numbers are calculated. These absolute errors are shown as a percentage of what was measured. MAPE is often employed because it is simple to understand and comprehend (Wargon et al. 2009). For instance, a MAPE value of 10% indicates that there is an average 10% discrepancy between the measured and estimated values. It is determined by the absolute difference to actual ratio. The daily average DNI for each month is used to calculate the variance.

For calculating MAPE of DNI data, the predicted mean irradiance (kWh/m^2/day) values from each season were compared with two weather stations' datasets (Table 4). First, data from Woonona (Popes Rd) weather station with station number 68108 and another from Bellambi AWS with station number 68228, with the input parameter from 2021 (BoM, 2022) were used in the validation process.

Table 4 Monthly mean DNI data from Wollongong weather stations (kWh/m^2/day) (BOM 2022).

2021	Jan	Feb	Mar	Apr	May	Jun	Jul	Aug	Sep	Oct	Nov	Dec
Woonona (Popes Rd) (68108)	5.7	4.6	3.8	3.9	2.8	2.5	2.8	3.6	4.6	5.6	4.4	5.5
Bellambi AWS (68228)	5.7	4.6	3.8	3.9	2.8	2.5	2.8	3.6	4.6	5.6	4.4	5.5

Table 5 compares average seasonal DNI data from weather stations in both suburbs to the predicted average DNI data from this study; both data are in kWh/m^2/day. Table 5 shows that both sets of data exhibit a similar trend. However, when the model's average solar irradiance data is compared to the data from both stations, there is a minor difference. For example, the daily mean solar irradiance value in winter and autumn is lower in the predicted data.

Table 5: Observed and predicted solar radiation data from Bureau stations.

Season/Station	Woonona (Popes Rd)	Bellambi AWS	Predicted
Winter	2.97	2.97	2.0
Autumn	3.50	3.50	2.6
Spring	4.87	4.87	4.2
Summer	5.27	5.27	4.9

The MAPE of the data was calculated in a spreadsheet, and its result is 19.7%. As shown in Table 6, Blasco et al. (2013) proposed four categories to evaluate MAPE results for assessing a forecasting model. The solar radiation modelling could be considered as a reliable model as it falls into a good forecasting model according to Blasco et al. (2013) explanation.

Table 6: MAPE table interpretation.

MAPE (%)	Explanation
<10	Highly accurate forecasting
10-20	Good forecasting
20-50	Reasonable forecasting
>50	Inaccurate forecasting

The independent variable t-test on the sample population of 40 structures from each of the two suburbs revealed that the yearly means for Cringila and Wombarra were 1106.09 kWh/m^2 and 943.07 kWh/m^2, respectively. If p-value is less than 0.05, the null hypothesis would be discarded. The result of p-value is 0.000002049, which supports the idea that the null hypothesis would be rejected. Here, p-value is significantly lower than 0.05, supporting the alternative hypothesis that the solar radiation annual means of the two suburbs are significantly different due to the escarpment shadow.

5.2 Solar Radiation Estimation

By performing solar PV energy simulations using the geospatial method with the aid of LiDAR data, building footprints, and suburb boundaries, the solar radiation output for each building rooftop was identified for Wombarra and Cringila suburbs, and variation in results due to the effect of seasons and escarpment in solar distribution at suitable rooftop areas is demonstrated.

5.2.1 Suburb boundaries

Figure 10 depicts the extracted suburb boundaries of Wombarra and Cringila. It is clear from the figure that the Wombarra suburb is located in the northern part, and the Cringila suburb is located in the southern part of Wollongong city.

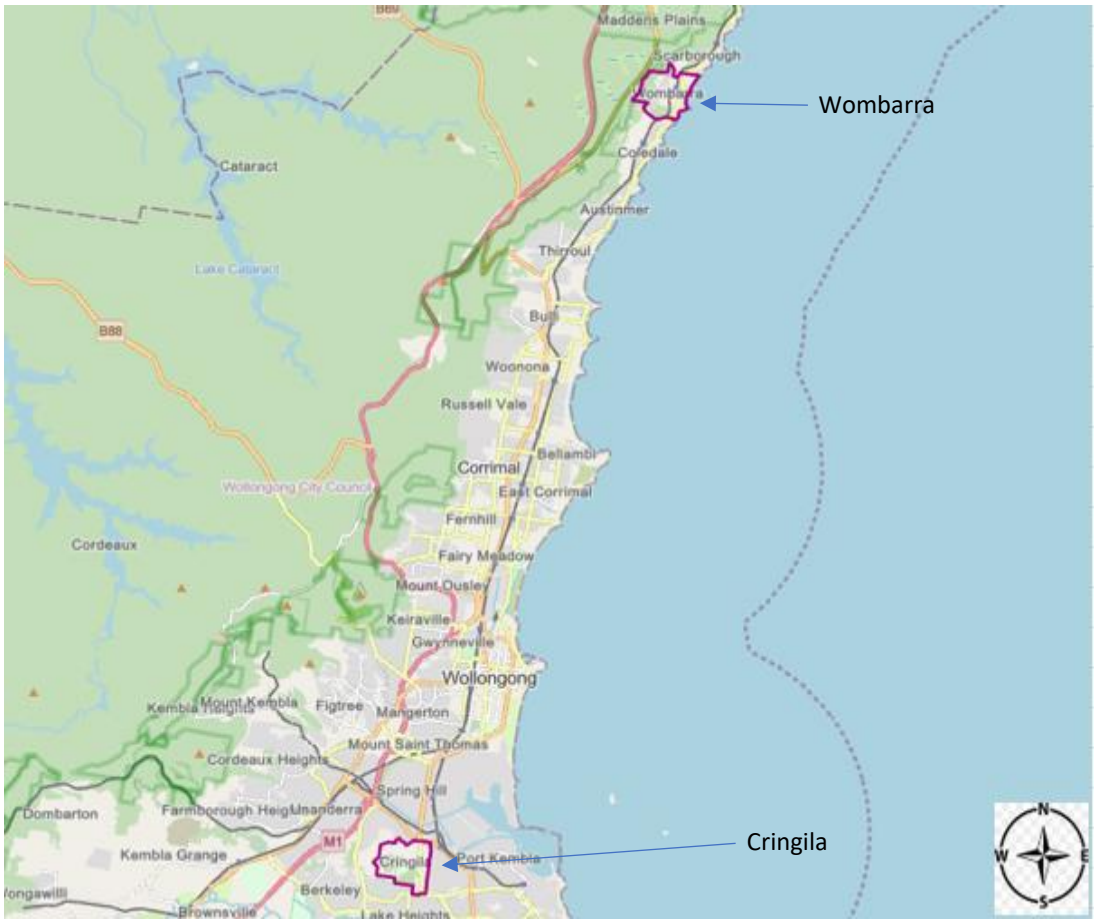

Figure 10: Wombarra and Cringila suburb boundaries in dark red.

As shown in Figure 11a, the Wombarra suburb is adjacent to the escarpment, and the escarpment is outside the suburb boundaries. This escarpment cast a shadow on the

Wombarra suburb's dwelling rooftops and to include the escarpment and ground features in the solar radiation analysis, a minimum 400-metre buffer was created. The escarpment is about 350 m tall (Macquarie 2013), and the maximum length of shadow in the summer is equal to the object's height, while the maximum length of shadow in the winter is 2.5 times the object's height (Williams 2020). Hence, the maximum length of the shadow would be 875 m (2.5 times 350 m) or approximately 1 km due to the escarpment. As a result, unlike Wombarra, the escarpment would not cast a shadow on the Cringila suburb's dwelling rooftops because it is 7 kms away from Cringila (Figure 11b).

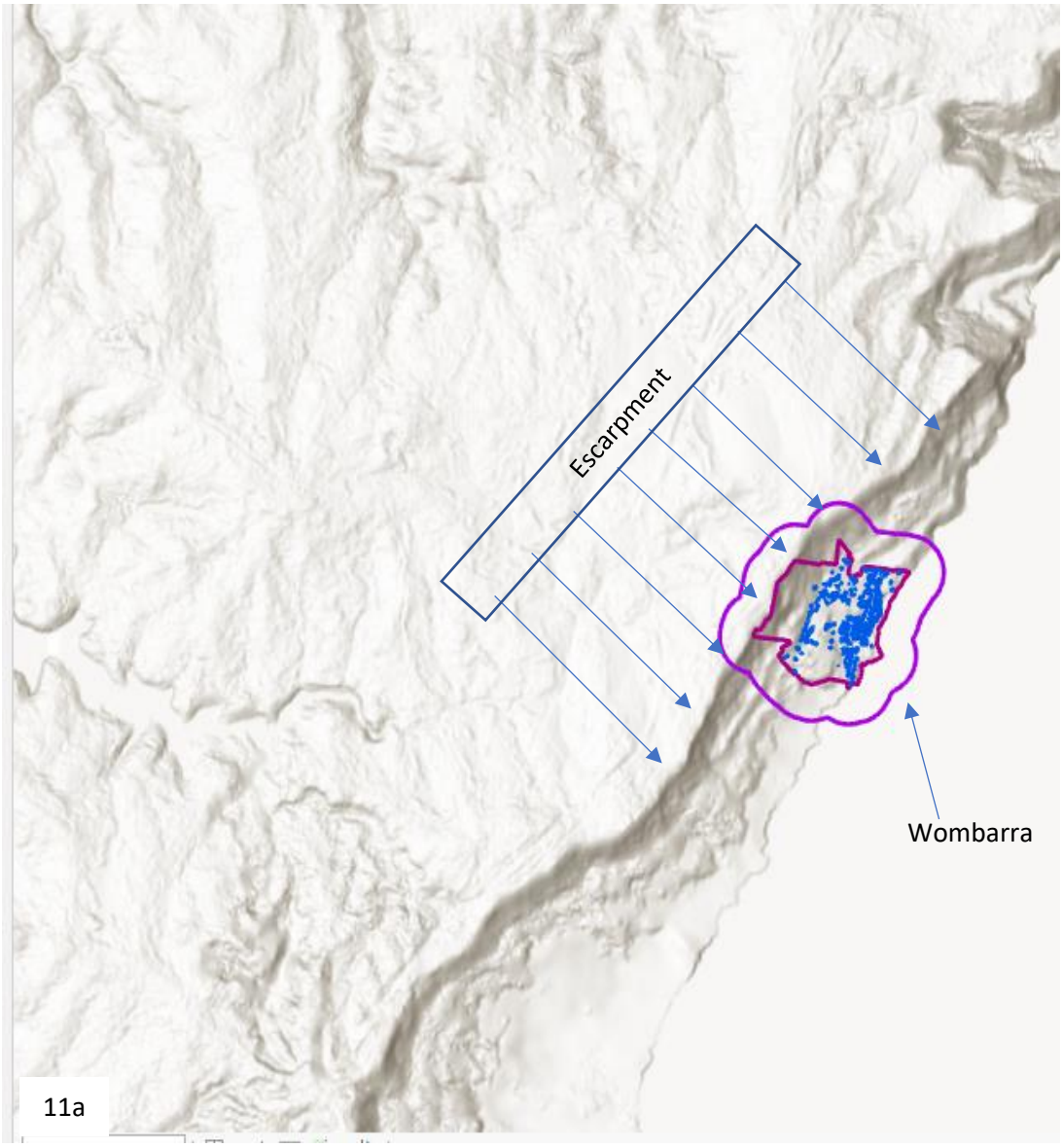
Escarpment
Wombarra
11a

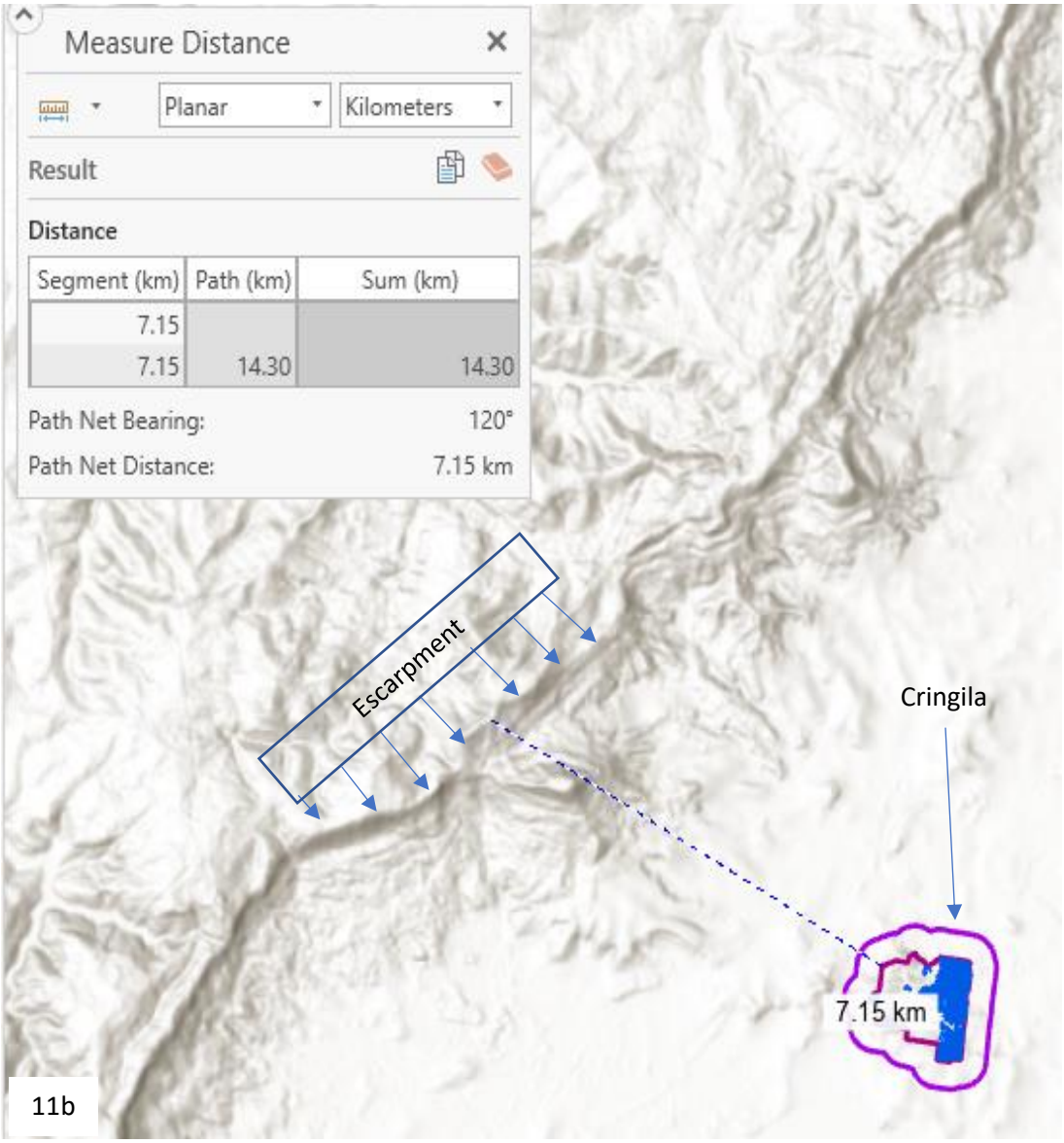

Figure 11: Suburb boundaries are in red, 400 metres buffer boundaries are in purple, building footprints are blue, and the escarpment is indicated with a dark blue colour block and arrows; Figure 11a: Escarpment is outside the Wombarra suburb boundary and inside the buffer boundary; Figure 11b: Escarpment is 7 kms away from Cringila suburb boundary.

5.2.2 LiDAR data

Figure 12 is the 2D view of the LiDAR point cloud in the study area. The points with high elevation are shown in dark red, and points with low elevation are shown in green and blue. The raw LiDAR data contains many undesirable points that represent the environment, like water and even cars on the street. Those points were out of scope for the analysis and unfiltered for the process. The useful points were gone through a series of classifications and separations.

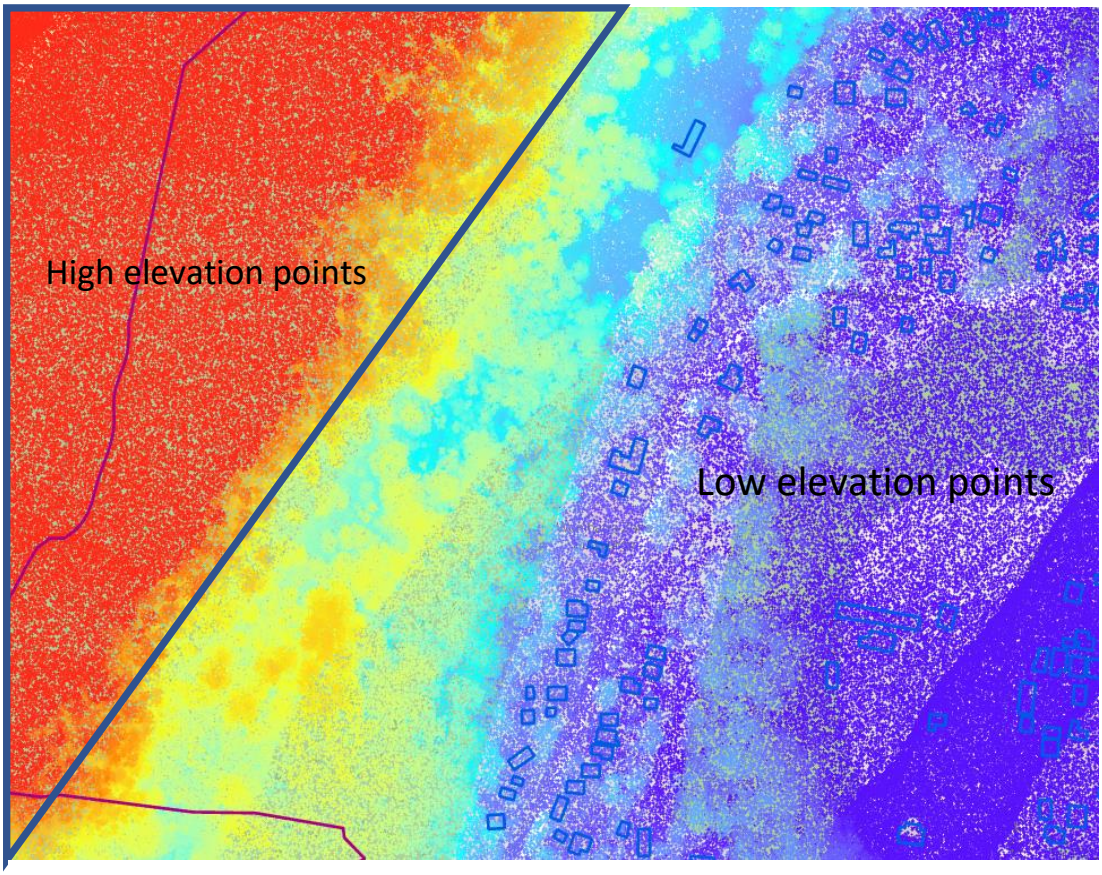

Figure 12: Visualization of LiDAR data (Wombarra); high elevation points are in red and low elevation points are in blue.

To include the above ground features in the analysis, LiDAR data was converted to a digital surface model (DSM) (Figure 13). The dark areas represent low elevations, and the light areas represent high elevations. The DSM model for the Wombarra suburb (Figure 13a) shows the elevation with light shading touching the west boundary due to the effect of the escarpment. Cringila, on the other hand, has a low elevation throughout and across its surroundings (Figure 13b).

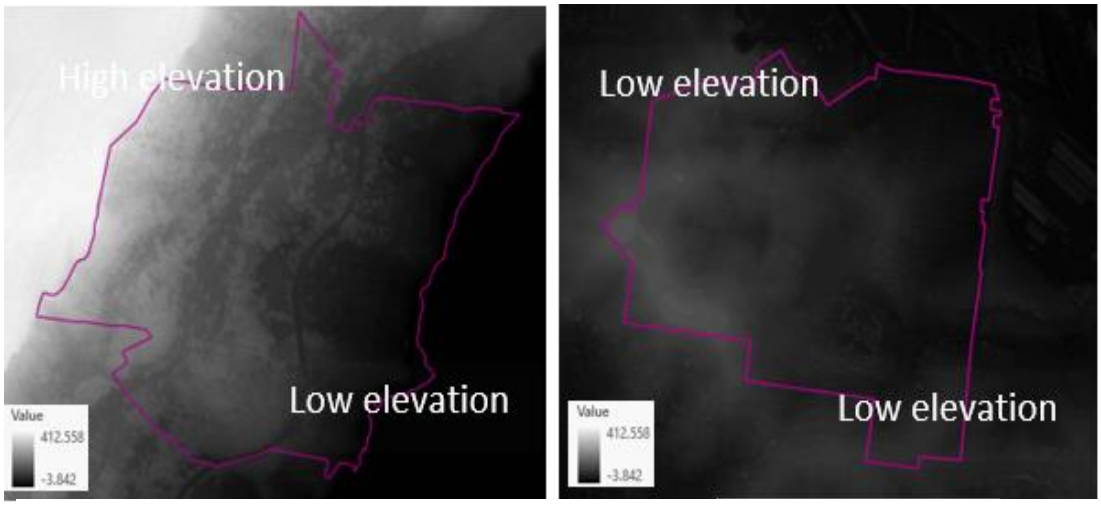

Figure 13: Light grey areas represent high elevation and dark grey areas represent low elevation; suburb boundaries are presented in red colour lines; Figure 13a: Wombarra DSM depicting high and low elevation; Figure 13b: Cringila DSM depicting high and low elevation.

5.2.3 Building footprints

Figures 14a and 14b show the building footprints of the suburbs of Wombarra and Cringila, respectively. These figures show that all rooftops of selected suburbs are covered in the assessment. There are 416 rooftop segments in Wombarra with an area of 48415 m^2 and 1178 rooftop segments in Cringila with an area of 118429.5 m^2. As a result, 1594 rooftop segments with a total rooftop area of 166844.5 metres square were identified.

Figures 14a and 14b: Building footprints in blue and suburb boundaries in red for the Wombarra and Cringila suburbs.

Figures 15 shows the intersection of the DSM model and the building footprints of the Wombarra and Cringila suburbs. The high elevation points are presented in light grey and the low elevation points presented in dark grey with suburb boundaries in red (Figure 15). In Wombarra dwellings are close to high elevation points on the west side and are close to low elevation points on the east side (Figure 15a). Whereas, In Cringila all dwellings are on low elevation points (Figure 15b).

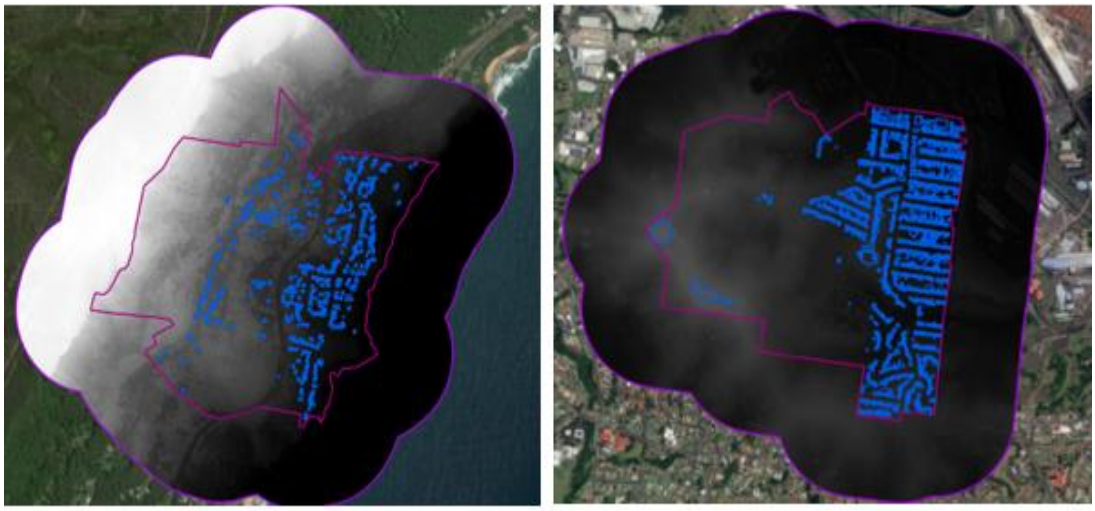

15a. Wombarra 15b. Cringila

Figure 15: Light grey areas represent high elevation and dark grey areas represent low elevation; suburb boundaries are presented in red colour lines; buffer boundaries are in purple; building footprints are in blue; Figures 15a and 15b: Intersection of DSM model and footprints in the Wombarra and Cringila suburbs.

5.2.4 Hillshade analysis and area solar radiation modeling

Figure 16 shows the result of the Hillshade analysis of shadow done by considering the effects of the local horizon at each cell. Shadow is observable mainly in the escarpment, tree canopy, and on the roof edge. The escarpment is clearly visible in Figure 16a, and shading can be observed more on Wombarra than on Cringila (Figures 16b and 16c). This is because Wombarra's western boundary is adjacent to the escarpment, and vegetation is dense, thus casting more shadow on rooftops than in Cringila, which is far from the escarpment. Apparently, the raster cells that are in the shadow do not have access to the incoming solar radiation. Thus, those areas are not considered suitable for solar PV installation.

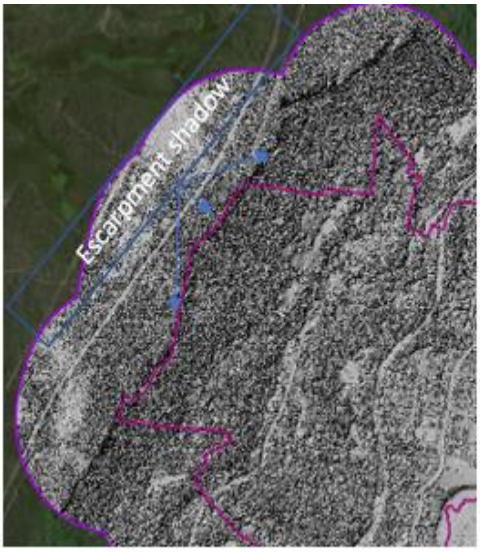

16a: Escarpment shadow (Wombarra)

16b: Wombarra

16c: Cringila

Figure 16: The grayscale 3D representation of the terrain surface using the Hillshade tool; suburb boundaries are presented in red colour lines; buffer boundaries are in purple; Figure 16a: Grayscale representation of the escarpment and surrounding high vegetation in Wombarra; Figure 16b: Grayscale representation of Wombarra suburb buildings and surroundings; Figure 16c: Grayscale representation of Cringila suburb buildings and surroundings.

In the next step, solar radiation on building rooftops was calculated for four seasons (Winter, Autumn, Spring, and Summer). Figure 17 shows the comparison of solar radiation in these two suburbs and across the four seasons. In the Wombarra suburb, solar radiation density is lower than in Cringila due to the escarpment and high vegetation density, which cast shadows on building rooftops across the seasons. Figure 17 depicts solar radiation per unit area for Cringila and Wombarra, with blue representing the lowest solar radiation, yellow

being the medium, and red representing the maximum solar radiation. Each of the Cringila maps (Figures 17a, 17c, 17e, and 17g) has a higher intensity of solar radiation than the Wombarra maps (Figures 17b, 17d, 17f, and 17h), as seen by the colours, which are darker in Cringila. When comparing the intensity of solar radiation in each season, the colours intensify from winter (Figures 17a and 17b) to autumn (Figures 17c and 17d) to spring (Figures 17e and 17f) to summer (Figures 17g and 17h). Maps therefore indicate that the intensity of solar radiation is highest in the summer and lowest in the winter.

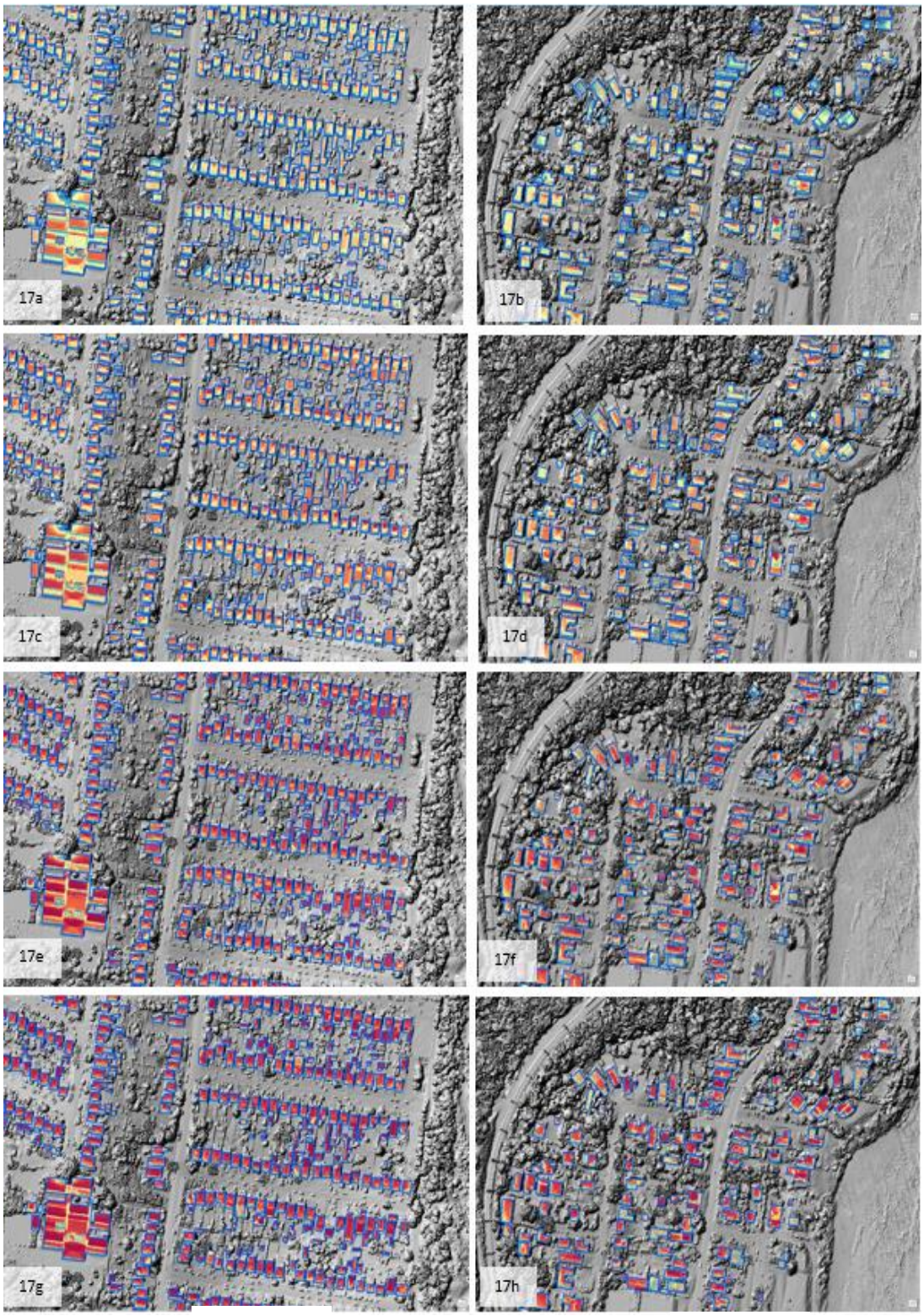

Figure 17: Cringila and Wombarra mean solar radiation maps for each building in all seasons, blue represents the lowest solar radiation, yellow is the median, and red represents the highest solar radiation; Figures 17a and 17b show solar radiation for Cringila and Wombarra in winter; Figures 17c and 17d show solar radiation for Cringila and Wombarra in autumn; Figures 17e and 17f show solar radiation for Cringila and Wombarra in spring; and Figures 17g and 17h show solar radiation for Cringila and Wombarra in summer.

Note that solar radiation was only calculated for buildings because the raster of building footprints was used as a mask. This auto-generated raster was in watt-hours per square. To make the raster easy to read, the unit was converted to kilowatt-hours per square metre (kWh/m^2). Figure 18a for Cringila and Figure 18b for Wombarra show the annual solar radiation of each building in blue and average annual solar radiation per building in orange. In Cringila, the average annual solar radiation is 1087 kWh/m^2/building, and in Wombarra it is 909 kWh/m^2/building. Given a certain minimum level of annual radiation, these numbers give an idea of how many buildings could have the feasibility of PV systems installed. Also, figures 18a and 18b show that average annual solar radiation per building in Cringila is higher than Wombarra.

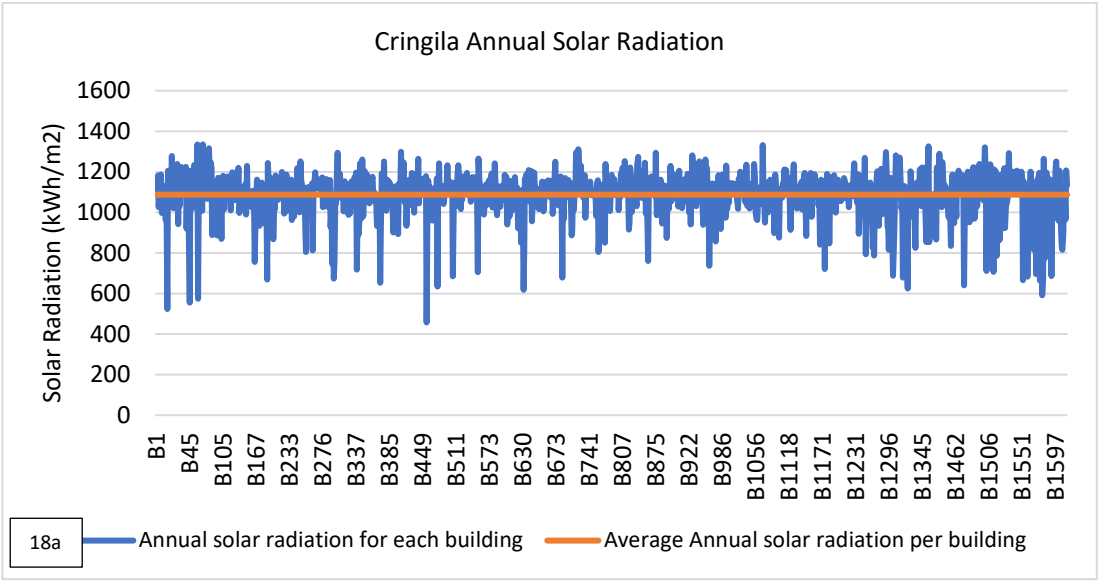

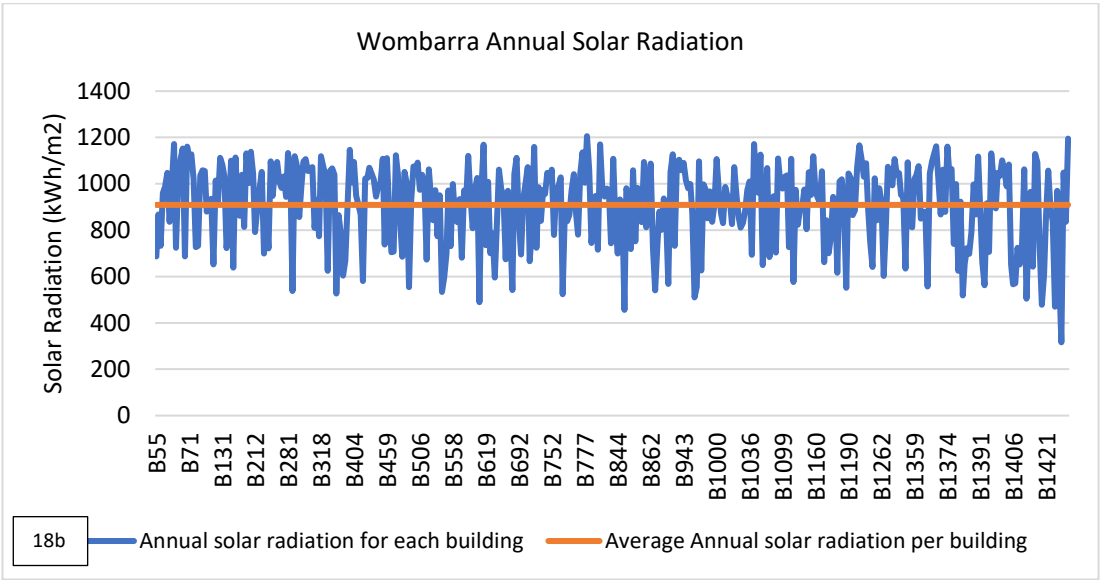

Figure 18a: Cringila annual solar radiation (kWh/m^2) for each building in blue and average annual solar radiation (kWh/m^2/ building) in orange; Figure 18b: Wombarra annual solar radiation (kWh/m^2) for each building in blue and average annual solar radiation (kWh/m^2/ building) in orange.

Table 7 shows the comparison of annual and seasonal mean solar radiation in Wombarra and Cringila. Wombarra suburb Mean solar radiation (kWh/m^2) on building rooftops is 10.8 % lower in winter, 2.6% lower in autumn, 6.9% lower in spring, and 7.4% lower in summer than in Cringila. As mentioned in section (Regional Setting Chapter 3), both the suburbs are similar in terms of dwelling structures, as 93.5% of dwelling structures in Cringila are matched with 96.4% of dwellings in Wombarra, but solar distribution varies because Wombarra is right beside the escarpment. Figure 19 shows season-wise per dwelling average solar radiation in Cringila and Wombarra (kWh/m^2). For every season it is lesser in Wombarra than in Cringila

(annual mean solar radiation: 1087 kWh/m^2 (Cringila), and 909 kWh/m^2 (Wombarra)). In winter, Wombarra in orange has 12.45 kWh/m^2 lesser solar radiation than Cringila in blue (Figure 19). In autumn, Wombarra in orange has 5.44 kWh/m^2 lesser solar radiation than Cringila in blue (Figure 19). In spring, Wombarra in orange has 23.17 kWh/m^2 lesser solar radiation than Cringila in blue (Figure 19). In summer, Wombarra in orange has 30.19 kWh/m^2 lesser solar radiation than Cringila in blue (Figure 19).

Table 7: Annual and seasonal mean solar radiation in Wombarra and Cringila.

Season	Cringila	Wombarra
Winter	128.16	115.71
Autumn	217.63	212.19
Spring	361.16	337.99
Summer	436.05	405.86
Annual	1087.00	909.00

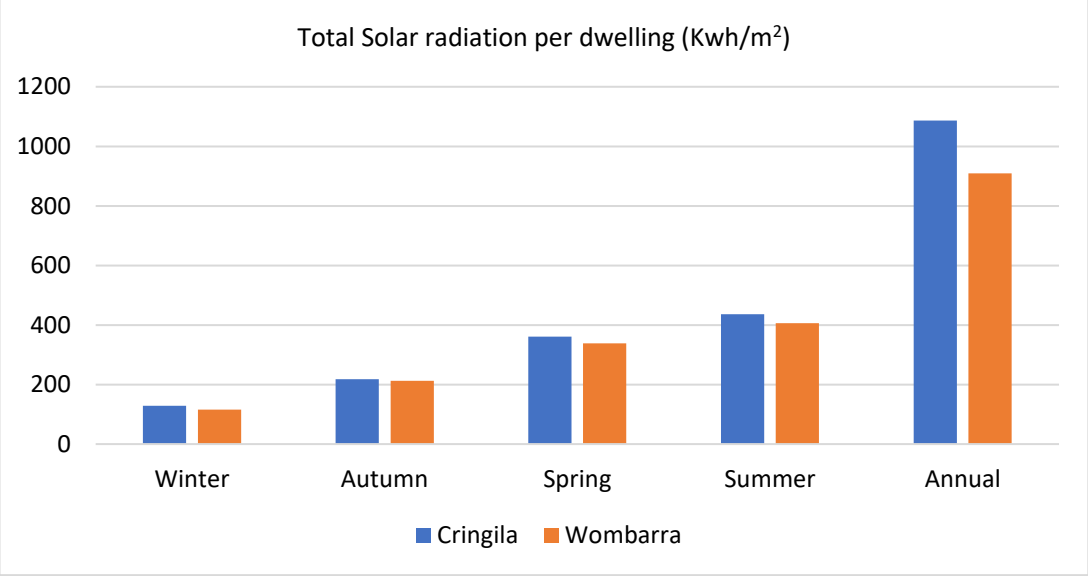

Figure 19: Annual and seasonal mean solar radiation chart for Wombarra in orange and Cringila in blue.

Wombarra has more shading than Cringila due to the escarpment. This shading across the seasons varies and decides the suitable rooftop area to be used in estimating the value of the rooftop solar PV energy. It is clear from Figure 20 that dwelling roofs in Cringila have a

higher distribution of suitable rooftop areas than in Wombarra. In summer (Figure 20a), the distribution of suitable rooftop area for Cringila is more between 70 to 80% (average for all the rooftops is 75%), while in Wombarra (Figure 20b) distribution is between 60 to 70% (average for all the rooftops is 60%). In spring (Figure 20c), for Cringila, the distribution is 70 to 80% (average for all the rooftops is 69%), while in Wombarra (Figure 20d), the distribution is between 50 and 60% (average for all the rooftops is 48%). In autumn, for Cringila (Figure 20e) distribution is 50 to 60% (average for all the rooftops is 57%), while in Wombarra (Figure 20f), it is at 20% and between 40 to 50% (average for all the rooftops is 33%). In winter, for Cringila (Figure 20g) distribution is 50 to 60% (average for all the rooftops is 59%), while in Wombarra (Figure 20h), it is at 20% and between 50 to 60% (average for all the rooftops is 36%). This shows that, in every season, Cringila has a more suitable rooftop area for solar PV installation than Wombarra.

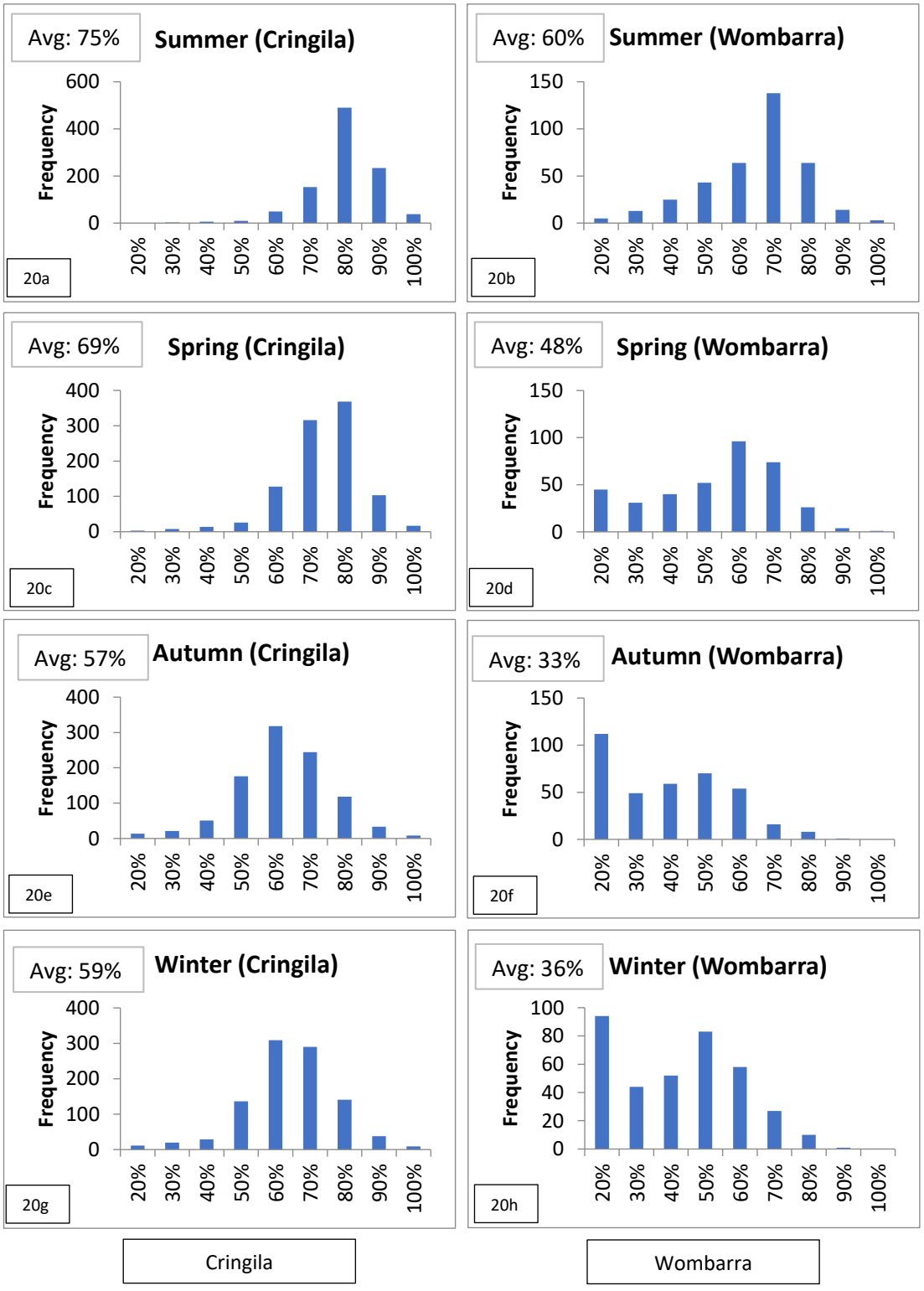

Figure 20: Suitable rooftop area distribution comparison at various seasons; Figures 20a and 20b show suitable rooftop area distribution for Cringila and Wombarra in summer; Figures 20c and 20d show suitable rooftop area distribution for Cringila and Wombarra in spring; Figures 20e and 20f show suitable rooftop area distribution for Cringila and Wombarra in autumn; and Figures 20g and 20h show suitable rooftop area distribution for Cringila and Wombarra in winter.

Figure 21 shows the comparison of both the suburbs with the number of buildings falling into the bracket of high and low solar radiation. In Summer, most of the buildings (count: 866) are having solar radiation of between 400 – 500 kWh/m^2, while in Wombarra most of the buildings (count: 215) are falling into the bracket of 300 – 400 kWh/m^2 (Figure 21a). In Spring, most of the buildings (count: 933) are having solar radiation of between 300 – 400 kWh/m^2, also in Wombarra most of the buildings (count: 220) are falling into the same bracket (Figure 21b). In Autumn, most of the buildings (count: 713) are having solar radiation of between 200 – 300 kWh/m^2, while in Wombarra most of the buildings (count: 270) are falling into the bracket of 100 – 200 kWh/m^2 (Figure 21c). In Winter, most of the buildings (count: 923) have solar radiation of between 100 and 200 kWh/m^2, while in Wombarra most of the buildings (count: 202) fall into the bracket of 0–100 kWh/m^2 (Figure 21d). As a result, Wombarra buildings are falling into a lower solar radiation bracket than Cringila buildings in each season. Figure 21 also depicts how the distribution of solar radiation varies throughout the year.

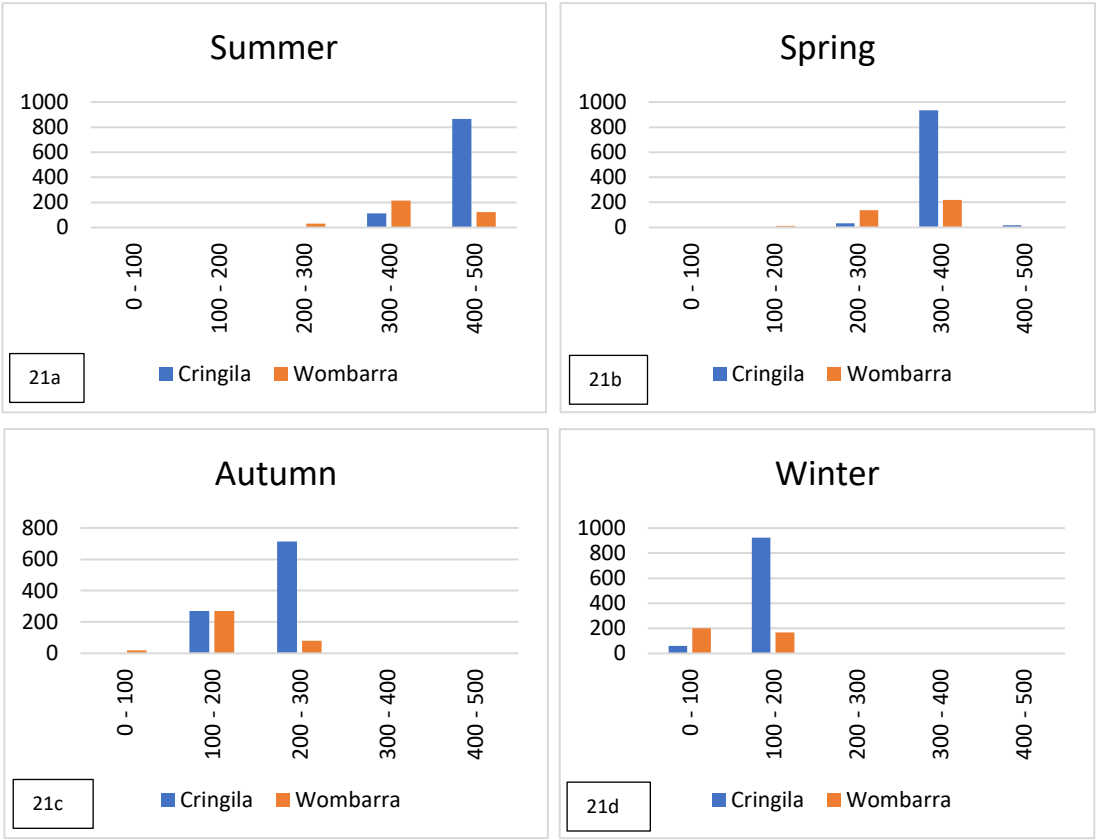

Figure 21: Count of buildings in the bracket of solar radiation (unit: kWh/m^2); Figures 21a, 21b, 21c, and 21d depict the number of buildings in various solar radiation brackets for Cringila and Wombarra in the summer, spring, autumn, and winter, respectively.

5.3 Electricity Potential

5.3.1. Rooftop slope and aspect

Slope values were divided into five groups (0.018°- 10°, 10°- 20°, 40°- 60°, and 60°- 87.323°) in order to find suitable rooftop slopes. A slope value of 0° indicates a level surface, while a value of 90° designates a perfectly vertical surface. The colour-coded classification of the rooftop slope is shown on the map in Figure 22.

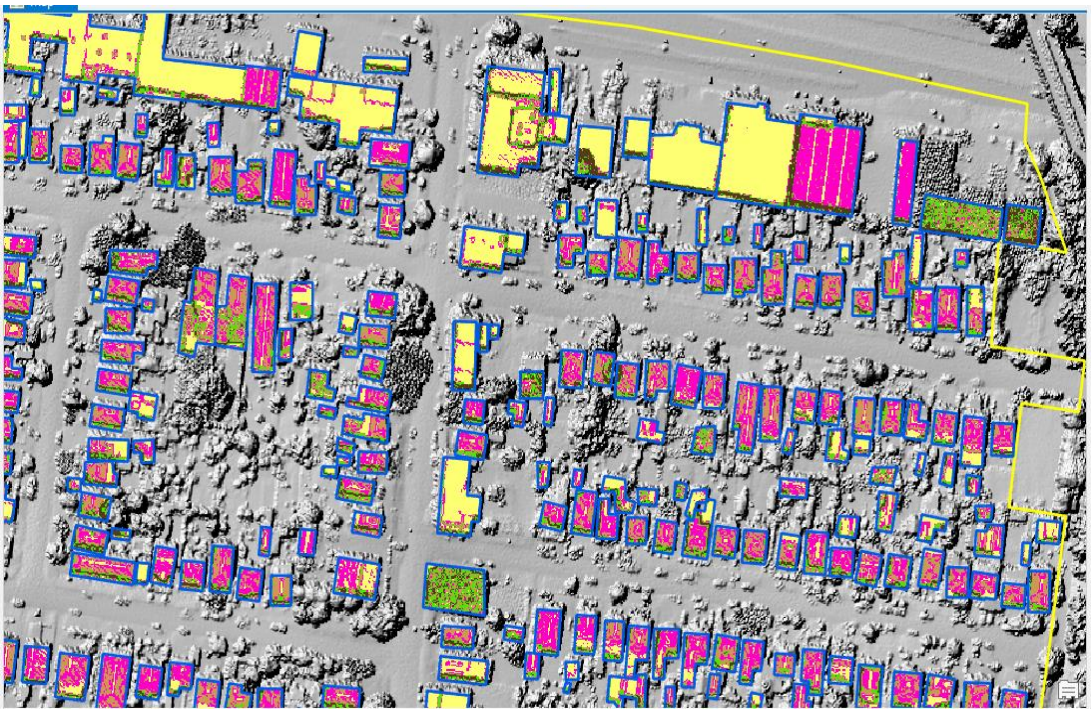

Figure 22: The Slope raster of the study area is created by the Surface Parameter Tool using DSM as input; yellow depicts the slope range of 0.018-10 degrees; pink depicts the slope range of 10-20 degrees; brown depicts the slope range of 20-40 degrees; green depicts the slope range of 40-60 degrees; black depicts the slope range of 60-87.323 degrees.

This slope raster is one of the necessary parameters to eliminate unsuitable roofs. Figures 23a and 23b show the classification and distribution of rooftops in these classes. Most of the rooftops fall into the classes (0.018-10) and (10-20), which shows that most of the rooftops are suitable for solar PV installation. Roofs with a slope of more than 60 degrees are seen as being too steep, and their installation and upkeep are expensive. Hence, rooftops having a slope of less than 60 degrees were considered for solar PV energy estimation.

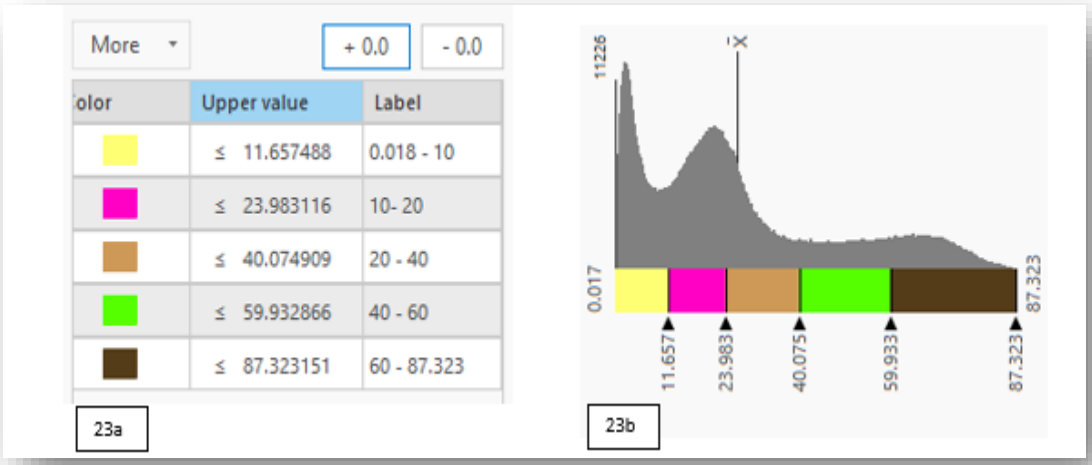

Figure 23: 23a. Classification of rooftop slopes; 23b. Distribution of Rooftops in the slope classes.

The average tilt angle of most of the rooftops in Cringila lies between 20 and 40 degrees as shown in the Figure 24a with orange dotted line, and in Wombarra, it is between 20 and 50 degrees as shown in the Figure 24b with orange dotted line. These ranges fall within the range of the optimum tilt angle of the PV panel, as shown in Figures 24a and 24b.

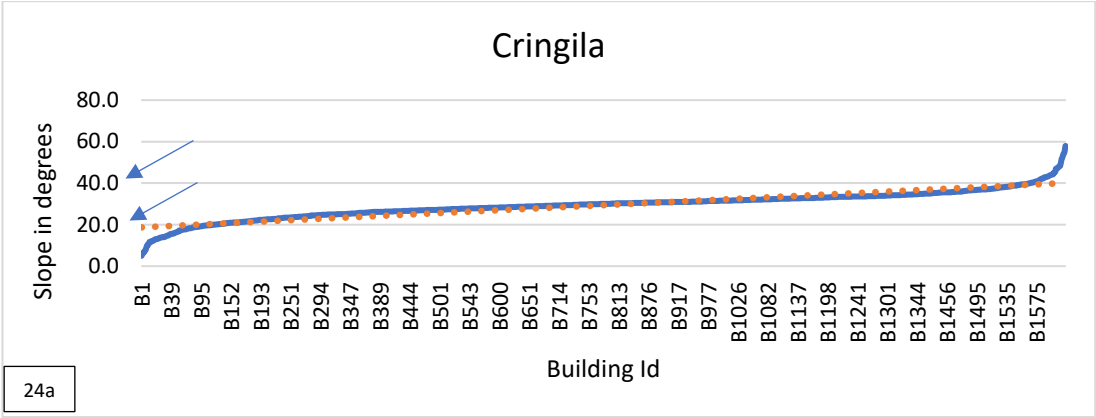

24a

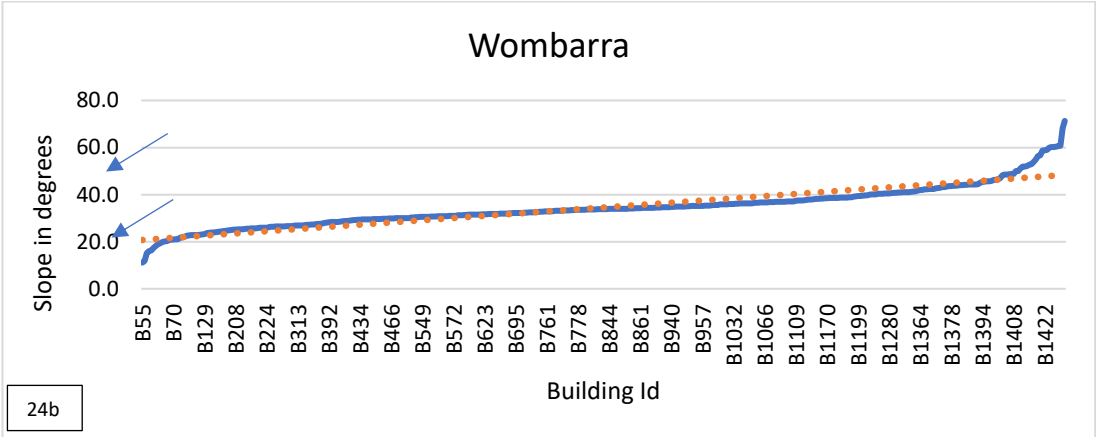

24b

Figures 24a and 24b: The average tilt angles of rooftops in Cringila and Wombarra; blue line depicts the actual slope of buildings; orange dotted line depicts the average slope trend; Figure 24a: Arrows pointing the average range of slopes in Cringila between 20 and 40 degrees; Figure 24b: Arrows pointing the average range of slopes in Wombarra between 20 and 50 degrees.

The aspect was categorized into standardized 8 categories: (i) (337.5 - 22.5) north, (ii) (22.5 – 67.5) northeast, (iii) (67.5 – 112.5) east, (iv) (112.5 – 157.5) southeast, (v) (157.5 – 202.5) south, (vi) (202.5 – 247.5) southwest, (vi) (247.5 – 292.5) west, (viii) (292.5 - 337.5) northwest. The aspect raster was used to filter out rooftops facing south. Figure 25 depicts north facing rooftops in red, south facing rooftops in cyan, east facing rooftops in yellow, and west facing rooftops in blue.

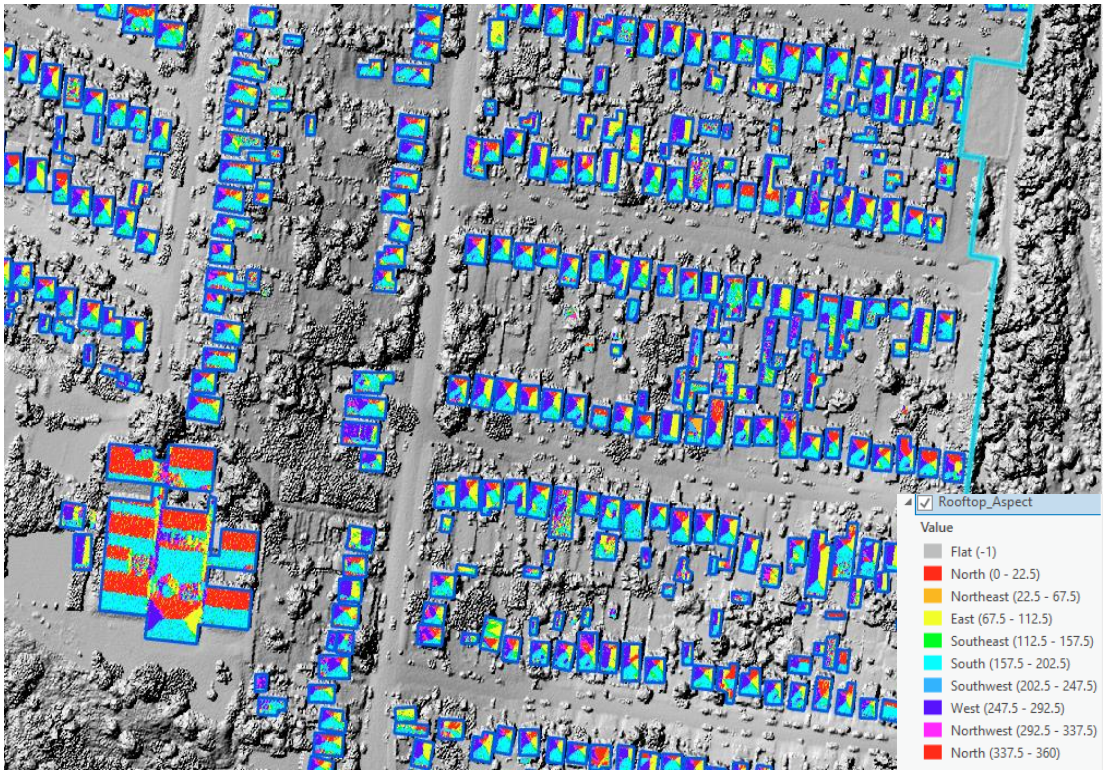

Figure 25: The aspect raster of the study area generated using the Surface Parameters tool; red roofs facing north, cyan roofs facing south, yellow roofs facing east, and blue roofs facing west (colour legend is provided in the figure).

5.3.2 Solar electricity potential calculation

There are 1178 building footprints in Cringila and 416 building footprints in Wombarra, with a total area of 118430 and 48415 square metres respectively. To determine the appropriate rooftop area for calculating electricity potential, roofs with slopes greater than 60 degrees, roofs facing south, and roofs with solar radiation less than 800 kWh/m^2 were eliminated. As a result, the suitable rooftop area for Cringila and Wombarra comes down to 55887 m^2 (47% of total rooftop area) and 19594 m^2 (40% of total rooftop area), respectively. Once the suitable rooftop area was derived, it was used to calculate potential electricity by multiplying area (m^2), mean solar radiation (kWh), panel efficiency (17.5%), and performance ratio (86%) for each rooftop. As a result, the annual electricity potential for Wombarra is 2778.3 Mwh and for Cringila is 9926.7 Mwh.

Figure 26 shows the electricity potential at different seasons and a comparison of both suburbs. Figure 27 shows the comparison of the estimated average electricity generation from solar PV in each season in kWh/day for a building. According to the Australian Govt. Energy Made Easy statistics, the annual electricity consumption per household in

Wollongong is 5707.6 kWh (Australian Energy Regulator 2022). For 1178 buildings, Cringila's total electricity consumption would be around 6723.6 Mwh. If all suitable rooftops were covered with solar PV panels, about an extra 48% of electricity consumption could be offset by solar PV energy for Cringila. In the case of Wombarra, for 416 buildings, total electricity consumption would be 2374.4 Mwh, if all suitable rooftops were covered with solar PV panels, about an extra 17% of electricity consumption can be offset by solar PV energy. The two suburbs could generate enough solar power to meet their energy needs and would have surplus power of 48% and 17%, respectively. It should be noted that the yearly energy numbers include both the commercial and residential segments. Hence , surplus energy generated by rooftop PV panels in these two suburbs could offset the gap in the neighbouring suburbs.

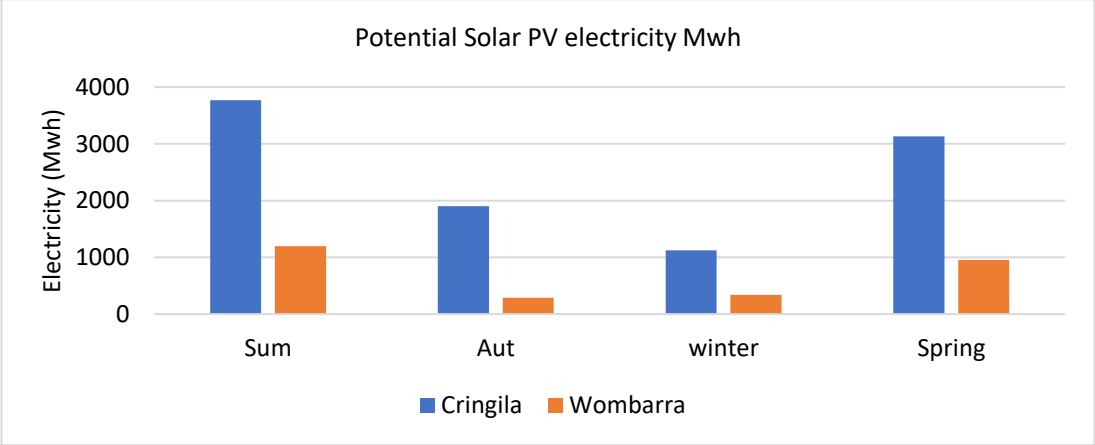

Figure 26: Electricity potential at different seasons for Cringila in blue and for Wombarra in orange.

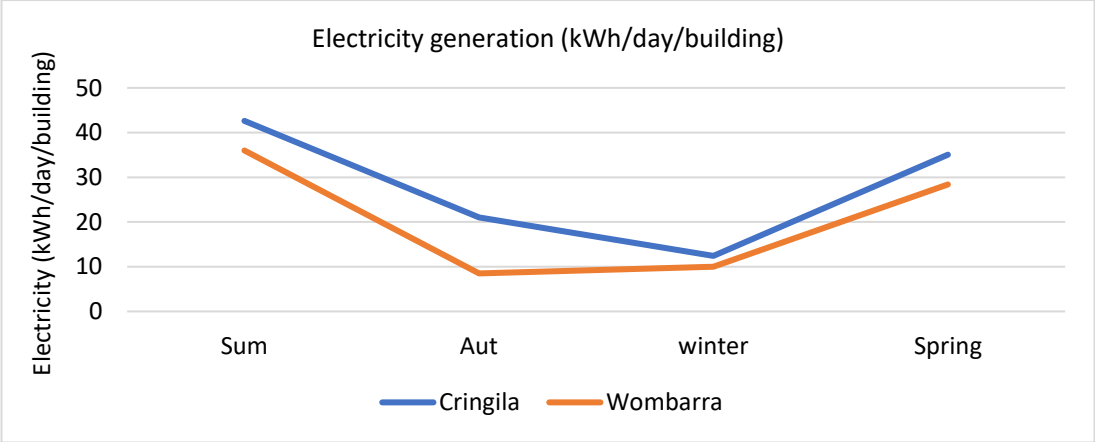

Figure 27: Seasonal trend of average electricity generation per day per building for Cringila in blue and for Wombarra in orange.

6. Discussion

This chapter summarizes the key findings and compares the solar PV energy output of two suburbs. In addition, it discusses the role that topographic features and the seasons play in the overall energy output.

6.1 Solar radiation and suitable rooftop area distribution for the area of interest

The findings demonstrate that electricity production in Wombarra is affected not only by the rooftop area but also by the amount of solar radiation reaching the roof surfaces, which is affected by the shading of the escarpment. Both suburbs share the same weather patterns, the number of rainy days, and types of buildings (ABS 2021a; ABS 2021d; World Weather Online 2022). However, the escarpment casts shadows on the Wombarra suburb's dwelling rooftops, and Cringila does not experience any escarpment-related shadowing. Consequently, even though the meteorological circumstances are the same, the solar PV energy output varies because of the escarpment's shadow. It is clear that the building rooftops in the Cringila suburb are better suited for the installation of rooftop solar PV panels since the majority of buildings have suitable rooftop areas greater than 55% in all seasons (Table 8). According to Table 8, buildings in the Cringila suburb have an average roof suitable area of 59 to 75% for solar panel installation, compared to 36 to 60% in the Wombarra suburb.

Table 8: Average suitable rooftop area per dwelling.

Season / Suburb	Cringila	Wombarra
Summer	75%	60%
Spring	69%	48%
Autumn	57%	33%
Winter	59%	36%

The ratio of the total suitable rooftop area to the total area of each suburb indicates which suburb is more suitable for installing solar PVs. In comparison to Wombarra, which has a suitable rooftop area of 19594 m^2 out of a total rooftop area of 48415 m^2, representing 40%, Cringila has a suitable rooftop area of 5587 m^2 out of a total rooftop area of 118429 m^2, representing 47%. These results suggest that the amount of solar energy that may reach the PV panel arrays in the suburb of Wombarra is constrained by the escarpment's shadow. Similar results were found in previous studies, Paidipati et al. (2008) conducted study in the

United states and determined that 46% of total rooftops area is suitable for rooftop PV. Ladner-Garcia & O'Neill-Carrillo (2009) conducted study in Puerto Rico and came to the conclusion that suitable rooftop area for PV installation is 50%. According to the research by Hofierka & Kanuk (2009) on rooftops in Bardejov, Slovakia, 59% of the overall rooftop surface area is suitable for solar panel installation. Santos et al. (2011) conducted study on Lisbon, Portugal and found that 49% of total rooftop area for PV installation is suitable. Odeh & Nguyen (2021) conducted study on Sydney, Australia and concluded that suitable rooftop area for the installation of solar PV is 50%.

The findings indicate that the solar radiation in Cringila is higher than in Wombarra in every season. As per the results, the average annual solar radiation for each dwelling in Wombarra is 178 kWh/m^2 lower than in Cringila (Cringila: 1087 kWh/m^2, Wombarra: 909 kWh/m^2). Consequently, the average annual potential electricity generation per dwelling in Wombarra is 20.6 kWh/m^2/day, while it is 27.6 kWh/m^2/day in Cringila. This escarpment shading effect is visible on solar radiation maps, that is, Cringila has a higher level of solar radiation in each season than Wombarra as shown in Figure 17. The results suggest that the role of shadowing is important in accurately estimating solar PV energy values along roofs. This research shows that the average yearly potential solar PV electricity is 7 kWh/m^2/day lesser in Wombarra than Cringila due to escarpment shadow cast on Wombarra rooftops. According to research by Ko et al. (2015), the output of solar panels is significantly impacted by the shadow effect created of adjacent building structures. Mishra et al. (2020) addressed that PV sites should not be under any kind of shade. Since the shadow is constantly shifting owing to the sun's motion, Alam et al. (2012) proposed that when shadow falls on PV, it rapidly reduces the performance of the Photovoltaic system.

According to the findings of the study, the amount of solar radiation varies seasonally throughout the year. Additionally, Figure 17 shows the seasonal variation in the solar radiation output, which is increasing from winter to autumn to spring to summer. Total solar potential for both suburbs come 4965.99 Mwh, 2188.04 Mwh, 1463.21 Mwh, and 4087.79 Mwh from summer, autumn, winter and spring respectively. Therefore, Cringila has a higher potential for solar rooftop installation per dwelling in each season. Other researches (Mishra et al. 2020, Chow et al. 2014) have found a similar trend that summer has the most prolonged hours of sunlight, with the fewest shadows, while winter has the least quantity of solar radiation due to short days and the sun's positioning casts a high number of shadows.

This study used a geospatial model to predict the seasonal and annual solar PV energy output of all types of buildings in the Wombarra and Cringila suburbs, using DSM, building footprints, and suburb boundaries. This model estimated and compared the solar PV energy output of two suburbs, taking into account seasonal patterns and topographical effects. The key findings show that topographic features and seasons have an impact on the distribution of solar radiation and suitable rooftop area, which in turn has an impact on the power generation capacity of solar PV panels (Dolara et al. 2015).

6.2 Solar PV energy potential of the area of interest

The results of this study show that Wombarra and Cringila have significant potential for producing electricity. It is possible to generate about 2778.3 Mwh for Wombarra and 9926.7 Mwh for Cringila from the 369 suitable building rooftops in the Wombarra suburb and the 983 suitable building rooftops in the Cringila suburb, each of which has an area of 19594 and 55887 m^2, respectively. If the potential rooftop areas of both suburbs were considered for solar PV electricity production, then the result shows that it could meet the total energy demand of these suburbs, and surplus power of 48% and 17% can be exported back to the grid, where it can be used by surrounding suburbs.

6.3 Possible change in CO_2 emissions

According to Zhao et al. (2021), in NSW, the average amount of CO_2 released by the power sector for energy production in 2021 was 0.81 kgCO2e/kWh. The total estimated annual electricity potential from solar PV panels on all the suitable rooftop areas for both suburbs is 12705 Mwh. This estimate could prevent 10291.1 tonnes of carbon dioxide emissions in both suburbs. In addition, the unused solar power of the dwellings could be exported back to the grid, reducing dependency on coal-fired power stations.

6.4 Validation

In terms of validation, the model employed achieved a MAPE of 19.7% which falls within the range of what is considered a good forecasting model; 10-20% (Blasco et al. 2013). This performance is similar to those in previous studies, for example, Rana & Rahman (2020) calculated MAPE of 18.14%, Chupong & Plangklang (2011) calculated MAPE of 16.83%, Pamain et al. (2022) calculated MAPE of 19.74%, and Lahouar et al. (2017) calculated MAPE of 18.95%. As a result, this model is considered to accurately represents the yearly solar PV energy potential of the rooftops in this study. However, there is a minor difference between

forecasted and actual mean solar irradiance output in winter and summer (winter: 0.97 kWh/m^2/day; summer: 0.37 kWh/m^2/day). Therefore, conducting a detailed analysis by physically inspecting the building rooftops of the chosen sites in each season would be recommended in order to make final decisions (Colak et al. 2020).

6.5 Implications of the findings

This model effectively incorporates seasonal effects as well as the slope and orientation of rooftops, surface characteristics in the area surrounding the target, and shading effects of topographic features. Therefore, the model could make it possible to anticipate PV output levels more accurately, while also providing a wealth of additional information, i.e., variation in energy output due to seasons and topographic features, and suitable building rooftops to install solar PV panels. In this regard, this method may assist in reducing the number of time-consuming site visits for data collection and also utilizes hidden spatial patterns in the area of interest. This would be beneficial because these site visits tend to take a significant amount of time. Further research could take into account the regional climatic characteristics, such as the amount of precipitation that occurs during the day in the chosen area.

This research provides a method for calculating the potential technical loss of rooftop PVs output by analyzing topographical structures via LiDAR data, building footprints, suburb and buffer boundaries. The framework offers an approach to the geospatial assessment of rooftop PV potential that is economical, efficient, and simple to apply on a suburban scale of a regional area. As the case study in Wollongong's suburbs demonstrates, the framework's distinguishing feature is its scalability between exact locations or vast areas, spanning multiple time scales and possessing topographical structure. In addition, the assessment results under this framework are credible; for instance, the calculated suitable rooftop areas are consistent with those found in studies by Paidipati et al. (2008), Ladner-Garcia & O'Neill-Carrillo (2009), Jofierka & Kanuk (2009), Santos et al. (2011), and Odeh & Nguyen (2021), indicating that the accuracy meets the criteria for a good forecasting model.

The implementation of solar panels in suburban areas will be the primary driver of innovation for Wollongong's renewable energy strategy, as outlined in the sustainable planning vision for Wollongong City 2030 (Wollongong City Council 2020). This model could be an integral part of the local government’s strategic decisions to install more solar panel systems for

maximum energy output and increased efficiency. This research suggests that municipal planners should prioritize the construction of buildings with large, undisrupted north-facing roof areas that can produce electricity from solar PV throughout the year and maximize the efficiency of solar panels. This is especially important in the suburbs, which are often located near any topographical feature and have demanding solar energy goals.

7. Conclusion

In view of growing energy demand and the fact that solar energy is an efficient and advantageous source of electricity, this study provides a framework to comprehend and determine the potential of solar power to produce electricity (Salahuddin & Alam 2015; Sampaio & González 2017). This report reviewed the existing literature on the subject, focusing on the studies that showed how vital an examination of topographical features and seasonality was to the overall energy output. All of the data sets were obtained from trustworthy sources.

This study identifies and estimates the solar radiation and suitable areas for rooftop PV and solar PV potential in the Wombarra and Cringila suburbs. The study area, located in the southeast region of Australia, receives abundant solar radiation throughout the year (BOM 2019). The study region includes a high building density and a high number of suitable building structures for solar PV systems, which means there is a significant opportunity for community solar initiatives. ArcGIS Pro is used to remove the areas that are not suitable for PV installation and to compute the solar radiation. This is accomplished by using the LiDAR data-based DSM model and processing it. The accurate calculation of topographic features, slope, aspect, and the orientation of the building rooftops in consideration of seasonality are critical points (Park et al. 2015) for the estimation of solar energy that was assessed using a GIS-based method. This algorithm promises a result with high accuracy in less data and less time for estimating solar energy production on flat and tilted surfaces, as well as classifying the ideal building to place solar PV panels to fulfil the user's energy requirements during a particular time period. It does this by avoiding assumptions, manual and machine-learning-based methods, and relying instead on empirical data.

The findings of this study also have implications for the estimation of the solar potential of suburban regions to a reasonable degree of precision. As was covered in chapter 2, estimating solar potential can be done in a variety of ways, with each method being tailored to a unique set of research areas and scales. For calculations of vast areas, a systematic method with numerous assumptions is frequently employed. The parameters that are used for calculating a city filled with tall structures are distinct from those used for calculating suburban areas in regional areas. As a result, the findings of this study offer a strategy for planning suburban areas that have a high building density but a height that is relatively low. It is clear that the geospatial method of separating the structure from its surroundings and

taking topographical features into account with seasonality analysis is particularly significant in this research region and may be duplicated elsewhere. Furthermore, while a manual correction is appropriate for large areas, it only serves to improve accuracy. In other words, when the study region is expansive, the level of accuracy may not be as great as it is in this study, and calculation time is frequently compensated.

The findings of the study have demonstrated that solar photovoltaic panels have the potential to play a considerable part in the studied areas in the process of displacing conventional fossil fuels. Overall, these solar panels have the capacity to meet one hundred percent of the peak energy demand in the suburb, as well as to supply any excess electricity to the requirements of the adjacent suburbs. There is room for additional investigation into this subject. For instance, one could estimate how much it would cost to put solar photovoltaic panels in the research regions and how long it would take for those panels to pay for themselves. In addition, this research does not take into account the fact that solar panels may already be installed in some buildings that are suited for their use. In future studies, a comparison between the currently installed PV panels on rooftops and their maximum capacity could be made. Future work might potentially involve creating a model by physically examining individual building rooftops. To encourage the development of solar energy, technical potential assessment is only the first step. Multiple obstacles are included in the road plans for PV integration in the built environment that are intended to be overcome. The effects of PV installations on building roofs on the economy and society should therefore be the subject of future research.

References

Alam, N, Coors, V, Zlatanova, S & Oosterom, P 2012, 'Shadow effect on photovoltaic potentiality analysis using 3D city models', *The International Archives of the Photogrammetry, Remote Sensing and Spatial Information Sciences*, vol. XXXIX-B8, pp. 209-14.

Alexander, C, Smith-Voysey, S, Jarvis, C & Tansey, K 2009, 'Integrating building footprints and LiDAR elevation data to classify roof structures and visualise buildings', *Computers, Environment and Urban Systems*, vol. 33, no. 4, pp. 285-292.

Almaghrabi, S, Rana, M, Hamilton, M & Rahaman, MS 2021, 'Forecasting regional level solar power generation using advanced deep learning approach', in *2021 International Joint Conference on Neural Networks (IJCNN)*, Shenzhen, China, 18-22 July.

Alqahtani, N & Balta-Ozkan, N 2021, 'Assessment of rooftop solar power generation to meet residential loads in the City of Neom, Saudi Arabia', *Energies*, vol. 14, no. 13, p. 3805.

Asumadu-Sarkodie, S & Owusu, PA 2016, 'The potential and economic viability of solar photovoltaic power in Ghana', *Energy Sources, Part A: Recovery, Utilization, and Environmental Effects*, vol. 38, no. 5, pp. 709-716.

Australian Bureau of Statistics 2021a, *Cringila 2021 Census All persons QuickStats*, Australian Bureau of Statistics, viewed 27 September 2022, <https://www.abs.gov.au/census/find-census-data/quickstats/2021/SAL11117>.

Australian Bureau of Statistics 2021b, *Digital boundary files*, Australian Bureau of Statistics, viewed 27 September 2022, <https://www.abs.gov.au/statistics/standards/australian-statistical-geography-standard-asgs-edition-3/jul2021-jun2026/access-and-downloads/digital-boundary-files>.

Australian Bureau of Statistics 2021c, *Regional population*, Australian Bureau of Statistics, viewed 25 August 2022, <https://www.abs.gov.au/statistics/people/population/regional-population/2021>.

Australian Bureau of Statistics 2021d, *Wombarra 2021 Census All persons QuickStats*, Australian Bureau of Statistics, viewed 27 September 2022, <https://www.abs.gov.au/census/find-census-data/quickstats/2021/SAL14381>.

Australian Bureau of Statistics 2022, *Population*, Australian Bureau of Statistics, viewed 13 October 2022, <https://www.abs.gov.au/statistics/people/population>.

Australian Energy Market Operator 2021, *About the National Electricity Market (NEM)*, Australian Energy Market Operator, viewed 13 October 2022, <https://aemo.com.au/en/energy-systems/electricity/national-electricity-market-nem/about-the-national-electricity-market-nem>.

Australian Energy Regulator 2022, *Understand and compare your home energy usage*, Australian Energy Regulator, viewed 25 October 2022, <https://www.energymadeeasy.gov.au/benchmark>.

Bahadori, A & Nwaoha, C 2013, 'A review on solar energy utilisation in Australia', *Renewable and Sustainable Energy Reviews*, vol. 18, pp. 1-5.

Baurzhan, S & Jenkins, GP 2016, 'Off-grid solar PV: Is it an affordable or appropriate solution for rural electrification in Sub-Saharan African countries?', *Renewable and Sustainable Energy Reviews*, vol. 60, pp. 1405-1418.

Baxter, J 2011, *Families in regional, rural and remote Australia*, Australian Institute of Family Studies, viewed 16 October 2022, <https://aifs.gov.au/research/research-reports/families-regional-rural-and-remote-australia>.

Benson, R, Paris, M, Sherry, J & Justus, C 1984, 'Estimation of daily and monthly direct, diffuse and global solar radiation from sunshine duration measurements', *Solar Energy*, vol. 32, no. 4, pp. 523-535.

Benti, NE, Aneseyee, AB, Asfaw, AA, Geffe, CA, Tiruye, GA & Mekonnen, YS 2022, 'Estimation of global solar radiation using sunshine-based models in Ethiopia', *Cogent Engineering*, vol. 9, no. 1.

Bergamasco, L & Asinari, P 2011, 'Scalable methodology for the photovoltaic solar energy potential assessment based on available roof surface area: Further improvements by ortho-image analysis and application to Turin (Italy)', *Solar Energy*, vol. 85, no. 11, pp. 2741-2756.

Blasco, BC, Moreno, JJM, Pol, AP & Abad, AS 2013, 'Using the R-MAPE index as a resistant measure of forecast accuracy', *Psicothema*, vol. 25, no. 4, pp. 500-506.

Boulahia, M, Djiar, KA & Amado, M 2021, 'Combined engineering—statistical method for assessing solar photovoltaic potential on residential rooftops: case of Laghouat in Central Southern Algeria', *Energies*, vol. 14, no. 6, p. 1626.

Breeze, P 2014, 'Electricity Generation and the Environment', in *Power Generation Technologies*, 2nd edn, Elsevier, United Kingdom, pp. 15-27.

Buffat, R, Grassi, S & Raubal, M 2018, 'A scalable method for estimating rooftop solar irradiation potential over large regions', *Applied Energy*, vol. 216, pp. 389-401.

Bureau of Meteorology 2019, *Average daily solar exposure*, Australian Government: Bureau of Meteorology, viewed 26 September 2022, <http://www.bom.gov.au/jsp/ncc/climate_averages/solar-exposure/index.jsp?period=an#maps>.

Bureau of Meteorology 2022, *Climate Data Online*, Australian Government: Bureau of Meteorology, viewed 09 October 2022, <http://www.bom.gov.au/climate/data/index.shtml?bookmark=200>.

Calcabrini, A, Ziar, H, Isabella, O & Zeman, M 2019, 'A simplified skyline-based method for estimating the annual solar energy potential in urban environments', *Nature Energy*, vol. 4, no. 3, pp. 206-215.

Chiew, F, Teng, J, Vaze, J, Post, D, Perraud, J, Kirono, D & Viney, N 2009, 'Estimating climate change impact on runoff across southeast Australia: Method, results, and implications of the modeling method', *Water Resources Research*, vol. 45, no. 10, p. W10414.

Chow, A, Fung, AS & Li, S 2014, 'GIS modeling of solar neighborhood potential at a fine spatiotemporal resolution', *Buildings*, vol. 4, no. 2, pp. 195-206.

Chupong, C & Plangklang, B 2011, 'Forecasting power output of PV grid connected system in Thailand without using solar radiation measurement', *Energy Procedia*, vol. 9, pp. 230-7.

Clean Energy Council 2020, *Clean Energy Australia Report 2020*, Clean Energy Council, viewed 14 September 2022, <https://assets.cleanenergycouncil.org.au/documents/resources/reports/clean-energy-australia/clean-energy-australia-report-2020.pdf>.

Clean Energy Council 2022, *Solar*, Clean Energy Council, viewed 14 October 2022, <https://www.cleanenergycouncil.org.au/resources/technologies/solar-energy>.

Clifton, J & Boruff, BJ 2010, 'Assessing the potential for concentrated solar power development in rural Australia', *Energy Policy*, vol. 38, no. 9, pp. 5272-5280.

Defaix, P, Van Sark, W, Worrell, E & de Visser, E 2012, 'Technical potential for photovoltaics on buildings in the EU-27', *Solar Energy*, vol. 86, no. 9, pp. 2644-2653.

Department of Climate Change, Energy, the Environment and Water 2022a, *Electricity generation*, Department of Climate Change, Energy, the Environment and Water, viewed 14 October 2022, <https://www.energy.gov.au/data/electricity-generation>.

Department of Climate Change, Energy, the Environment and Water 2022b, *Photovoltaic systems*, Department of Climate Change, Energy, the Environment and Water, viewed 02 October 2022, <https://www.yourhome.gov.au/energy/photovoltaic-systems>.

Department of Planning and Environment 2019, *NSW Electricity Strategy*, Department of Planning and Environment, viewed 13 October 2022, <https://www.energy.nsw.gov.au/sites/default/files/2022-08/2019_11_NSW_ElectricityStrategyOverview.pdf>.

Dolara, A, Leva, S & Manzolini, G 2015, 'Comparison of different physical models for PV power output prediction', *Solar Energy*, vol. 119, pp. 83-99.

Doorga, JRS, Rughooputh, SD & Boojhawon, R 2019, 'High resolution spatio-temporal modelling of solar photovoltaic potential for tropical islands: Case of Mauritius', *Energy*, vol. 169, pp. 972-987.

Dwyer, J 2018, *Big Strategic Planning Changes for Local Government in NSW*, Mecone, viewed 31 August 2022, <https://mecone.com.au/articlesandnews/big-strategic-planning-changes-for-local-government-in-nsw/>.

Energy Networks Australia 2017, *Electricity Network Transformation Roadmap: Final Report*, Energy Networks Australia, viewed 14 October 2022, <https://www.energynetworks.com.au/assets/uploads/entr_final_report_april_2017.pdf>.

Environmental Systems Research Institute 2019, *What is lidar data?*, Environmental Systems Research Institute, viewed 05 October 22, <https://desktop.arcgis.com/en/arcmap/10.3/manage-data/las-dataset/what-is-lidar-data-.htm>.

Environmental Systems Research Institute 2021a, *ArcGIS Pro 2.9*, Environmental Systems Research Institute, viewed 02 August 2022, <https://www.esri.com/en-us/arcgis/products/arcgis-pro/overview>.

Environmental Systems Research Institute 2021b, *Area Solar Radiation*, Environmental Systems Research Institute, viewed 23 October 2022, <https://pro.arcgis.com/en/pro-app/2.9/tool-reference/spatial-analyst/area-solar-radiation.htm>.

Environmental Systems Research Institute 2021c, *Hillshade function*, Environmental Systems Research Institute, viewed 23 October 2022, <https://pro.arcgis.com/en/pro-app/2.9/help/analysis/raster-functions/hillshade-function.htm>.

Environmental Systems Research Institute 2021d, *How Slope works*, Environmental Systems Research Institute, viewed 22 September 2022, <https://pro.arcgis.com/en/pro-app/2.9/tool-reference/spatial-analyst/how-slope-works.htm>.

Environmental Systems Research Institute 2021e, *How solar radiation is calculated*, Environmental Systems Research Institute, viewed 23 October 2022, <https://pro.arcgis.com/en/pro-app/2.9/tool-reference/spatial-analyst/how-solar-radiation-is-calculated.htm>.

Environmental Systems Research Institute 2021f, *What is ArcPy?*, Environmental Systems Research Institute, viewed 23 October 2022, <https://pro.arcgis.com/en/pro-app/2.8/arcpy/get-started/what-is-arcpy-.htm>.

Falklev, EH 2017, 'Mapping of solar energy potential on Tromsøya using solar analyst in ArcGIS', Master's thesis, UiT The Arctic University of Norway, Norway.

Farzaneh, A, Monfet, D & Forgues, D 2019, 'Review of using building information modeling for building energy modeling during the design process', *Journal of Building Engineering*, vol. 23, pp. 127-135.

Florio, P, Peronato, G, Perera, A, Di Blasi, A, Poon, KH & Kämpf, JH 2021, 'Designing and assessing solar energy neighborhoods from visual impact', *Sustainable Cities and Society*, vol. 71, p. 102959.

Freitas, S & Brito, MC 2019, 'Solar façades for future cities', *Renewable Energy Focus*, vol. 31, pp. 73-79.

Freitas, S, Catita, C, Redweik, P & Brito, MC 2015, 'Modelling solar potential in the urban environment: State-of-the-art review', *Renewable and Sustainable Energy Reviews*, vol. 41, pp. 915-931.

Fu, P & Rich, PM 1999, 'Design and implementation of the Solar Analyst: an ArcView extension for modeling solar radiation at landscape scales', in *Proceedings of the Nineteenth Annual ESRI User Conference*, vol. 1, pp. 1-31.

Fu, P & Rich, PM 2002, 'A geometric solar radiation model with applications in agriculture and forestry', *Computers and Electronics in Agriculture*, vol. 37, no. 1-3, pp. 25-35.

Fu, P 2000, '*A geometric solar radiation model with applications in landscape ecology'*, Doctor of Philosophy thesis, University of Kansas, Kansas.

Gagnon, P, Margolis, R, Melius, J, Phillips, C & Elmore, R 2018, 'Estimating rooftop solar technical potential across the US using a combination of GIS-based methods, lidar data, and statistical modeling', *Environmental Research Letters*, vol. 13, no. 2, p. 24027.

Geoscience Australia 2022a, *Solar Energy*, Geoscience Australia, viewed 14 October 2022, <https://www.ga.gov.au/scientific-topics/energy/resources/other-renewable-energy-resources/solar-energy>.

Geoscience Australia 2022b, *Elvis - Elevation and Depth - Foundation Spatial Data*, Geoscience Australia, viewed 22 September 2022, <https://elevation.fsdf.org.au/>.

Ghaleb, B & Asif, M 2022, 'Assessment of solar PV potential in commercial buildings', *Renewable Energy*, vol. 187, pp. 618-630.

Ghosh, S & Vale, R 2006, 'The potential for solar energy use in a New Zealand residential neighbourhood: a case study considering the effect on CO2 emissions and the possible benefits of changing roof form', *Australasian Journal of Environmental Management*, vol. 13, no. 4, pp. 216-225.

Glenn 2022, *The 50 largest cities and towns in Australia: Pandemic edition*, Informed Decisions, viewed 28 October 2022, <https://blog.id.com.au/2022/population/population-trends/the-50-largest-cities-and-towns-in-australia-pandemic-edition/>.

Gooding, J, Edwards, H, Giesekam, J & Crook, R 2013, 'Solar City Indicator: A methodology to predict city level PV installed capacity by combining physical capacity and socio-economic factors', *Solar energy*, vol. 95, pp. 325-335.

Güney, T 2019, 'Renewable energy, non-renewable energy and sustainable development', *International Journal of Sustainable Development & World Ecology*, vol. 26, no. 5, pp. 389-397.

Harder, E & Gibson, JM 2011, 'The costs and benefits of large-scale solar photovoltaic power production in Abu Dhabi, United Arab Emirates', *Renewable Energy*, vol. 36, no. 2, pp. 789-796.

Heo, J, Song, K, Han, S & Lee, D-E 2021, 'Multi-channel convolutional neural network for integration of meteorological and geographical features in solar power forecasting', *Applied Energy*, vol. 295, p. 117083.

Hofierka, J & Kaňuk, J 2009, 'Assessment of photovoltaic potential in urban areas using open-source solar radiation tools', *Renewable Energy*, vol. 34, no. 10, pp. 2206-14.

Hong, T, Lee, M, Koo, C, Jeong, K & Kim, J 2017, 'Development of a method for estimating the rooftop solar photovoltaic (PV) potential by analyzing the available rooftop area using Hillshade analysis', *Applied Energy*, vol. 194, pp. 320-332.

Ineichen, P 2016, 'Validation of models that estimate the clear sky global and beam solar irradiance', *Solar Energy*, vol. 132, pp. 332-344.

Informed Decisions 2021, *Wollongong City: About the profile areas*, Informed Decisions, viewed 16 October 2022, <https://profile.id.com.au/wollongong/about>.

Informed Decisions 2022, *Wollongong City Council population forecast*, Informed Decisions, viewed 27 September 2022, <https://forecast.id.com.au/wollongong>.

International Energy Agency 2021a, *Coal 2021: Analysis and forecast to 2024,* International Energy Agency, viewed 13 October 2022, <https://iea.blob.core.windows.net/assets/f1d724d4-a753-4336-9f6e-64679fa23bbf/Coal2021.pdf>.

International Energy Agency 2021b, *World Energy Outlook 2021*, International Energy Agency, viewed 13 October 2022, <https://www.iea.org/reports/world-energy-outlook-2021>.

International Energy Agency 2022, *Global Energy Review: CO2 Emissions in 2021*, International Energy Agency, viewed 13 October 2022, <https://www.iea.org/reports/global-energy-review-co2-emissions-in-2021-2>.

Ironbark Sustainability 2021, *Wollongong emissions snapshot*, Ironbark Sustainability, viewed 27 October 2022, <https://snapshotclimate.com.au/locality/municipality/australia/new-south-wales/wollongong/2020/fy>.

Isaksson, E & Karpe Conde, M 2018, '*Solar power forecasting with machine learning techniques',* Degree Project in Mathematics, KTH Royal Institute of Technology, Stockholm.

Jakubiec, JA & Reinhart, CF 2013, 'A method for predicting city-wide electricity gains from photovoltaic panels based on LiDAR and GIS data combined with hourly Daysim simulations', *Solar Energy*, vol. 93, pp. 127-143.

Jiang, H, Yao, L, Lu, N, Qin, J, Liu, T, Liu, Y & Zhou, C 2022, 'Geospatial assessment of rooftop solar photovoltaic potential using multi-source remote sensing data', *Energy and AI*, vol. 10, p. 100185.

Jo, JH & Otanicar, T 2011, 'A hierarchical methodology for the mesoscale assessment of building integrated roof solar energy systems', *Renewable Energy*, vol. 36, no. 11, pp. 2992-3000.

Julieta, S-R, José-Julio, R-B & Pablo, Y-R 2022, 'A methodology to estimate the photovoltaic potential on parking spaces and water deposits. The case of the Canary Islands', *Renewable Energy*, vol. 189, pp. 1046-1062.

Jung, J, Han, S & Kim, B 2019, 'Digital numerical map-oriented estimation of solar energy potential for site selection of photovoltaic solar panels on national highway slopes', *Applied Energy*, vol. 242, pp. 57-68.

Jung, Y, Jung, J, Kim, B & Han, S 2020, 'Long short-term memory recurrent neural network for modeling temporal patterns in long-term power forecasting for solar PV facilities: Case study of South Korea', *Journal of Cleaner Production*, vol. 250, p. 119476.

Kabir, E, Kumar, P, Kumar, S, Adelodun, AA & Kim, K-H 2018, 'Solar energy: Potential and future prospects', *Renewable and Sustainable Energy Reviews*, vol. 82, pp. 894-900.

Karteris, M, Slini, T & Papadopoulos, A 2013, 'Urban solar energy potential in Greece: A statistical calculation model of suitable built roof areas for photovoltaics', *Energy and Buildings*, vol. 62, pp. 459-468.

Knight, G, Lockhart, N & Christopher, T 2021, 'Toward zero emissions: An initiative of Renew Illawarra', *Renew: Technology for a Sustainable Future*, no. 156, pp. 29-38.

Ko, L, Wang, J-C, Chen, C-Y & Tsai, H-Y 2015, 'Evaluation of the development potential of rooftop solar photovoltaic in Taiwan', *Renewable Energy*, vol. 76, pp. 582-95.

Labed, S & Lorenzo, E 2004, 'The impact of solar radiation variability and data discrepancies on the design of PV systems', *Renewable Energy*, vol. 29, no. 7, pp. 1007-1022.

Ladner-Garcia, H & O'Neill-Carrillo, E 2009, 'Determining realistic photovoltaic generation targets in an isolated power system', in *2009 IEEE Power & Energy Society General Meeting*, pp. 1-5.

Lahouar, A, Mejri, A & Slama, JBH 2017, 'Importance based selection method for day-ahead photovoltaic power forecast using random forests', in *2017 International Conference on Green Energy Conversion Systems (GECS)*, Hammamet, Tunisia, 23-25 March

Li, HX, Edwards, DJ, Hosseini, MR & Costin, GP 2020, 'A review on renewable energy transition in Australia: An updated depiction', *Journal of Cleaner Production*, vol. 242, p. 118475.

Li, Y & Liu, C 2017, 'Estimating solar energy potentials on pitched roofs', *Energy and Buildings*, vol. 139, pp. 101-107.

Lukač, N, Žlaus, D, Seme, S, Žalik, B & Štumberger, G 2013, 'Rating of roofs' surfaces regarding their solar potential and suitability for PV systems, based on LiDAR data', *Applied Energy*, vol. 102, pp. 803-812.

Macquarie, PC 2013, 'Valuing landscape, performing landscape: a case study of the Illawarra escarpment', Doctor of Philosophy thesis, University of Wollongong, Wollongong.

Mahmud, K, Azam, S, Karim, A, Zobaed, S, Shanmugam, B & Mathur, D 2021, 'Machine learning based PV power generation forecasting in Alice Springs', *IEEE Access*, vol. 9, pp. 46117-46128.

Margolis, R, Gagnon, P, Melius, J, Phillips, C & Elmore, R 2017, 'Using GIS-based methods and lidar data to estimate rooftop solar technical potential in US cities', *Environmental Research Letters*, vol. 12, no. 7, p. 74013.

Markos, FM & Sentian, J 2016, 'Potential of solar energy in Kota Kinabalu, Sabah: An estimate using a photovoltaic system model', *Journal of Physics: Conference Series*, vol. 710, no. 1, p. 12032.

Maxar 2020, *Satellite Imagery*, Maxar, viewed 22 October 2022, <https://www.maxar.com/products/satellite-imagery>.

Melius, J, Margolis, R & Ong, S 2013, *Estimating rooftop suitability for PV: a review of methods, patents, and validation techniques*, National Renewable Energy Laboratory, Denver, viewed 10 September 2022, <https://www.nrel.gov/docs/fy14osti/60593.pdf>.

Meyerson, FA, Merino, L & Durand, J 2007, 'Migration and environment in the context of globalization', *Frontiers in Ecology and the Environment*, vol. 5, no. 4, pp. 182–190.

Microsoft 2020, *Australia Building Footprints*, github, viewed 22 September 2022, <https://github.com/microsoft/AustraliaBuildingFootprints>.

Mishra, T, Rabha, A, Kumar, U, Arunachalam, K & Sridhar, V 2020, 'Assessment of solar power potential in a hill state of India using remote sensing and Geographic Information System', *Remote Sensing Applications: Society and Environment*, vol. 19, p. 100370.

Moriarty, P & Honnery, D 2012, 'What is the global potential for renewable energy?', *Renewable and Sustainable Energy Reviews*, vol. 16, no. 1, pp. 244-252.

Narayanan, R, Parthkumar, P & Pippia, R 2021, 'Solar energy utilisation in Australian homes: A case study', *Case Studies in Thermal Engineering*, vol. 28, p. 101603.

National Oceanic and Atmospheric Administration 2021, *What is lidar?*, National Oceanic and Atmospheric Administration, viewed 15 August 2022, <https://oceanservice.noaa.gov/facts/lidar.html>.

Nettesheim, FC, Conto, Td, Pereira, MG & Machado, DL 2015, 'Contribution of topography and incident solar radiation to variation of soil and plant litter at an area with heterogeneous terrain', *Revista Brasileira de Ciência do Solo*, vol. 39, no. 3, pp. 750-762.

Ng, C-F, Choong, C-K, Ching, S-L & Lau, L-S 2019, 'The impact of electricity production from renewable and non-renewable sources on CO2 emissions: evidence from OECD countries', *International Journal of Business & Society*, vol. 20, no. 1, pp. 365-382.

Nguyen, HT & Pearce, JM 2010, 'Estimating potential photovoltaic yield with r. sun and the open source Geographical Resources Analysis Support System', *Solar Energy*, vol. 84, no. 5, pp. 831-843.

Odeh, S & Nguyen, TH 2021, 'Assessment method to identify the potential of rooftop PV systems in the residential districts', *Energies*, vol. 14, no. 14, p. 4240.

OpenStreetMap 2022, *Wollongong topographic map*, Topographic map, viewed 29 September 2022, <https://en-au.topographic-map.com/map-tnd5k/Wollongong/>.

Paidipati, J, Frantzis, L, Sawyer, H & Kurrasch, A 2008, *Rooftop photovoltaics market penetration scenarios*, NREL/SR-581-42306, National Renewable Energy Lab.(NREL), Golden, CO (United States).

Pamain, A, Rao, PK & Tilya, FN 2022, 'Prediction of photovoltaic power output based on different non-linear autoregressive artificial neural network algorithms', *Global Energy Interconnection*, vol. 5, no. 2, pp. 226-35.

Park, J-K, Das, A & Park, J-H 2015, 'A new approach to estimate the spatial distribution of solar radiation using topographic factor and sunshine duration in South Korea', *Energy Conversion and Management*, vol. 101, pp. 30-39.

Quicke, A 2021, *Climate of the Nation 2021: Tracking Australia's attitudes towards climate change and energy*, The Australia Institute, viewed 13 September 2022, <https://australiainstitute.org.au/wp-content/uploads/2021/10/211013-Climate-of-the-Nation-2021-WEB.pdf>.

Rahman, MM & Vu, X-B 2020, 'The nexus between renewable energy, economic growth, trade, urbanisation and environmental quality: a comparative study for Australia and Canada', *Renewable Energy*, vol. 155, pp. 617-627.

Rana, M & Rahman, A 2020, 'Multiple steps ahead solar photovoltaic power forecasting based on univariate machine learning models and data re-sampling', *Sustainable Energy, Grids and Networks*, vol. 21, p. 100286.

Rana, M, Rahman, A & Jin, J 2020, 'A data-driven approach for forecasting state level aggregated solar photovoltaic power production', in *2020 International Joint Conference on Neural Networks (IJCNN)*, pp. 1-8.

Rathore, PKS, Chauhan, DS & Singh, RP 2019, 'Decentralized solar rooftop photovoltaic in India: On the path of sustainable energy security', *Renewable Energy*, vol. 131, pp. 297-307.

Ravimohan, A, Stafford, T & Twomey, P 2014, 'Financial incentives and solar PV adoption in NSW', Honours Thesis, The University of New South Wales, New South Wales.

Reddy, BS & Nathan, HSK 2013, 'Energy in the development strategy of Indian households—the missing half', *Renewable and Sustainable Energy Reviews*, vol. 18, pp. 203-210.

Redweik, PM, Catita, C, & Brito, MC 2018, '3D local scale solar radiation model based on urban LiDAR data', *International Archives of the Photogrammetry, Remote Sensing and Spatial Information Sciences*, vol. XXXVIII-4/W19, pp. 265–269.

Rogers, SR, Manning, I & Livingstone, W 2020, 'Comparing the spatial accuracy of digital surface models from four unoccupied aerial systems: Photogrammetry versus LiDAR', *Remote Sensing*, vol. 12, no. 17, p. 2806.

Salahuddin, M & Alam, K 2015, 'Internet usage, electricity consumption and economic growth in Australia: A time series evidence', *Telematics and Informatics*, vol. 32, no. 4, pp. 862-878.

Salehabadi, A, Ahmad, MI, Ismail, N, Morad, N & Enhessari, M 2020, 'Overview of energy, society, and environment towards sustainable and development', *Energy, Society and the Environment: Solid-State Hydrogen Storage Materials*, Springer, Singapore, pp. 1-8.

Sampaio, PGV & González, MOA 2017, 'Photovoltaic solar energy: Conceptual framework', *Renewable and Sustainable Energy Reviews*, vol. 74, pp. 590-601.

Santos, T, Gomes, N, Brito, M, Freire, S, Fonseca, A & Tenedório, JA 2011, 'Solar potential analysis in Lisbon using lidar data', in *Proc. in 31st EARSeL symposium and 35th general assembly Prague*, pp. 13-20.

Sartori, I & Hestnes, AG 2007, 'Energy use in the life cycle of conventional and low-energy buildings: A review article', *Energy and Buildings*, vol. 39, no. 3, pp. 249-257.

Schiffer, MB 2009, 'The impact of electricity: development, desires and dilemmas by Tanja Winther', *American Anthropologist*, vol. 111, no. 4, pp. 546–547.

Schüler, D, Wilbert, S, Geuder, N, Affolter, R, Wolfertstetter, F, Prahl, C, Röger, M, Schroedter-Homscheidt, M, Abdellatif, G, Guizani, AA, Balghouthi, M, Khalil, A, Mezrhab, A, Al-Salaymeh, A, Yassaa, N, Chellali, F, Draou, D, Blanc, P, Dubranna, J & Sabry, OMK 2016, 'The enerMENA meteorological network – Solar radiation measurements in the MENA region', in *AIP Conference Proceedings*, American Institute of Physics, Melville, vol. 1734, no. 1, p. 150008.

Sen, Z 2008, *Solar energy fundamentals and modeling techniques: atmosphere, environment, climate change and renewable energy*, Springer, London.

Sewchurran, S & Davidson, IE 2021, 'Why solar PV is such a lucrative option for South African municipal customers', in *2021 Southern African Universities Power Engineering Conference/Robotics and Mechatronics/Pattern Recognition Association of South Africa (SAUPEC/RobMech/PRASA)*, IEEE, Potchefstroom, South Africa, 27-29 January.

Shahsavari, A & Akbari, M 2018, 'Potential of solar energy in developing countries for reducing energy-related emissions', *Renewable and Sustainable Energy Reviews*, vol. 90, pp. 275-291.

Singh, A 2022, *Why and How do Seasons Change on Earth?*, Planets Education, viewed 08 October 2022, <https://planetseducation.com/what-causes-seasons-change/>.

Solar Market 2022, *Different Types of Solar Panels*, Solar Market, viewed 02 October 2022, <https://www.solarmarket.com.au/residential-solar/different-types-of-panels/>.

SolarSena 2021, *Calculating Optimal Azimuth Angle for Solar Panels*, SolarSena, viewed 22 August 2022, <https://solarsena.com/calculating-optimal-azimuth-angle-solar-panels/>.

Suomalainen, K, Wang, V & Sharp, B 2017, 'Rooftop solar potential based on LiDAR data: Bottom-up assessment at neighbourhood level', *Renewable Energy*, vol. 111, pp. 463-475.

Sykes, J 2022, *Solar Panels Wollongong: Compare costs & installers*, Solarchoice, viewed 27 September 2022, <https://www.solarchoice.net.au/blog/solar-power-system-prices-wollongong-nsw/>.

Taminiau, J & Byrne, J 2020, 'City-scale urban sustainability: Spatiotemporal mapping of distributed solar power for New York City', *Wiley Interdisciplinary Reviews: Energy and Environment*, vol. 9, no. 5, p. e374.

Taylor, A 2022, *Australia leads world in rooftop solar as share of renewables jumps to 35%*, viewed 27 September 2022, <https://www.minister.industry.gov.au/ministers/taylor/media-releases/australia-leads-world-rooftop-solar-share-renewables-jumps-35>.

Teofilo, A, Radosevic, N, Tao, Y, Iringan, J & Liu, C 2021, 'Investigating potential rooftop solar energy generated by Leased Federal Airports in Australia: Framework and implications', *Journal of Building Engineering*, vol. 41, p. 102390.

Tovar-Pescador, J, Pozo-Vázquez, D, Ruiz-Arias, J, Batlles, J, López, G & Bosch, J 2006, 'On the use of the digital elevation model to estimate the solar radiation in areas of complex topography', *Meteorological Applications*, vol. 13, no. 3, pp. 279-287.

Tyagi, V, Rahim, NA, Rahim, N, Jeyraj, A & Selvaraj, L 2013, 'Progress in solar PV technology: Research and achievement', *Renewable and Sustainable Energy Reviews*, vol. 20, pp. 443-461.

Wargon, M, Guidet, B, Hoang, TD & Hejblum, G 2009, 'A systematic review of models for forecasting the number of emergency department visits', *Emergency Medicine Journal*, vol. 26, no. 6, pp. 395-399.

Wiginton, L, Nguyen, HT & Pearce, JM 2010, 'Quantifying rooftop solar photovoltaic potential for regional renewable energy policy', *Computers, Environment and Urban Systems*, vol. 34, no. 4, pp. 345-357.

Williams, DK 2020, *Tree Distance for Solar Gain*, Sfgate, viewed 29 October 2022, <https://homeguides.sfgate.com/tree-distance-solar-gain-104280.html>.

Wollongong City Council 2020, *Sustainable Wollongong 2030: A Climate Healthy City*, Wollongong City Council, viewed 01 July 2022, <https://our.wollongong.nsw.gov.au/sustainable-wollongong-2030-a-climate-healthy-city>.

World Economic Forum 2021, *Why buildings are the foundation of an energy-efficient future*, World Economic Forum, viewed 13 September 2022, <https://www.weforum.org/agenda/2021/02/why-the-buildings-of-the-future-are-key-to-an-efficient-energy-ecosystem>.

World Weather Online 2022, *Wombarra Annual Weather Averages*, Zoomash Ltd, viewed 16 August 2022, <https://www.worldweatheronline.com/wombarra-weather-averages/new-south-wales/au.aspx>.

Yesilmaden, HM & Dogru, AO 2019, 'Finding the Best Locations for Photovoltaic Panel Installation in Urbanized Areas', *Feb-Fresenius Environmental Bulletin*, vol. 28, no. 2, p. 619.

Yu, M & Halog, A 2015, 'Solar photovoltaic development in Australia—a life cycle sustainability assessment study', *Sustainability*, vol. 7, no. 2, pp. 1213-1247.

Zalamea, E & Alvarado, RG 2014, 'Roof characteristics for integrated solar collection in dwellings of RealEstate developments in Concepción, Chile', *Revista de la Construcción. Journal of Construction*, vol. 13, no. 3, pp. 36-44.

Zhang, K, Yan, J & Chen, S-C 2006, 'Automatic construction of building footprints from airborne LIDAR data', *IEEE Transactions on Geoscience and Remote Sensing*, vol. 44, no. 9, pp. 2523-2533.

Zhao, E, May, E, Walker, PD & Surawski, NC 2021, 'Emissions life cycle assessment of charging infrastructures for electric buses', *Sustainable Energy Technologies and Assessments*, vol. 48, p. 101605.

Zuo, J & Zhao, Z-Y 2014, 'Green building research–current status and future agenda: A review', *Renewable and Sustainable Energy Reviews*, vol. 30, pp. 271-281.

Appendices

Appendix A.

The literature sources that make up the various components of the “section 2.2: Extent of study area” are listed in the table below. It is a comparison of studies with their methodology, and more significantly, it examines whether or not these studies include seasonality, topographic feature, rooftop characteristic, impediments, and shading analysis. Additionally, it examines whether or not any validation is being done.

Author	(Jo & Otanicar 2011)	(Alqahtani & Balta-Ozkan 2021)
Title	"Evaluation of integrated solar energy systems on roofs of buildings"	"Evaluation of solar rooftop power for residential buildings"
Area of Evaluation	The city of Chandler in Arizona - The Phoenix metropolitan area	City of Neom, Saudi Arabia
Scale	Country	3 Dwellings analysed
Dwelling Type	Commercial and Government buildings Rooftops	Residential buildings
Solar irradiation	NASA Global analysis data	Fixed tilt angle of 28 degree and aspect of 0 degree are used. Solar irradiation data from NASA surface meteorology and fixed tilt (19-30 degree) was taken
Roof area calculation	Quickbird remote sensing data photographs of 0.6 m per pixel and GIS building footprints were utilised for the detection of building rooftops using an object-orientated approach (Definiens developer program). After importing the data into ArcGIS, the computation of area was carried out.	Rooftop area is taken from data provided by Ministry of housing, Personal communication, 23 July 2020 (15-20m square) and available area provided by previous investigators (80% of total Rooftop area)
PV potential identification	RETScreen PV sizing software to evaluate electricity production	HOMER Pro software is used for PV sizing on the basis of load profiles
Have validation	Yes	No
Slope and Aspect	Yes	Yes
Shading analysis	Yes	No
Topographic feature	No	No
Seasonality Analysis	No	No

(Buffat et al. 2018)	(Boulahia, Djiar & Amado 2021)	(Suomalainen, Wang & Sharp 2017)
"Calculating the potential for rooftop solar radiation across large scale areas"	"Statistical Approach for determining residential rooftop solar photovoltaic	"Using LiDAR data, estimate rooftop solar potential"
2250 Km Square area of Switzerland	Municipality of Laghouat, Algeria	2250 square Km in Auckland Region
Country	City	City
3 million building' s rooftops	Residential rooftop	Residential buildings
DSM, which is produced from LIDAR, is provided by Swisstopo with a spatial resolution of 0.5 m square to determine slope and aspect. The data from the heliostats on the solar irradiance was used to determine the efficiency	Solar radiation analysis is done by Ladybug tool	Lidar data (provided by Auckland council) is used for the assessment of solar potential with the resolution of 1 m square, DSM data is analysed in the ArcGIS tool
Because no single source was able to cover such a large area, the footprints of individual buildings were collected using a combination of Open Street Map, cadastral surveys, and SwissTLM	Number of houses, full roof area, and statistical data about the selected buildings is taken from the Laghouat urban master plan.	Building Footprints shapefile is provided by Auckland Council, 2013 census data and analysed in ArcGIS to calculate rooftops area.
PV efficiency calculated using the single diode selected panel properties and inverter efficiency	Assumption made on PV efficiency at 17% and energy losses at 75%	Assumption made based on common installation sizes 2 to 3.5 KW panels
Yes	No	Solar radiation results are verified by an online solar radiation calculator (SolarView) developed by National Institute of Water and Atmospheric Research (NIWA)
Yes	Yes	Yes
Yes	Yes	Yes
No	No	No
No	No	No

(Ghosh & Vale 2006)	(Gagnon et al. 2018)	(Odeh & Nguyen 2021)
"Assessment of solar energy potential in a New Zealand residential neighbourhood"	"Estimating the US's technical potential for rooftop solar"	"Identify the rooftop PV potential"
Glen Innes, Auckland	USA country	Sydney City - 4 suburbs (Erskineville, Newton,
Suburb	Country	City
Roofs of built-up areas	All type of buildings	Residential buildings
ArcGIS is used to calculate solar efficient roof areas considering shading, slope and orientation.	Roof suitability factor, tilt, aspect and shading identified from Lidar data; NREL' s System Advisor Model (SAM) for energy simulation.	Annual energy production for each roof is calculated through SunSPoT tool
Aerial photographs are used to calculate total building roof area in ArcGIS tool. Suitable rooftop area is calculated by using sample of 60 buildings to place 0.6m*1.2m size panels in ArcGIS tool	Lidar data is used from US department (2006-14) with a resolution of 1 m square, survey data is used, and extrapolation is being done for building count	Suitable roof area is digitized and calculated for each roof in SunSPot tool
PV potential is taken from previous studies	PV potential is considered on assumption basis i.e., 160 W per m square. System loss of 14.08% taken on assumption basis	PV array of 1.75Kw capacity
Not done	Google Project sunroof is used for the roof suitability validation	PVSYST and SunSPot results were compared.
Yes	Yes	Yes
No	No	No
No	No	No
No	No	No

(Teofilo et al. 2021)	(Roberts et al., 2019)	(Roberts et al., 2018)	(Jung et al., 2020)
"Investigating potential rooftop solar energy generated by Leased Federal Airports in Australia"	"How Much rooftop solar can be installed in Australia"	"Analysis of Rooftop Solar Potential on Australian Residential Buildings"	"Long term power forecasting for solar PV using LSTM NN (Machine
21 Airports throughout Australia	Australia	Australia	South Korea
Country		Country	One Solar Power Plant
Airport buildings	All type of buildings	All type of buildings	Solar Power Plant
Area solar radiation tool in ArcGIS Pro	APVI solar map used to calculate solar insolation	ArcGIS tool used to include tilt and orientation. Solar radiation tool and hillshade tool used for insolation and	DEM model used to identify solar radiation data
Rooftop polygon outlines are digitized in ArcGIS Pro 2.4 using its World Imagery, which were taken by MAXAR with a resolution of 0.5 m rooftop area is calculated.	Available roof space generated by OMNILINK using the PSMA Geoscape database	Lidar data and DSM model with 1 m sq resolution used	No
10 Kw of fixed panel considered with 14.08% loss and North direction	PV sizing and efficiency is not suburb specific. PV capacity assumed to be equivalent to insolation. Information	Generic 250 watt module considered with the dimension of 1m*1.6m	Machine learning forecasting model used with historical data of 164 power plants for Korea power
Not done	No	No	Yes
Yes	Yes	Yes	Yes
No	Yes	Yes	Yes
No	No	No	Yes
No	No	No	No

(Jung et al., 2019)	(Heo et al, 2021)	(Fu and Rich, 2002)	(Clifton and Boruff, 2010)	(Mahmud et al., 2021)	(Nettesheim et al., 2015)
"Estimate solar energy potential for site selection on national highway"	"Convolutional neural network for integration of geographical	"Correlation of average soil temperature with insolation and	"Concentrated Solar power prediction"	"Machine learning based power	"Contribution of Topography and Incident Solar Radiation to
National Highway in Gongju city, South Korea	South Korea	Rocky Mountain Biological Laboratory (RMBL), Gunnison County, Colorado,	Wheatbelt area of Western Australia	Alice Spring, Northern territory,	Marambaia Island, State of Rio de Janeiro, Brazil
City	One solar Power plant	One building	City	City	City
No	No	No	No	All type of buildings	No
Digital numerical maps are used to prepare elevation contours and thus solar radiation modelling being done	Contour map and DEM model used to identify solar radiation	Calculated Insolation maps from DEM model	DEM model is used to calculate solar radiation in ArcGIS	Historical solar irradiance data used	GIS modelling being done on DEM model
No	No	No	No	No	No
No	Machine learning model	No	No	Historical PV power output data used	No
No	No	Yes	No	Yes	Yes
Yes	Yes	Yes	Yes	No	Only Slope considered
Yes	Yes	Yes	Yes	No	Yes
Yes	Yes	Yes	Yes	No	Yes
No	Yes	No	No	Yes	No

(Jiang et al., 2022)
“ Geospatial assessment of rooftop solar photovoltaic
Jiangsu Province, China with area of 107,200 km^2
State
All type of buildings
Geostationary satellite photos were used to record the solar radiation pattern
Building footprints are typically divided into grids so that spatial computations may be made more easily, and the ratio of rooftop space to total area is reflected in each grid
Global Solar Energy Estimator (GSEE) is used for the photovoltaic (PV) electricity
Yes
No
No
No
No